HOKKAIDO UNIVERSITY

Title	Characterization and Modeling of Alkali-Silica Reaction of Reactive Siliceous Materials in Conducting Model and Mortar Experiments
Author(s)	Baingam, Lalita
Citation	北海道大学. 博士(工学) 甲第12469号
Issue Date	2016-09-26
DOI	10.14943/doctoral.k12469
Doc URL	http://hdl.handle.net/2115/63435
Type	theses (doctoral)
File Information	Lalita_Baingam.pdf

Instructions for use

Hokkaido University Collection of Scholarly and Academic Papers : HUSCAP

Characterization and Modeling of Alkali-Silica Reaction of Reactive Siliceous Materials in Conducting Model and Mortar Experiments

By

Lalita BAINGAM

A thesis submitted in partial fulfillment of the requirements for the degree of Doctor of Engineering

Examination Committee: Prof. Toyoharu NAWA
Prof. Tsutomu SATO
Prof. Naoki HIROYOSHI
Associate Prof. Kiyofumi KURUMISAWA

Doctor' s Thesis
Division of Sustainable Resources and Materials
Graduate School of Engineering, Hokkaido University
September 2016

ACKNOWLEDGEMENTS

Herewith I would like to record my appreciate to all the people who contributed by some means or others to the successful completion of this dissertation.

I sincerely appreciate to my supervisor, Professor Toyoharu NAWA, whose guidance, encouragement and advice from the beginning step to the final level enabled me to develop an understanding of the subjects. Under his instruction with patience, knowledge, and talent about the concrete science, it was a strongly contributed to elevate the quality of this research work to fulfill the doctor degree requirement with fruitful achievements and publications. Every moment of his valuable time that he spent in guiding and teaching me towards the completion of this work is sincerely and gratefully acknowledged. I wish to express profound gratitude to Associate Professor Kiyofumi KURUMISAWA for his advice, supervision , and crucial assistance, which made him a backbone of this research and so to this dissertation. Special thanks go to Dr. Eiji IWASUTKI for his assistance to get the data of reactive chert materials and experimental instrument used in this work.

I wish to express my sincere appreciations to Professor Tsutomu SATO and Professor Naoki HIROYOSHI who served as my dissertation committee members, and give me important guidance during my first step into studies of "Investigation of Alkali-Silica Reaction of Reactive Siliceous Materials in Conducting Model Experiments" and gave good advice and guidance since the start until the completion. I wish to acknowledge to Associate Professor Elakneswaran YOGARAJAH for his help and suggestions about PHREEQC simulation.

I wish to thank Natalya Shmakova, coordinator of English Engineering Education Program (e3), for her indispensable help dealing with administration matters during my stay. I thank MEXT for providing financial support through Monbukagakusho scholarship during my tenure at Hokkaido University, Japan. I convey special acknowledge to laboratory members for their help to carry out the experiments and useful discussion during the weekly seminar. I would like to thank Naoya Nakagawa, engineering official (Department of Applied Physics) for allowing me to use ^{29}Si-MAS NMR and suggested me to analyze the results properly. I would like to express special thanks to all staff at the Graduate School of Engineering, Hokkaido University for their help in providing facilities and materials for my experiments.

Certainly, I much to express special thanks to my family for their long-distance encouragement. They always give me a greatest love, willpower and financial support until the completion of this thesis. Finally, I would like to thank my friends who supported in every aspect for my life more enjoyable during my PhD life.

ABSTRACT

The use of certain aggregate in harden concrete may cause in a particular chemical process in which various silica forms of aggregate react with alkali hydroxides dissolved in the pore solution of concrete, attributing to the alkali silica reaction (ASR). The ASR can produce hydrous calcium-alkali silicate and alkali-silicate gels. This so-called ASR gel adsorbs water and the resulting in swelling expansion, causes cracks in the aggregate grains and in the surrounding cement paste matrix leading to loss of strength and reductions in the elastic modulus and durability of the concrete. Therefore, ASR is a major liability for the durability of concrete structures. Generally, the expansion process occurs due to the formation of gel by the ASR reaction. It may be deduced that the rate of expansion due to ASR depends on both the contents of ASR as well as on the capacity available for swelling of the gel.

The main objective of the research in this dissertation is to clearly understanding the ASR mechanism as a cause of damage. One way to approach the mechanism is to analyze the chemical compositions and structure of ASR products. A chemical model is presented here to simulate the ASR formation volume in deteriorated concrete due to ASR. The ASR formation was studied with experiments involving siliceous materials (Yoro-chert, Seto- chert, Silica sand, and Pyrex glass) and $Ca(OH)_2$ with alkalinity under accelerated conditions at different temperatures (60, 70, and 80°C). The investigation employed Inductively Coupled Plasma Atomic Emission Spectrometry (ICP-AES), X-Ray Diffraction (XRD), ^{29}Si Nuclear Magnetic Resonance (^{29}Si-NMR), Scanning Electron Microscopy with Energy Dispersive X-Ray Analysis (SEM/EDX), and Electron Prove Micro-Analyzer (EPMA) analysis. The ICP-AES, XRD, ^{29}Si-NMR, SEM/EDX, and EPMA results showed that the formation of ASR occurred in model system is compatible to C-S-H product. Considering these results, the prediction of ASR products was made using PHREEQC program, in which the results were in line with the experiment data. Additionally, the reactive pyrex glass was assumed to be the most reactive material in this work. The expansion measurements were conducted by mean of ASTM 227 standard (mortar testing), indicating the conclusion that PG is a highly reactive compound inducing expansion due to ASR. The dissertation is organized into seven chapters with the references. The contents of each chapter are presented as follows.

In Chapter 1, the study context and motivation, the significance for practice, the objectives of the study and the research methodology are viewed. Attention in Chapter 2 had been paid to the basic chemical reaction, the model description of ASR expansion, the identification of ASR in deteriorated structures, the laboratory identification of ASR products and the examination of quality of aggregates. In Chapter 3, the materials and experiments (including model system, simulation of phase assemblage and ASR-induced expansion of mortar) carried out in this investigation are revealed. The results and discussion of model system are described in Chapter 4. It is well-known that ASR is a chemical reaction which is highly sensitive to temperature. With the dissolution rate of soluble silica determined by ICP-AES analysis, the increasing temperature increases in the contents of soluble silica. It has been pointed out here that the Ca ions have an effect on the content of free soluble silica in pore solution of cement matrix. This is because when Ca ion is almost consumed, the contents of soluble silica remarkably increased in the solution. For investigation of insoluble products, the C-S-H formed in model system can be attributed to the ASR occurring between the available SiO_2 and Ca ions. In XRD results, the greater calcium hydroxide consumption supports the idea that Ca ions play an important role in accelerating the ASR reaction, with ASR formation of chemical compositions similar to C-S-H. It was noticeable that by the addition of small content of calcium hydroxide, the XRD peaks of C-S-H peaks located 29.0° 2θ shift to 30.0° 2θ and became broader. The spectra of ^{29}Si Nuclear Magnetic Resonance (^{29}Si-NMR) indicated a more reasonable relationship between ASR gel and C-S-H when Ca ions are present in particular. It is believed that alkali silicate hydrate (Na/K-S-H) may be supposed to be the first product in the sequence of the ASR.

Prior to the completed C-S-H formation, C-Na/K-S-H (the Q^1 site dominantly) could be formed by the incorporation of Ca ions into Na/K-S-H. Later, excess Ca ions are closely involved in the precipitation of ASR gel, likely to form a more polymerized structure of C-S-H (dominated by the Q^2 site). With lower amounts of Ca ions, the Q^3 site becomes detectable and finally, the presence of C-Na/K-S-H and Na/K-S-H may be attributed to the complete consumption of CH. According to SEM/EDX observation, the Ca/Si ratios of solid samples can be identified. For this result, we also assume the precipitation of C–S–H with an Ca/Si ratio of 0.83 for chert sample and that of 1.66 for Pyrex glass sample. Consequently, the chemical sequence of ASR gel formation for Yoro-chert and Pyrex glass was simulated by PHREEQC program (more detailed in Chapter 5). The sequence in the simulated process of ASR can be divided into 4 steps and the simulation model tends to give predictions of C-S-H, C–Na–S–H, and Na-S-H that are in agreement with the experimental data from the corresponding tests, as mentioned previously in the XRD and ^{29}Si-NMR results. Hence our simulation strongly confirms that sequence of the ASR of Pyrex glass is the same as those of both cherts (Yoro and Seto). This also suggests that the ASR examination using Pyrex glass can be used for and would be effective to understand the chemical and physical behavior of the ASR induced expansion of mortar and concrete. For this reason, the expansion measurement made at constant temperatures of 40°C, using two alkali constants (0.6 and 1.2%), allow the ASR reactivity of Pyrex glass to be investigated in this research (shown in Chapter 6). Supporting the evidence by EPMA, the formation of ASR existed in the cracked in the Pyrex glass or in the rim near the reactive site. For ASR product, it was found that at inside the cracks of Pyrex glass, high intensities of Si, Na and K with low Ca were investigated, in which the Ca/Si ratios of ASR gel were less than 1.0.

One of the important constituents of this study is to associate the dissolution rate of soluble silica with mortar expansion due to ASR. Based on Arrhenius law, three parameters including the constant rate of dissolution at 40°C, the dissolution rate of soluble silica at 40°C and the activation energy (E_a) could be determined by considering the dissolution rate of soluble silica at different temperatures (60, 70, and 80°C) in model system. The results show a strong relationship between the rate of dissolution of Si from aggregate in the model and its contribution to ASR-induced expansion of mortar under temperature of 40 °C. A quantitative consideration was given to the damage of mortar from a point of view of the relationships among the expanded mortar, the dissolution rate of soluble silica, and the gel composition of each reactive-siliceous materials. Ultimately, the simulation confirmed that the ASR gel formation is relevant to the expansion of mortar. The summary of results is revealed and contributed to the recommendations for future works in Chapter 7.

TABLE OF CONTENTS

CHAPTER 4 MODEL SYSTEM

CHAPTER 5 SIMULATION OF PHASE ASSEMBLAGE

CHAPTER 6 ASE-INDUCED EXPANSION OF MORTAR

CHAPTER 7 CONCLUSIONS AND FUTURE WORKS

CHAPTER 1 INTRODUCTION

1.1 STUDY CONTEXT AND MOTIVATION

The use of certain aggregate in harden concrete may cause in a particular chemical process in which various silica forms of aggregate react with alkali hydroxides dissolved in the pore solution of concrete, attributing to the alkali silica reaction (ASR). These alkali hydroxides are derived from the sodium, potassium and calcium in Portland cement and other cementitious materials, and irregularly from certain type mineral components within aggregates. The ASR can produce hydrous calcium-alkali silicate and alkali-silicate gels. This so-called ASR gel absorbs water and the resulting swelling expansion, causes cracks in the aggregate grains and in the surrounding cement paste matrix leading to loss of strength and reductions in the elastic modulus and durability of the concrete, and consequently damages the concrete structure, resulting in shortening of the service-life of concrete structures, leading to the generally acknowledged understanding that ASR is a major liability for the durability of concrete structures. Field investigation found the signs of concrete distress in the form of cracking that are visible on the surface of deteriorated concrete due to ASR. For examples, map cracking pattern and crack with an opaque white coating on the surface of a hydroelectric concrete dam [1] were inspected as shown in **Figs. 1.1-1.2**, respectively. Additionally, Fernandes 2004 [2] reported a special case of ASR characteristics in term of efflorescence, such as translucent gel and sticky gel (**Fig. 1.3**).

It is well-known that the main effect of ASR is a long-term structural deterioration and it is difficult to control the progress of the reaction, which results in a progressive decrease of concrete durability and service life. Consequently, damage to hardened concrete arising due to ASR is increasingly observed with the increasing use of concrete and extending service life of concrete components. Concrete deterioration due to the ASR moderately takes place in a few years but is strongly aggressive. On the other hand, the accelerated test methods have become increasingly essential to be able to investigate ASR for a short time under the several conditions. Experiments have been carried out by accelerated test methods to estimate the potential reactivity of aggregates before their use in concrete in order to avoid later problems arising from ASR-affected structures [3-4] and there are investigations of the residual expansion of existing concrete structures damaged by ASR [5-7]. There are a number of standards for evaluating ASR reactivity, for instance the American Society for Testing and Materials (ASTM) codes, which include the C289, C294, C1260, and C1293 standards [8-11].

Previous investigation [12] referred the existence of ASR in the concrete. The inspection of damaged structure in Aichi prefecture (Japan) reported the presence of cracks and exudations similar to the symptoms of ASR process and stated that the deterioration of concrete was owing to the ASR by the reaction of reactive chert aggregates. In laboratory experiment by [12], these chert aggregates including Yoro-chert and Seto-chert were used to study the characteristics of ASR conforming to the method of JIS A1146 (mortar-bar test). The results showed the significantly different of expansion-time relationship between Yoro-chert and Seto-chert (More detailed in chapter 5).

The present work is a part of laboratory program, which aims to establish the model system to simulate the ASR formation in concrete with accelerating conditions at highly alkaline and temperature. Four siliceous samples including Pyrex glass (PG), Yoro-chert (Yo), Seto-chert (Se) and Silica sand (SS) were investigated. The experiments describe the results of ASR generated through a reactive system conducted to gain a more comprehensive understanding of the ASR mechanism of formation and the role of Ca on ASR formation by an analysis of Inductively Coupled Plasma Atomic Emission Spectrometry (ICP-AES), X-Ray Diffraction (XRD), Scanning Electron Microscopy with Energy Dispersive X-Ray Analysis (SEM/EDX), ^{29}Si Nuclear Magnetic Resonance (^{29}Si-NMR) analysis and Electron Probe Micro-Analyzer (EPMA). Correlating these experimental data with previous studies [13-16][17] leads to insight into the

sequence of reaction, particularly the ASR formation in the presence of calcium hydroxide. The sequence of the ASR can be demonstrated to divide into 4 steps, which is relevant to the species predicted to be formed by ASR, including C-S-H, C-Na-S-H, and Na-S-H suggested by the PHREEQC program. With ICP-AES, the silica dissolution at different temperatures of PG, Yo, Se and SS can be determined. From the temperature dependence of the dissolution rate, the constant rate of dissolution, the dissolution rate of soluble silica, and the activation energy (E_a) at any temperature can be estimated on the basis of the Arrhenius law. This comprehensive effort has been developed to take understanding of the relationship between dissolution rate of soluble silica and expansion behaviors of mortars containing ASR-reactive materials.

Fig. 1.1 Map cracking pattern on the surface of dam [1]

Fig. 1.2 Cracks with an opaque white coating on surface of dam [1]

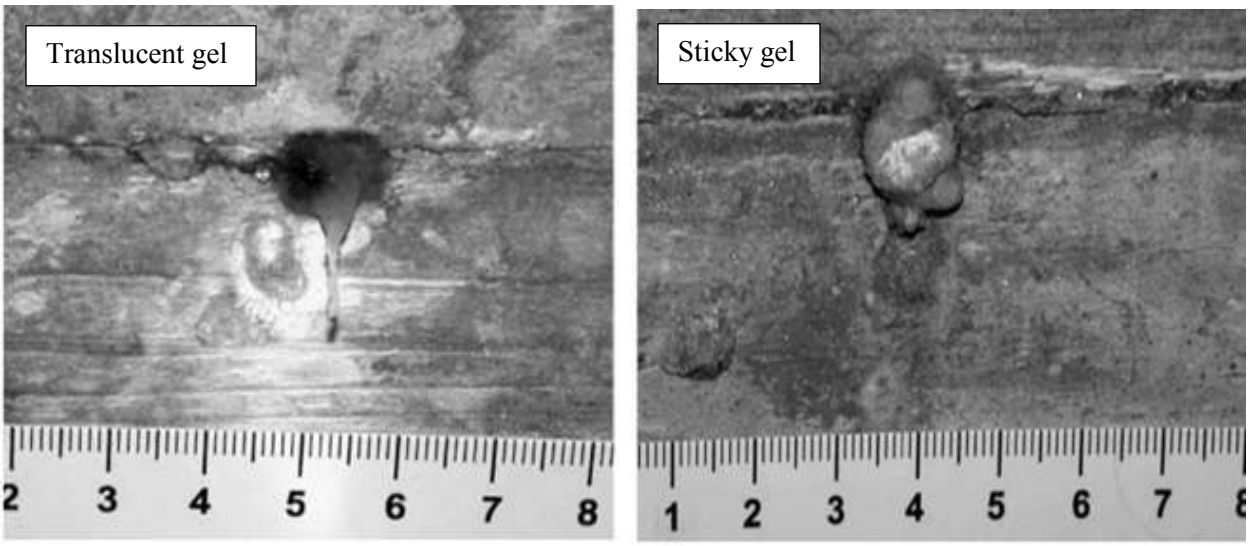

Fig. 1.3 Efflorescence gel [2]

1.2 SIGNIFICANCE FOR PRACTICE

Generally, the mechanism of ASR expansion can be divided into two aspects: (1) a reaction between reactive Si and alkalis in the pore solutions, yielding an ASR sol/gel; and (2) a humidity change influence on the volume of gel expansion. However, the ASR mechanism remains unclear because some products of ASR do not produce the deleterious expansion. Recent theory related to the first aspect detailed that, when reactive silica is in contact with strong alkali ions including K, Na, and Ca ions, the ASR reaction occurs spontaneously, generating an ASR gel, acting like a phase that is possibly congruent to Ca-rich ASR gel, at the boundary of the reactive aggregate [18]. Several types of ASR gel have also been reported as follows: ASR gel without Ca content, like alkali-silicate hydrate (Na/K-S-H); and ASR gel being incorporated with Ca, calcium-alkali silicate (C-S-H) or high alkali- and low Ca-silicate hydrate (C-Na/K-S-H). Hou et al [13] highly recommended the conversion of the tobermorite type C-S-H to be shown as ASR gel, like C-Na/K-S-H, due to the exhaustion of calcium hydroxide (CH) in the reacting system. Hou et al. [14] also reported that dissolved silica reacts initially with CH to produce more depolymerized C-S-H, which is similar to a pozzolanic reaction, and when Ca ions are depleted, dissolved silica starts to react with existing C-S-H and form a silica-rich polymerized C-S-H. They also insisted that finally the amount of silica dissolved in the active site further increases until starting of gelation of ASR product. Kim and Olek [15] also proposed very similar reaction sequence suggested by Hou et al [14]. The ASR is initiated by the dissolution of silica due to an attack by hydroxyl ions, and in the presence of calcium ions which is supplied by $Ca(OH)_2$ from cement paste, the tobermorite type C–S–H is generally stable. After consumption of the available calcium ion, the Si concentration in the solution starts to increase, which promotes the formation of highly polymerized, high alkali and C–(Na/K)–S–H. Continuous increase in the concentration of silica ions leads to subsequent formation of Na/K-S-H gel. They also confirmed the chemical sequence of the alkali–silica reaction (ASR) process by a thermodynamic model for closed reactive system consisting of mixture of reactive silica mineral, calcium hydroxide, and alkali hydroxide solution [16]. From these results, it seems reasonable that calcium ion has a significant role in the build-up of expansive pressure, resulting in cracking of both aggregate and surrounding cement paste. Ichikawa and Miura [18][19] proposed that the existence of a semi-permeable rigid reaction rim is generated from the reaction of Ca ions, and covers the ASR-affected aggregate, resulting in enough expansive pressure which can be eventually generated to crack the aggregate as well as the surrounding cement paste.

However, a reaction rim consisting of calcium-rich silica gel at the aggregate-cement paste interface of reactive aggregate has ‘‘banding’’ effect, which obviously prevent ASR-related expansion until the critical pressure on cracking. Therefore, there is no general agreement that calcium-rich ASR gel generates either more or less ASR-related expansion in concrete. Katayama [20] distinguished different kinds of ASR with differences in composition, location, and accompanying expansion characteristics. Further clarification is needed to determine which ASR compositions may increase the volume of gel to exceed the tolerance of aggregate and cement paste, resulting in the cracking of concretes. One way to better understand the mechanism is to analyze the compositions and structure of ASR products.

As mentioned above, the expansion process occurs due to the formation of gel by the ASR reaction. The main factors that contribute to the ASR formation are reactive aggregate, highly alkaline conditions, and the moisture content in the pore solution. In particular, the aggregate used has a strong influence on the swelling mechanism generated by the reactions. This is because with reactive aggregate free silica is easily dissociated in the pore solution by the activity of hydroxide (OH^-). Highly reactive compounds tend to result in making more silica available for the ASR reaction. It is accepted that ASR is a chemical reaction which is highly sensitive to temperature [21-22]. Thus, a rise in temperature may be considered to be involved in increases in the dissolution rate of soluble silica. With more silica available in the pore solution then results in greater amounts of ASR product that in turn may induce expansion by water absorption, due to the swelling characteristics of the gel. The swelling of the gel is related to its chemical composition. Garcia-Diaz et al. [23] proposed a damage mechanism due to ASR by detailing a swelling curve divided into 4 periods: (i) The Q_0 tetrahedron formed from dissolution followed by reaction with alkali and Ca ions, producing Q_0 products such as calcium silicate hydrate (C-S-H) and calcium silicate hydrate C-Na/K-S-H, with no appreciable swelling; (ii) A transition from Q_4 to Q_3 increases the yield of Q_3 tetrahedra in the aggregate, which is responsible for the swelling and cracking; (iii) The dissolution and precipitation process in period two occurs while Q_0 products fill the cracks generated by the swelling; (iv) The swelling is asymptotic and the reaction continues to produce more Q_0 and Q_3 further filling the cracks. The parameters Q_0, Q_3, and Q_4 are $H_2SiO_4^{2-}$, $SiO_{5/2}$, and $^-SiO_2$, respectively in all of the periods. It may be deduced that the rate of expansion due to ASR depends on both the contents of ASR as well as on the capacity available for swelling of the gel. A study to determine the relation of expansion due to ASR to the degree of reaction has been reported [24-25]. The use of SEM image analysis by Haha et al. [24] showed that for potentially reactive ASR, the degree of reaction of aggregate is around 0.3%. Buteel et al. 2002 [25] developed a chemical method for quantitative characterization of ASR by considering two reaction degrees: the number of moles generated by siloxane bond break up inside the aggregate and the number of moles of monomers and small polymers obtained from dissolution. Additionally, the reported activation energy of reactive flint aggregate by [25] is approximately 78 kJ/mol. This activation energy value is close to the activation energy breaking siloxane bonds, which would be the limiting step of the dissolution process. Additionally, Kawamura et al., [26] revealed that both yoro-chert and pyrex glass are deleterious materials that prone to ASR problem but the mortar with pyrex glass expanded rapidly when compared with yoro-chert mortar. The high expansion of pyrex glass mortar was related to the amount of silica dissolution. Therefore, the rate of dissolution of soluble silica is an important factor in the ASR reaction and is related to the ambient temperature. Based on this, it may be assumed that at high temperatures, this condition accelerates the ASR, yielding more ASR gel in the pore solution and causing significant expansion. However, few studies have focused on the relationships among the ASR-induced expansion, the dissolution rate of soluble silica and the gel composition, particular in the difference of siliceous material.

1.3 OBJECTIVES OF THE STUDY

This research aims to establish the model experiments for simulating ASR formation in concrete with accelerating conditions. The main objectives of this study are as followed:

- To demonstrate the chemical sequence of ASR for different siliceous materials
- To understand the role of Ca ions on ASR process
- To simulate the precipitated species of ASR products
- To investigate the phase assemblages of ASR from different siliceous materials
- To associate the gel formation and its contribution to ASR-induced expansion of mortar

The experiments describe the results of ASR generated through a reactive system conducted to gain a more comprehensive understanding of the ASR mechanism of formation by an analysis of ICP-AES, XRD, SEM/EDX ^{29}Si-NMR and EPMA results. This comprehensive effort has been developed to take understanding of the mechanism of ASR-affected structures and the effect of Ca on ASR formation.

Expansion measurements made at different alkali contents, using a constant temperature at 40°C, allow the effect of the alkali content on the ASR of these reactive components to be investigated and reported in detail in this study. The results make it possible to relate the ASR-induced expansion of mortar and the estimated amount of dissolved silica from the reactive silica in the alkali solution. Moreover, it was found that the dissolution rate of soluble silica in Pyrex glass is quite different from Yo, Se, and SS, the three other compounds investigated here. This points to PG as a highly reactive compound, contributing to the ASR reaction. The use of Pyrex glass in expansion measurements clearly confirmed that the expansion behavior of mortars was due to the ASR reactivity of PG.

With XRD and ^{29}Si-NMR data for solids, the sequence of the ASR can be demonstrated to divide into 4 steps. To confirm the produced ASR relevant to C-S-H, the geochemical speciation program PHREEQC program will be used to simulate the phase assemblage formation of different siliceous materials following that occurring with this accelerated method, and compared to the results obtained from Q-XRD in mass units of gram. The Q-XRD stands for the quantitative analysis by XRD. **Fig. 1.4** illustrates the thesis structure in this study.

1.4 RESEARCH METHODOLOGY

The progress of this study on the simulate the ASR formation in concrete will be done in several steps, in which it can be classified as:

1.4.1 Model system

The study is aim to gain fundamental information on the ASR by characterizing pore solutions and reaction products in a model system for ASR. In model system, the materials including silica sand, reactive chert aggregates and reactive glass were conducted at highly alkaline and temperature conditions. At each reaction time, liquid samples with or without CH were filtrated and provided for an Inductively Coupled Plasma Atomic Emission Spectrometry (ICP-AES) analysis in order to investigate the dissolution rate of soluble silica. After filtration, dehydrated solid samples mixed with or without CH under temperature of 70 and 80° C was provided for investigating the chemical components and structure using X-Ray Diffraction (XRD) and a ^{29}Si Nuclear Magnetic Resonance (^{29}Si-NMR). The major tasks that can be obtained by ASR model system are:

- With ICP-AES, the silica dissolution of two chert-aggregates, pyrex glass and silica sand can be determined and from temperature dependence of dissolution rate, the activation energy can be estimated by Arrhenius law.
- With ICP-AES, silica dissolution of chert and pyrex glass can be determined and provide ion concentration data for the simulation of PHREEQC program.
- With ^{29}Si-NMR and XRD- Rietveld analysis, the ASR products (C-S-H and C-Na-S-H) are formed that promotes the reactivity of chert aggregates and pyrex glass.
- With ^{29}Si-NMR and XRD- Rietveld analysis demonstrates the sequence of the ASR reaction (C-S-H, C-Na-S-H and Na-S-H) and provides details of the changes in the ASR product compositions.

1.4.2 Simulation of phase assemblage

According to ^{29}Si-NMR and XRD- Rietveld analysis, the results confirmed that the formation of ASR in ASR model system is congruent to C-S-H, C-Na-S-H and Na-S-H, which were observed in the insoluble products of both chert aggregates and pyrex glass solids. However, the ^{29}Si-NMR result of insoluble product, in particular pyrex glass, was not able to clearly demonstrate the sequence of ASR because the reactions among reactive silica mineral, calcium hydroxide and alkali hydroxide solution happen rapidly. According to the thermodynamic model by Kim and Olek [16], the prediction of precipitated species by the mass action equation with equilibrium constants at 70 and 80°C for several ASR products could be estimated by using PHREEQC program in order to verify the sequence of ASR of different siliceous materials. The data from ICP-AES and XRD- Rietveld is useful and provided for PHREEQC simulation.

1.4.3 ASR-induced expansion of mortar

The mortar bar test was carried out in the method of ASTM C227 to show the characteristic of ASR of reactive glass. The mortar bar was tested in order to obtain the magnitude of expansion at constant temperature. Moreover, this study aims to investigate the role that alkali content has on the ASR expansion rate of mortar bars. In this work, the study is intended to relate the gel formation to the mortar due to ASR by considering quantitative parameters including the activation energy of each material, the rate constant at 40°C and the degree of reaction estimated by dissolution rate of soluble silica.

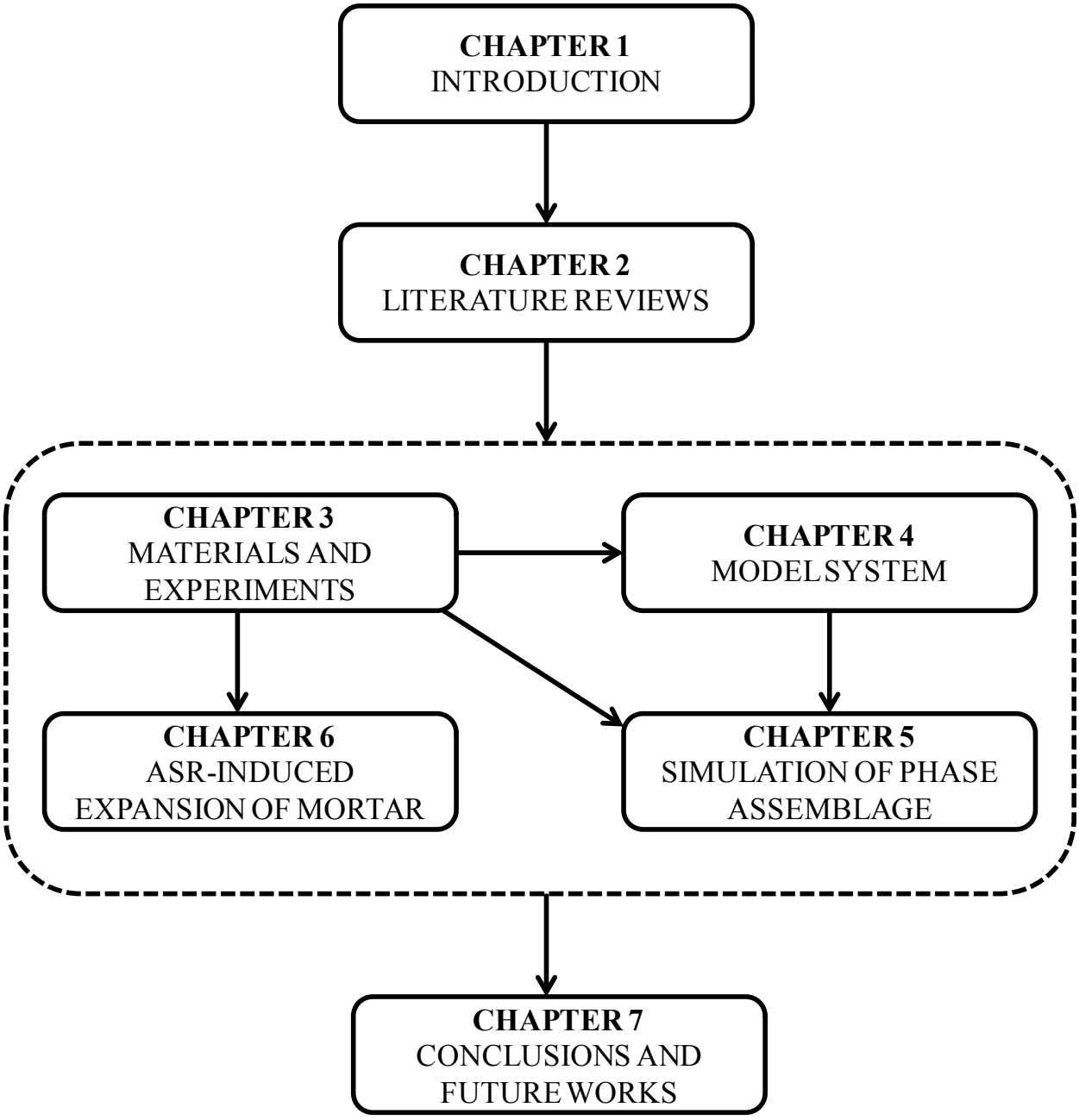

Fig. 1.4 Thesis structure

REFERENCES

[1] A. Shayan and J. Grimstad (2006), Deterioration of concrete in hydroelectric concrete gravity dam and its characterisation, Cement and Concrete Research, 36, 371-383

[2] I. Fernandes, F. Noronha, M. Teles (2004), Microscopic analysis of alkali-aggregate reaction products in a 50-year-old concrete, Materials Characterization, 53, 295-306

[3] A. Shayan, J. Grimstad. Deterioration of concrete in a hydroelectric concrete gravity dam and its characterisation. Cem Concr Res 2006;36(2):371 – 383.

[4] I. Fernades. Composition of alkali–silica reaction products at different locations within concrete structures. Mater Charact 2009;60(7): 655 – 668

[5] D. Lu, L. Mei, Z. Xu, M. Tang, X. Mo, B. Fournier. Alteration of alkali reactive aggregates autoclaved in different alkali solutions and application to alkali–aggregate reaction in concrete: (I) Alteration of alkali reactive aggregates in alkali solutions. Cem Concr Res 2006;36(6):1176–1190.

[6] M. Kawamura, K. Iwahori. ASR gel composition and expansive pressure in mortars under restraint. Cem Concr Comp 2004;26(1): 47-56.

[7] Federal highway administration, Alkali-aggregate reactivity (AAR) workshops for engineers and practitioners. U.S. department of transportation 2012.

[8] Test method for potential alkali-silica reactivity of aggregates (chemical method). ASTM international 2007. Retrieved from http://www.astm.org/Standards/C289.htm.

[9] Test method for constituents of natural mineral aggregates. ASTM international. Retrieved from http://www.astm.org/Standards/C294.htm.

[10] Test method for potential alkali-silica reactivity of aggregates (mortar-bar method). ASTM international 2007. Retrieved from http://www.astm.org/Standards/C1260.htm.

[11] Test method for determination of length change of concrete due to alkali-silica reaction (concrete prisms test). ASTM international.
Retrieved from http://www.astm.org/Standards/C1293.htm.

[12] E. Iwatsuki, K. Morino. Characteristics of alkali silica reaction of siliceous sedimentary rocks. JSMS 2008;57(10): 967-972.

[13] X. Hou, R J. Kirkpatrick. Structural investigation of alkali silicate gels. J Am Ceram Soc 2005; 88 (4): 943-949.

[14] X. Hou, L.J. Struble, R.J. Kirkpatrick. Formation of ASR gel and the roles of C-S-H and portlandite. Cem Concr Res 2004;34(9):1683-1696.

[15] T. Kim, J. Olek. Chemical sequence and kinetics of alkali-silica reaction part I Experiment. J Am Ceram Soc 2014; 97(7):2195-2203.

[16] T. Kim, J. Olek. Chemical Sequence and Kinetics of Alkali–Silica Reaction Part II. A Thermodynamic Model, J. Am. Ceram. Soc. 2014; 97(7) pp.2204–2212.

[17] X.D. Cong, R.J. Kirkpatrick. 29Si MAS NMR spectroscopic investigation of alkali silica reaction product gels. Cem Concr Res 1993 ; 23(4):811-823.

[18] T. Ichikawa, M. Miura. Modified model of alkali-silica reaction. Cem Concr Res. 2007;37(9):1291–1297.

[19] Ichikawa T (2009) Alkali–silica reaction, pessimum effects and pozzolanic effect. Cem Concr Res 39:716–726

[20] T. Katayama. Late-expansive ASR in a 30-year old PC structure in eastern Japan.14th ICAAR 030411-KATA-05. Austin;Texas: USA:2012.

[21] A.D. Jensen, S. Chatterji, P. Christensen, N. Thaulow, H. Gudmundsson. STUDIES OF ALKALI-SILICA REACTION-PART I A COMPARISON OF TWO ACCELERATED TEST METHODS, Cement and Concrete Research, 12, 641-647.

[22] R.N Swamy, a.A.-A.M.M., Influence of Alkali Silica Reaction on The Engeneering Properties of Concrete. Alkali in Concrete, ASTM STP 930, Ed,V.H. Dodson, American society for testing and material journal, Philadelphia (1986), 69-86.

[23] E.Garcia-Diaz, J.Riche, D.Bulteel and C. Vernet (2006), Mechanism of damage for the alkali-silica reaction, Cement and Concrete Research, 36, 395-400
[24] M.B. Haha, E. Gallucci, A. Guidoum, K.L. Scivener, Relation of expansion due to alkali silica reaction to the degree of reaction measured by SEM image analysis, Cement and Concrete Research, 37 (2007), 1206-1214.
[25] D. Bulteel, E. Garcia-Diaz, C. Vernet, H. Zanni Alkali-silica Reaction A Method to Quantify the Reaction Degree. Cem Concr Res, 32 (2002), 1199-1206.
[26] M. Kawamura, K. Iwahori. ASR gel composition and expansive pressure in mortars under restraint., Cement and Concrete Composites, 26 (2004), 47-56.

CHAPTER 2 LITERATURE REVIEWS

In this present work the focus is the simulation the ASR formation in concrete structure. Therefore, the main objective of the literature reviews is to give an overview about what is well-known on the ASR process in concrete. Attention had been paid to the basic chemical reaction, the model description of ASR expansion, the identification of ASR in deteriorated structures, the laboratory identification of ASR products and the examination of quality of aggregates. The previous simulation of ASR products by Kim and Olek [2] will be described in Chapter 5 and the previous work on mortar expansion by Iwatsuki [2] is discussed in Chapter 6.

2.1 REACTION MECHANISM

2.1.1 What is ASR ?

The Alkali-aggregate reaction (AAR) is the reaction between the alkali in pore solution of concrete and minerals of aggregates, under humidity condition. Most minerals in aggregate are siliceous and some carbonate materials. Thus, the deleterious reaction of AAR can be grouped as two [3-5]:

- Alkali-silica reaction (ASR) that aggregate contains form of silica reacts with alkali in pore solution to form ASR gel. This gel can absorb water to swell, causing the enough pressure to damage concrete.
- Alkali-carbonate reaction (ACR) is observed with certain dolomitic rocks. The breakdown of dolomite is related to expansion. The deterioration caused by ACR is similar to ASR.

A simplified description for ASR gel was summarized in two steps. The first is a rupture of the aggregate siloxane networks caused by the attack of hydroxide (OH^-) to produce alkali silicate and silicic acid (Eq. 2.1). This weak acid production of silicic immediately reacts with further hydroxyl ions, forming alkali silicate, so called alkali-silica gel (ASR gel), as shown in Eq. 2.2. Secondly, ASR gel causes expansion by the absorption of free water (Eq. 2.3). When the ASR gel is generated, it is diffused away from aggregate into pores, and then acts with calcium ions (Ca^{2+}) in the cement paste to form alkali-calcium-silicate hydrate gel. It is generally accepted that there are three conditions to induce ASR in concrete: the presence of reactive aggregate, a high level of alkalinity, and a sufficient moisture [6].

$$\equiv Si-O-Si\equiv +R^+ + OH^- \longrightarrow \equiv Si-O-R+H-O-Si\equiv \quad (2.1)$$

$$\equiv Si-O-H+R^+ + OH^- \longrightarrow \equiv Si-O-R+H_2O \quad (2.2)$$

$$\equiv Si-O-R \ + nH_2O \longrightarrow \equiv Si-O^- -(H_2O)_n + R^+ \quad (2.3)$$

where R^+ denotes an alkali ions such as sodium and Potassium ions (Na^+ and K^+)

n is assigned to the hydration number

2.1.2 The model description of ASR expansion

The expansion process of ASR according to Wang and Gillott [7] can be divided into 4 steps:

- Initial reaction on the silica grain
- The attack of hydroxide on silixane groups
- Ion exchange of Na^+, K^+ or Ca^{2+} for protons of silanol groups and the formation of swelling alkali-silica complex

- The ion exchange of Ca^{2+} for alkali ions in the alkali-silica complex and the formation of non-swelling alkali-silica-lime complex. This happens because Ca-O bond have a much higher electrostatic energy than $Na^{+}(K^{+})$-O.

In step 4, the presence of non-swelling alkali-silica-lime complex cannot produce a harmless but it would induce the release of alkali ions which are available for further reaction of swelling alkali-silica complex.

In case of the pressure to exert expansion, Hansen [8] proposed the theory that the expansion of ASR is due to the hydraulic pressure generated through the process of osmosis, in which it can generate depending a solution (aqueous sodium silicate), an external supply of solvent (water) and a semipermeable membrane (such as cement paste or mortar surrounding reactive site). The expansion may occurs after the products becomes plastic or fluid due to the alkali-silica complex imbibes water.

However, an important property governing the gel mobility or swelling is its viscosity. In 2006, Garcia et al. [9] revealed a damage mechanism for ASR by NMR investigation and distinguished the swelling curves of mortar into 4 steps (**Fig. 2.1**). The parameters Q_0, Q_3 and Q_4 are $H_2SiO_4^{2-}$, $SiO_{5/2}$ and $^{-}SiO_2$, respectively in any periods.

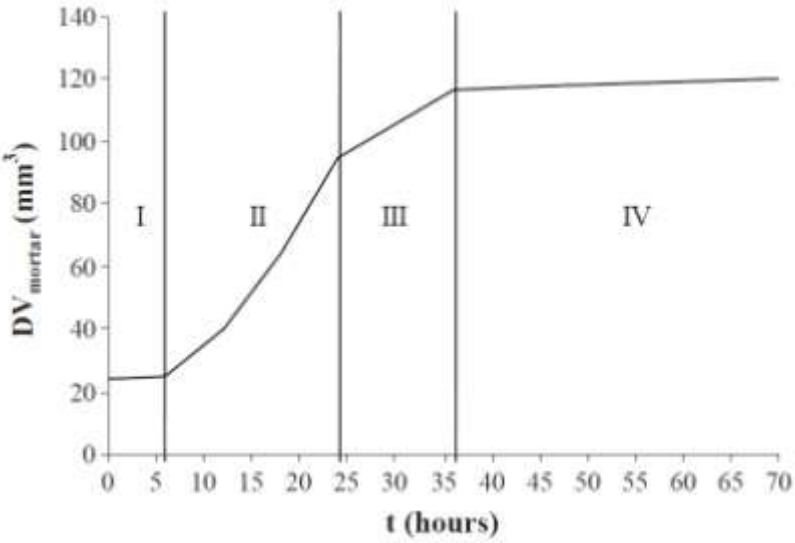

Fig. 2.1 Schematic subdivision of swelling curve

- Period I (first 6 h of autoclaving): the reaction is a dissolution precipitation process: the Q_0 tetrahedrons formed from Q_3 and Q_4 tetrahedrons dissolution react with calcium hydroxide and alkalis to form calcium silicate hydrate (C-S-H), calcium alkali silicate hydrate (C-Na-S-H or C-K-S-H). These products are called Q_0 products of ASR. The mortar bar does not swell during this period.
- Period II (between 6 h to 24 h of autoclaving): the formation of Q_0 products is slow down and stopped. A regular increase in Q_3 product occurs in the aggregate during this period. The transition Q_4 to Q_3 is expansive and is responsible for swelling and cracking phenomena in aggregate. The pore volume of the aggregate increase five fold. The aggregate swelling is amplified by cracking in the cement paste . A linear relationship between the mortar swelling and aggregate swelling.
- Period III (between 24 to 36 h of autoclaving): the swelling mechanism described above occurs, but the dissolution-precipitation process described in period I starts again: the Q_0 products fill part of the cracks generated by the swelling.

- Period IV (beyond 36 h of autoclaving): the swelling is asymptotic even though the reaction continues: the Q_0 and Q_3 products fill the cracks generated by the swelling. It is a period where the pore volume of the aggregate decreases because of the filling of the cracks.

Concerning the highly reactive aggregate, it is reported that ASR mostly exists at rim of reactive site. Refer to Ichikawa et al. [10], they found the development of dense and dark reaction rim that is generated by the reaction of alkali silicate and calcium ions, as shown in **Fig. 2.2**. Ultimately, they proposed mechanism of the ASR-induced deterioration of concrete according to following steps (see **Fig. 2.3**);

- OH^- and R^+ ions in the pore solution de-polymerize silica-rich aggregate to convert to fluid hydrated alkali silicate. The surface region of the aggregate is homogeneously covered with the alkali silicate. Consumption of OH^- ions by the reaction assists the dissolution of Ca^{2+} ions into the solution.
- The Ca^{2+} ions easily penetrate into the soft alkali silicate hydrated to re-polymerize the silicate. The aggregate is now tightly packed with a rigid reaction rim that allows the penetration of not alkali silicate but R^+ , Ca^{2+}, OH^- ions. The Ca^{2+} ions penetrate much slower that the R^+ ions.
- The OH^- and R^+ ions penetrate through the reaction rim to convert the fresh silicate into bulky alkali silicate. The resultant expansive pressure is stored in aggregate. The accumulated pressure cracks the aggregate and surrounding cement paste when the pressure exceeds the tolerance of the aggregate surrounded by the reaction rim and the cement paste.

This model claims that the ASR does not cause the deterioration, if the ASR is completed before the formation of ASR. This means that the use of fly ash and bottom ash do not induce the concrete deterioration due to ASR because their pozzolanic reaction can absorb alkali ions, and therefore reduce the concentration of OH^- and R^+ ions.

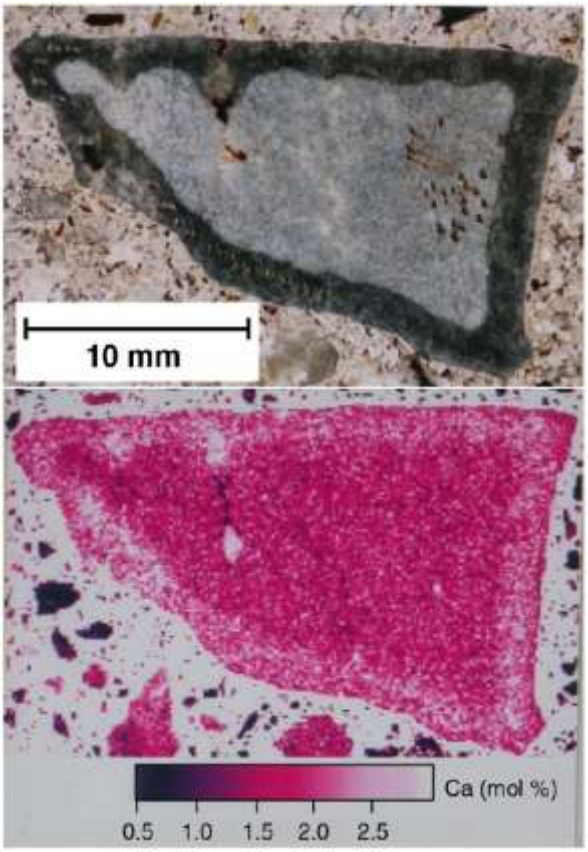

Fig. 2.2 Cross section (top) and it false color element mapping of calcium (bottom) for ASR-affected andesite.

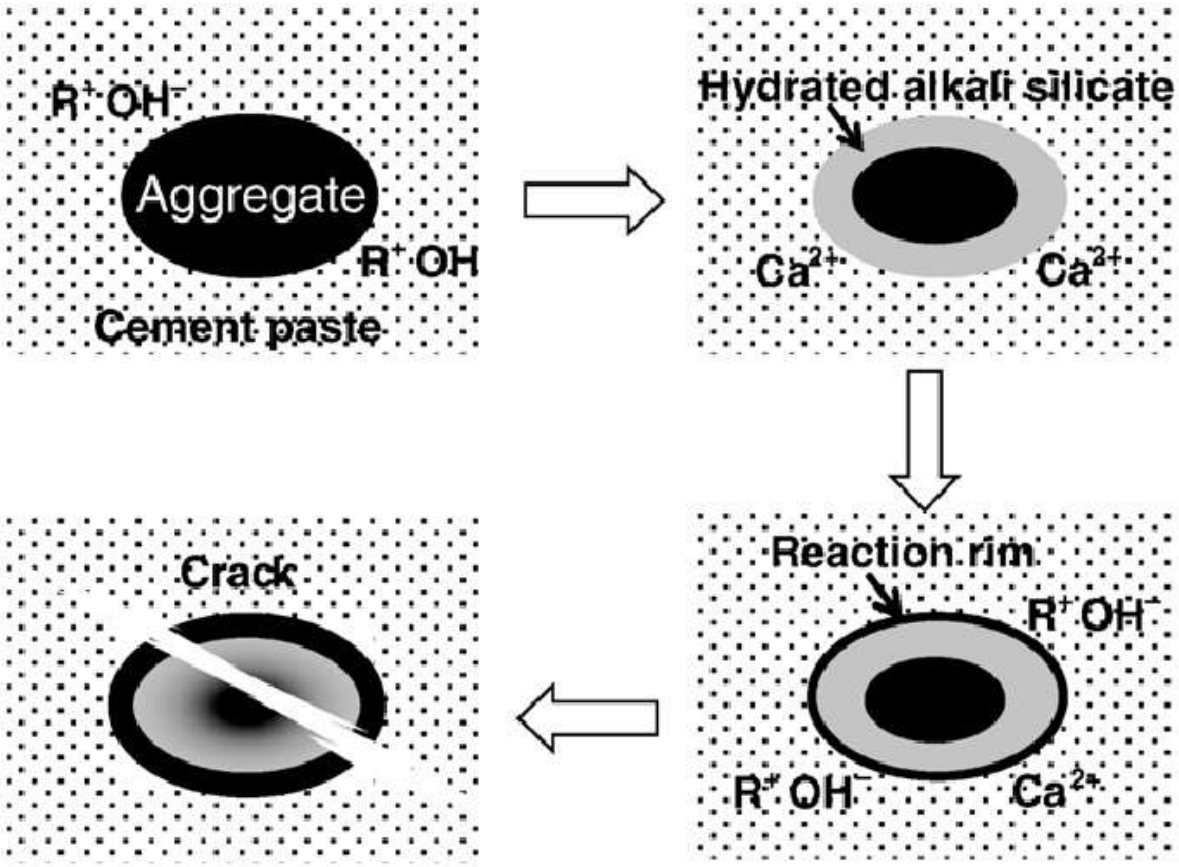

Fig. 2.3 Schematic representation of the mechanism of ASR-induced cracking of concrete

2.2 IDENTIFICATION OF ASR

2.2.1 Field evidence of ASR

A field survey is normally the first stage for identifying the possible presence of ASR. The visual signs attribute to the ASR symptom as follows:

- **Map-cracking pattern** is a matrix of fine cracks on the surface of concrete. **Fig. 2.4 (D)** shows the Map-cracking pattern of an exterior column of the power station investigated by [11]

- **Gel exudation through cracks** may occur for some period of time. This present gel is associated with the severe stress develops inside damaged structures. For example, Fernandes et al. [12] revealed the existence of efflorescence and exudations of ASR gel. They found the advanced cases of deterioration that may be translucent and moist or sticky (**Fig. 1.2**) which called efflorescence gel.

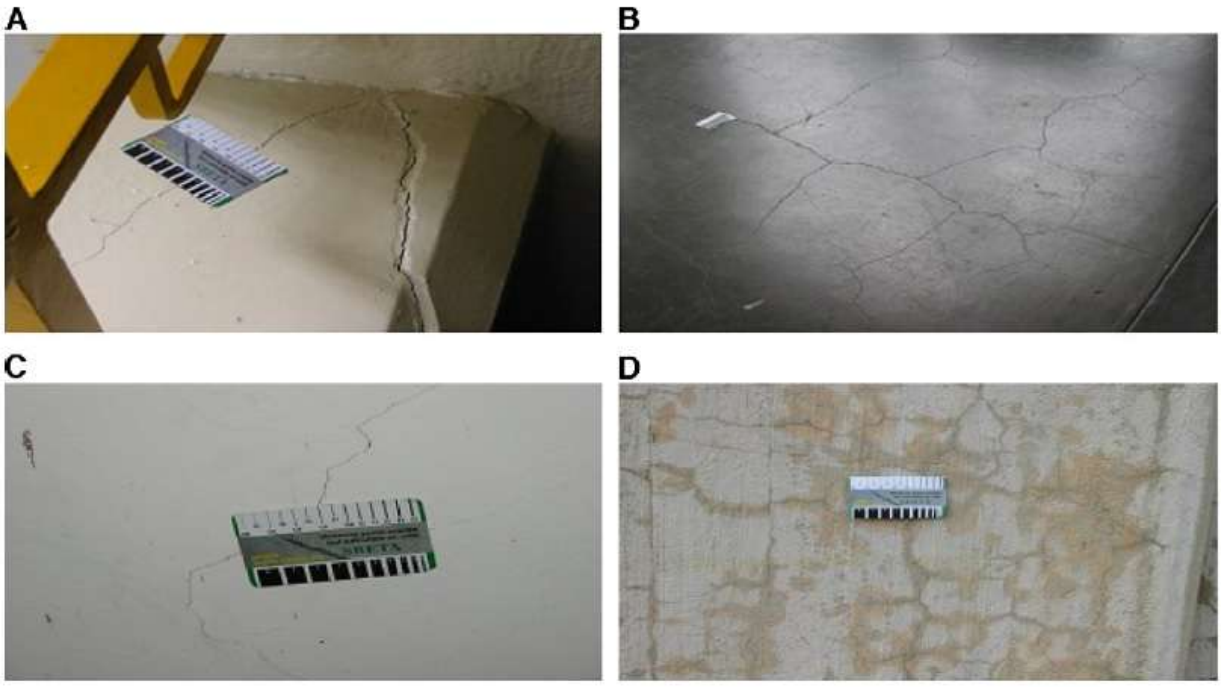

Fig. 2.4 (A) Cracking at the beam of the assembly bay. (B) Crack pattern in the second slab in front of the Roll-a-door of the assembly bay. (C) Cracking observed on the staircase wall on the floor below the assembly bay floor. (D) Map-cracking pattern of an exterior column of the power station. Similar cracking is also present on the exterior wall.

2.2.2 Microstructural evidence

Numerous methods is intended to show the microstructural evidence of the existence of ASR in deteriorated concrete. The common techniques are presented as follows.

- **Uranyl-acetate treatment under UV light**

Hollis et al. (2004) [13] provided technique that has been found useful in performing petrographic examinations of hardened concrete and its constituent materials. It introduced the investigation of ASR by uranyl-acetate treatment procedure. After applied uranyl-acetate solution to wet surface of specimens, ASR gel will be fluorescent under the short-wave UV light (**Fig. 2.5**). However, this technique still has limited use because not only ASR gel but also ettringite can be fluorescent under UV light.

- **SEM/EDX**

It is generally accepted that the ASR product increases in a volume with water absorption and exerts an expansive pressure inside the aggregate and paste, causing cracking and loss of strength of concrete. In recent years, researchers [11][12][14] have been observing the ASR products by SEM/EDX in order to confirm that deteriorated concretes were caused by ASR. The results revealed that ASR product is compose of main three elements (Si, Na/K and Ca), where various in Ca contents of gel deposit in different locations of cement matrix. **Figs 2.6-2.7** presents the crystalline ASR product and its EDX, showing high content of Si and K [11]. According to Fernandes (2009) [14], the gel is composed of silicon with variable amount of potassium, sodium and calcium. Especially for the different in location of

gel deposits, it was found that gel formed in cracked aggregate has low content of calcium (See **Fig. 2.8**), while the ASR gel with high intensities of Si and Ca existed around an aggregate particle (**Fig. 2.9**).

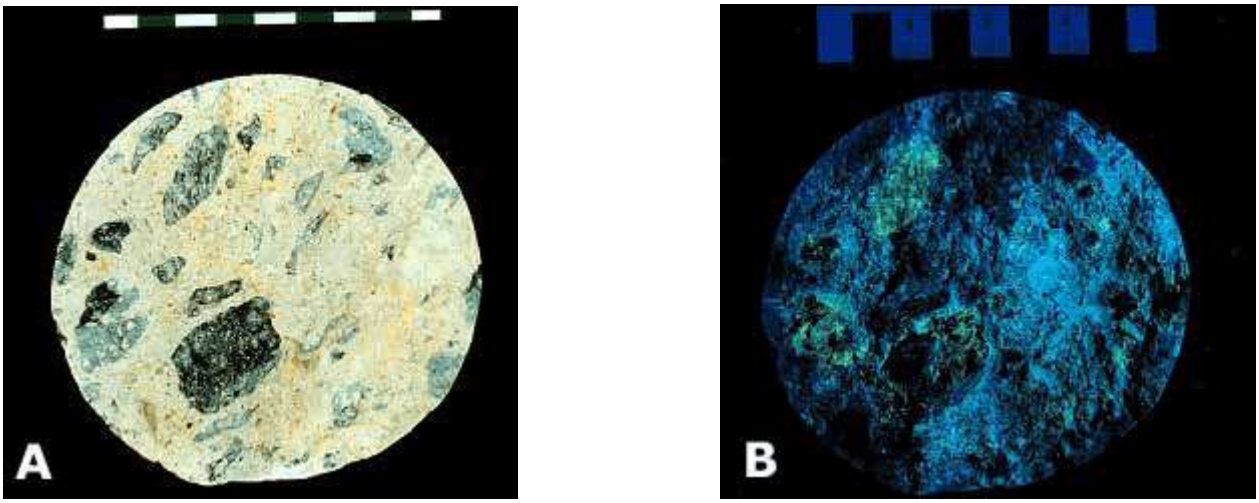

a) Concrete in the light

b) Concrete under UV-light, showing fluorescent ASR gel

Fig. 2.5 ASR gel investigation by uranyl-acetate treatment procedure

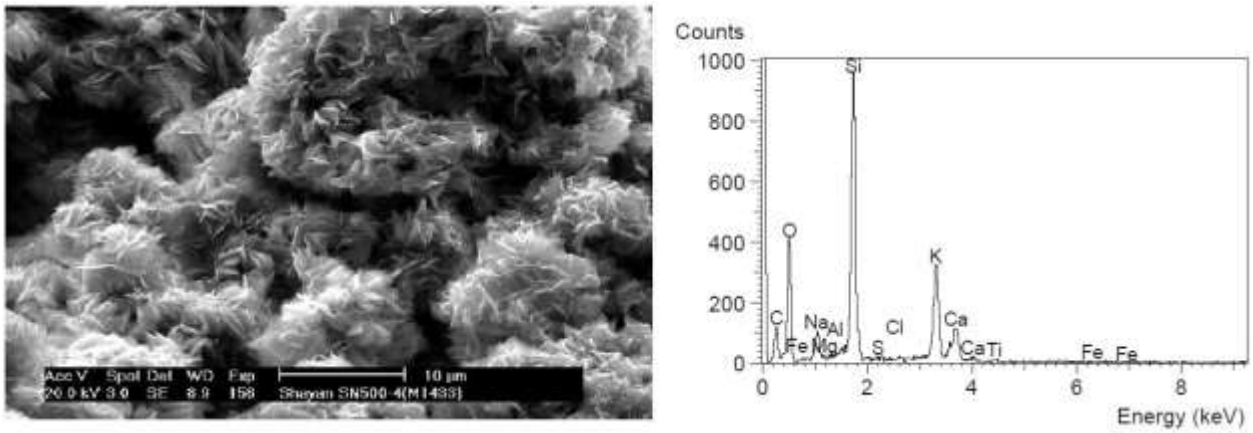

Fig. 2.6 Crystalline ASR product and its EDX composition

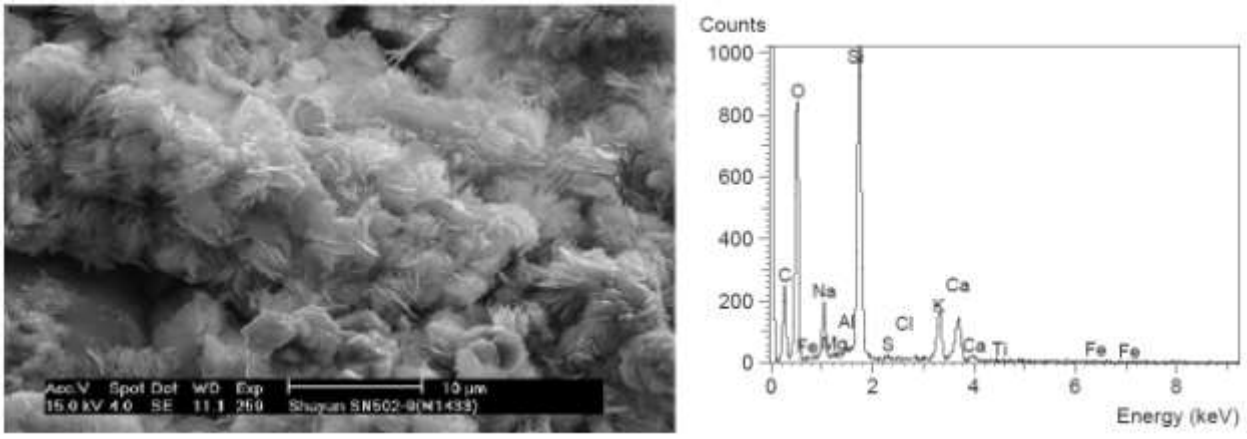

Fig. 2.7 Crystalline ASR product within aggregate and its EDX composition

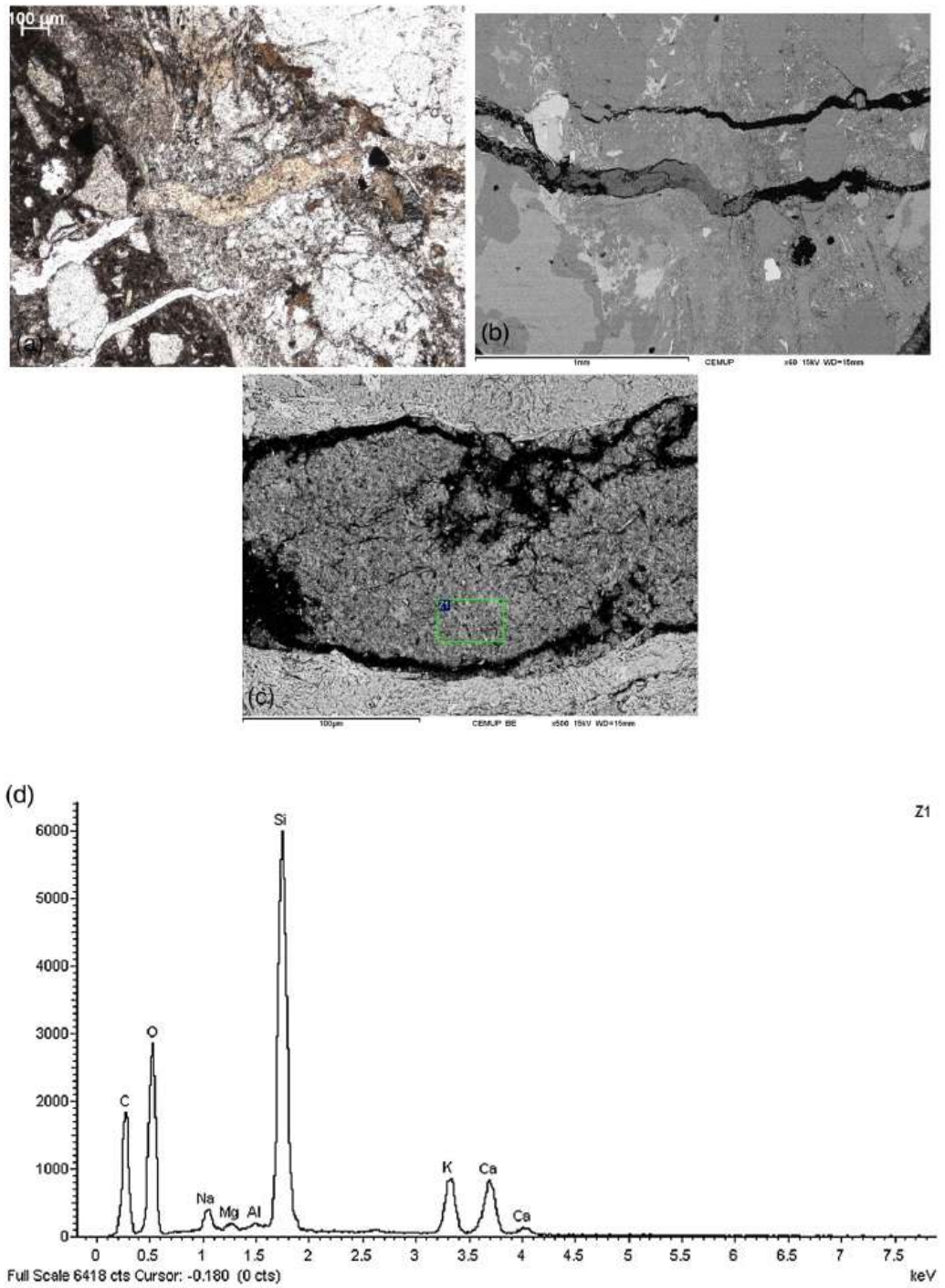

Fig. 2.8 Photomicrograph of a thin section of deteriorated structure (a) Gel partially filling cracks in the aggregate particle and extending to the cement paste, observed by polarizing microscope. (b-c) image of the same cracks by SEM (d) EDX at location Z1 in C

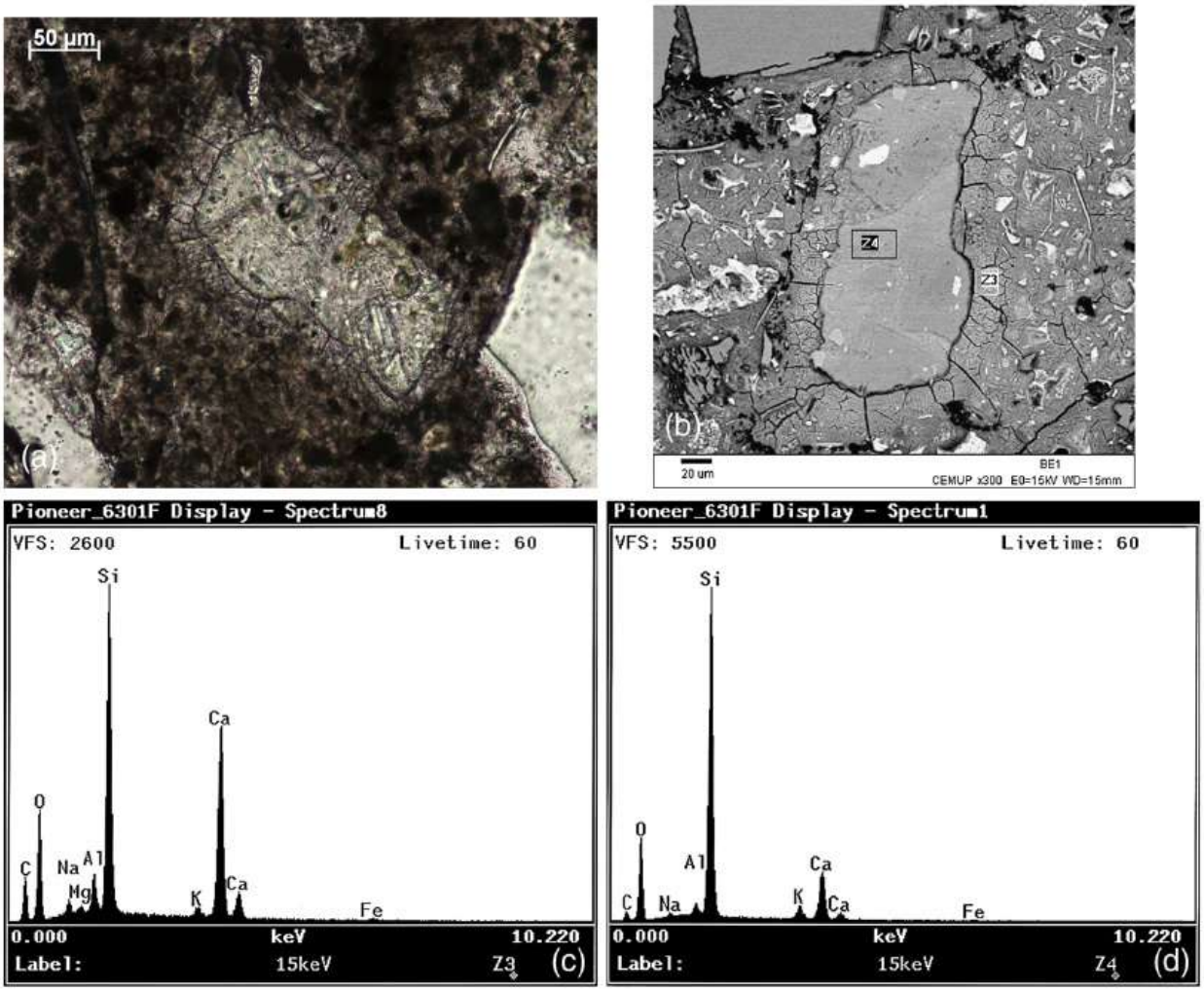

Fig. 2.9 Photomicrograph of a thin section of deteriorated structure: (a) Gel under polarizing microscope; (b) image of the thin-section under SEM; (c) EDS at Z3 in (b) obtain at interior rim; EDS at Z4 in (b) obtain in the interior of the reacted particle.

2.2.3 Locations of ASR and its compositions

The study of Katayama [15] confirmed the RC foundation of a PC structure has undergone combined ASR of late-expansive sedimentary rocks (sandstone, mudstone, chert) and early-expansive volcanic rocks (andesite, dacite, rhyolite) in the sand and gravel aggregates. **Figs. 2.10-2.11** shows ASR gel filling cracks within aggregates particle under polarizing microscopy and SEM, respectively. Regarding the migration of ASR gel along cracks from the reacted aggregate into cement paste, conversion occurs between alkali ions (Na,K) in the ASR gel and Ca ions in the cement paste, contributing the ASR gel in the crack present various compositions and its accompanying expansion. In **Fig. 2.12**, ASR gel on the [Ca/Si]-[Ca] / [Na+K] diagram was plotted. The chemical composition of ASR products, principally the calcium contents and the moisture, may link to the locations and volume of ASR formation on essential for damage to concrete. It was found that some existing ASR products with rich Ca content were in the cracks of cement paste or in the air voids.

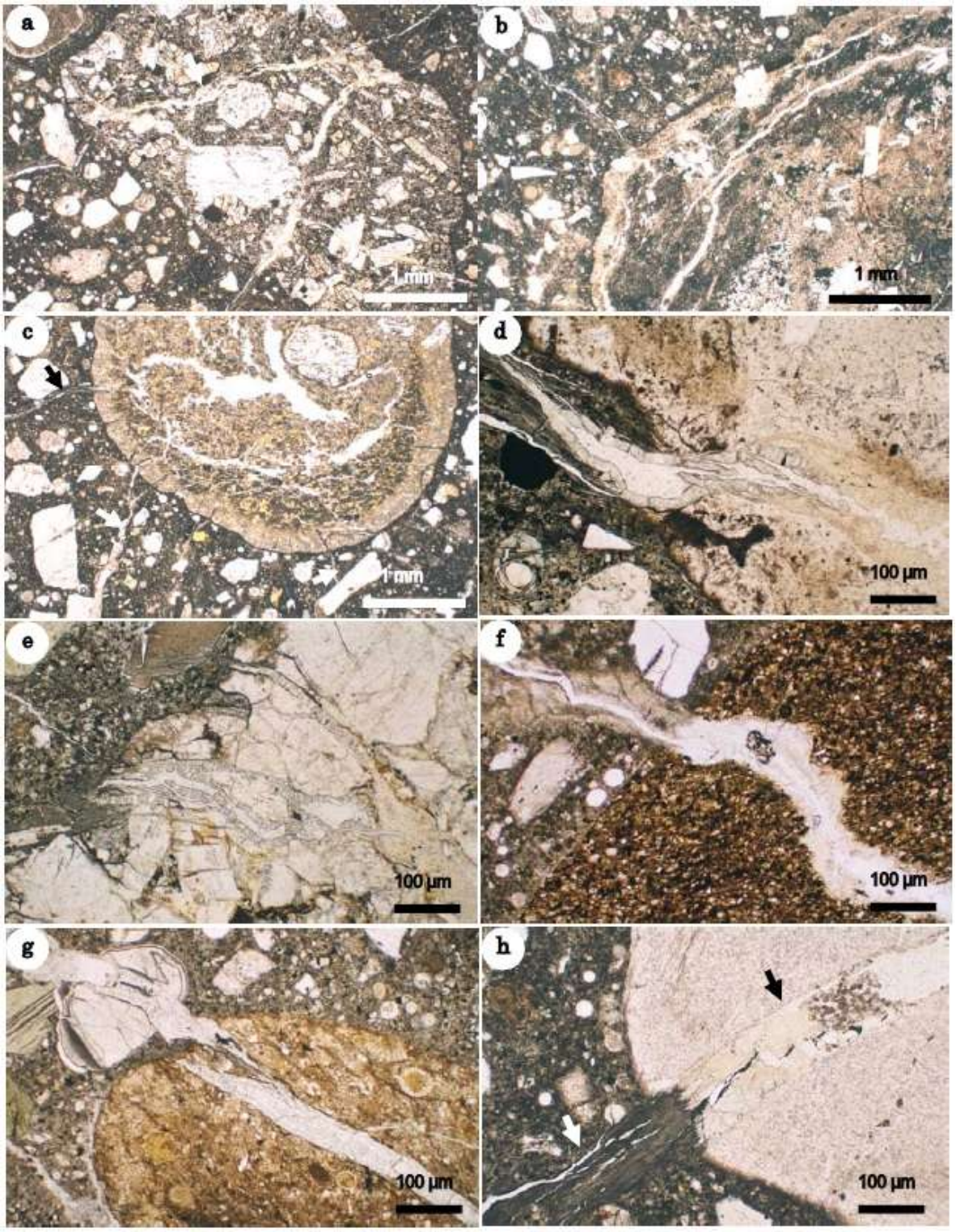

Fig. 2.10 ASR gel filling cracks within aggregate particles: a) Andesite in sand and b) dalcite in gravel c) Glassy rhyolite in the sand popping out with radial expansion cracks d) Silicified rhyolitic tuff e) sandstone and f) mudstone in gravel, forming a plugs of ASR gel within cracks at the aggregate-cement

paste interface g) Radiolarian siliceous mudstone precipitating ASR gel in the adjacent air void h) Chert in gravel forming a plug of ASR gel exuding into cement paste.

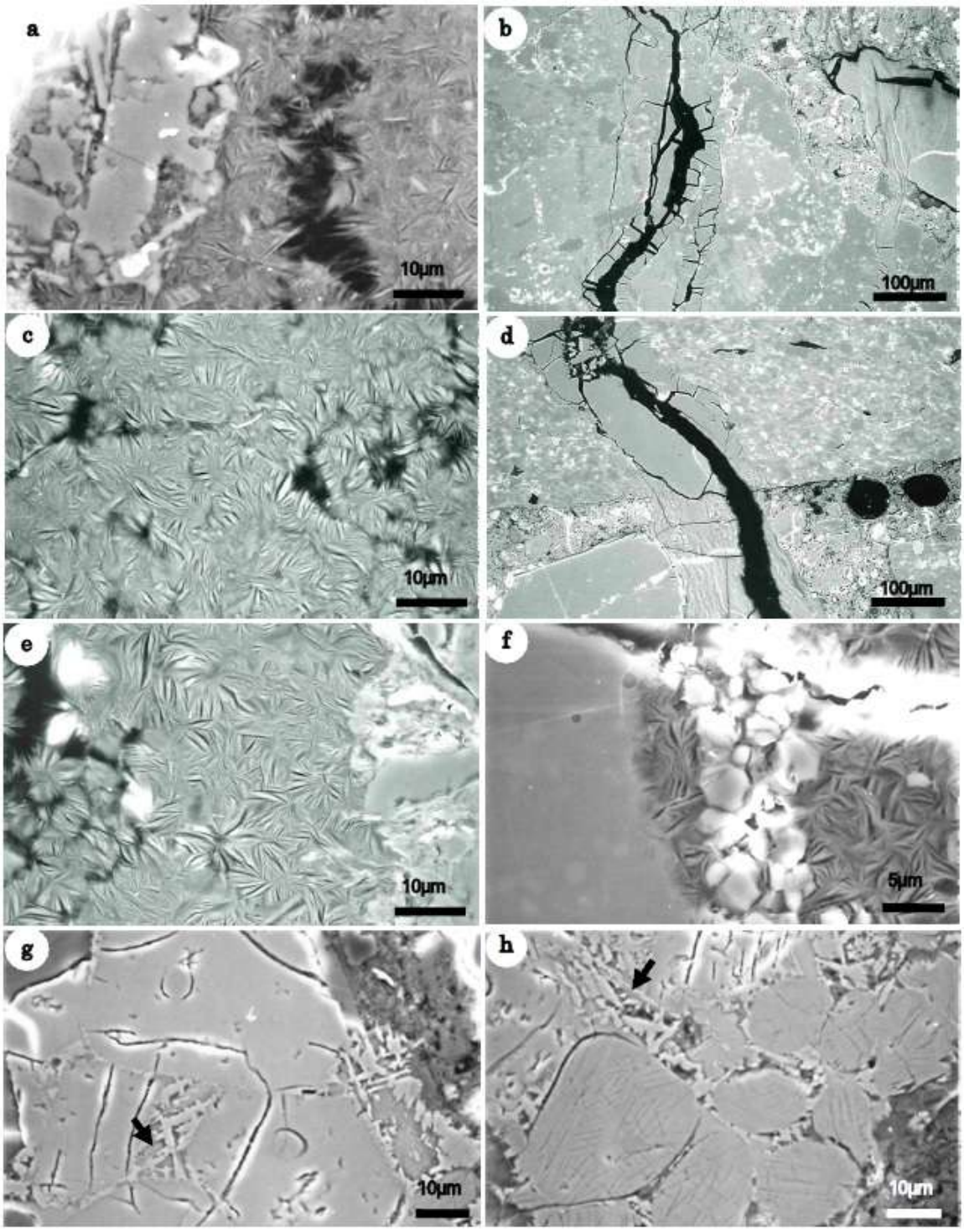

Fig. 2.11 a) Cristobalite particles in dacite converting to rosette crystals with fedorite to shlykovite composition. ASR products in sand stone: b) ASR gel and c) rosette crystals with fedorite composition. ASR product in mudstone d) ASR gel and e) rosette crystals with fedorite composition formed from

cryptocrystalline quartz f) Cryptocrystalline quartz in chert converting to ASR gel, now rosettes with mountainite composition Unhdrated cement particle rich in g) alite, and in h) belite, commonly associated with finegrained interstitial aluminate (dark) and ferrite

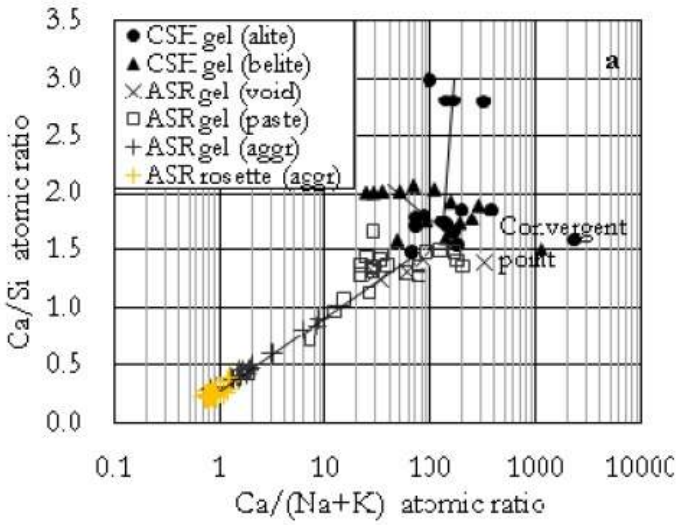

Fig. 2.12 Compositional trend of ASR products in reacted dalcite, sandstone, mudstone and chert in concrete

2.3 LABORATORY FORMATION OF ASR

Some previous research works [16-18] investigated the reaction between silica, alkali hydroxide and calcium hydroxide in order to clearly understand the effect of Ca ions on ASR formation. The investigation employed ICP, XRD and ^{29}Si-NMR to analyze the chemical components and structures of hydrated products.

For instance, the use of reactive opal in accelerated method of Hou et al. [16] showed the ASR development in mortar and concrete involves a reaction sequence of normal cement hydration (including the production of calcium hydroxide and Ca-rich, depolymerized C-S-H). The insoluble product was examined by XRD and ^{29}Si-NMR (**Fig. 2.13**). In XRD result of Opal+NaOH+$Ca(OH)_2$, the broad peaks at 7.15°2θ and 29.2°2θ initially appear and then increase in relative intensity. This indicated the formation of product like C-S-H. Parallel to the changes in ^{29}Si MAS NMR spectra presents substantial increase in the silicate polymerization of C-S-H (the conversion of Q^1 to Q^2 dominantly) as a reaction proceeds and the formation and subsequent transformation of Na-S-H gel due to the consumption of calcium hydroxide.

Similarly, the ^{29}Si-NMR result (See **Fig. 2.14**) of model system between microsilica, portlandite and highly alkaline solution was conducted by [17]. They revealed the major role of Ca in the type of products formed:

- Silica is dissolved by the alkaline solution until saturation is reached. When portlandite is present, it reacts with the dissolved silica forming C-S-H with a low Ca/Si ratio that contain alkalis (Q^1 presently). As a consequence, silica is removed from the solution enabling further silica dissolution. Because this process proceeds until portlandite is consumed, the amount of portlandite present determines how much silica can be dissolved.

- Silica dissolution starts with the formation of Q^3 sites and the ensuring formation of Q^1 and Q^2 sites in the presence of calcium. The Q^1 and Q^2 based calcium silicate structures are close to that of C-S-H.
- The total amount of Q^3 sites in the different samples is very similar but the amount of Q^1 and Q^2 sites increases with the increasing portlandite content. At the same time, the average Ca/Si ratio of reaction products is increasing.

It can be notice that the amount of chemically bound water in the reaction products decreases with the decreasing relative amount of Q^3 sites and increasing Ca/Si ratio.

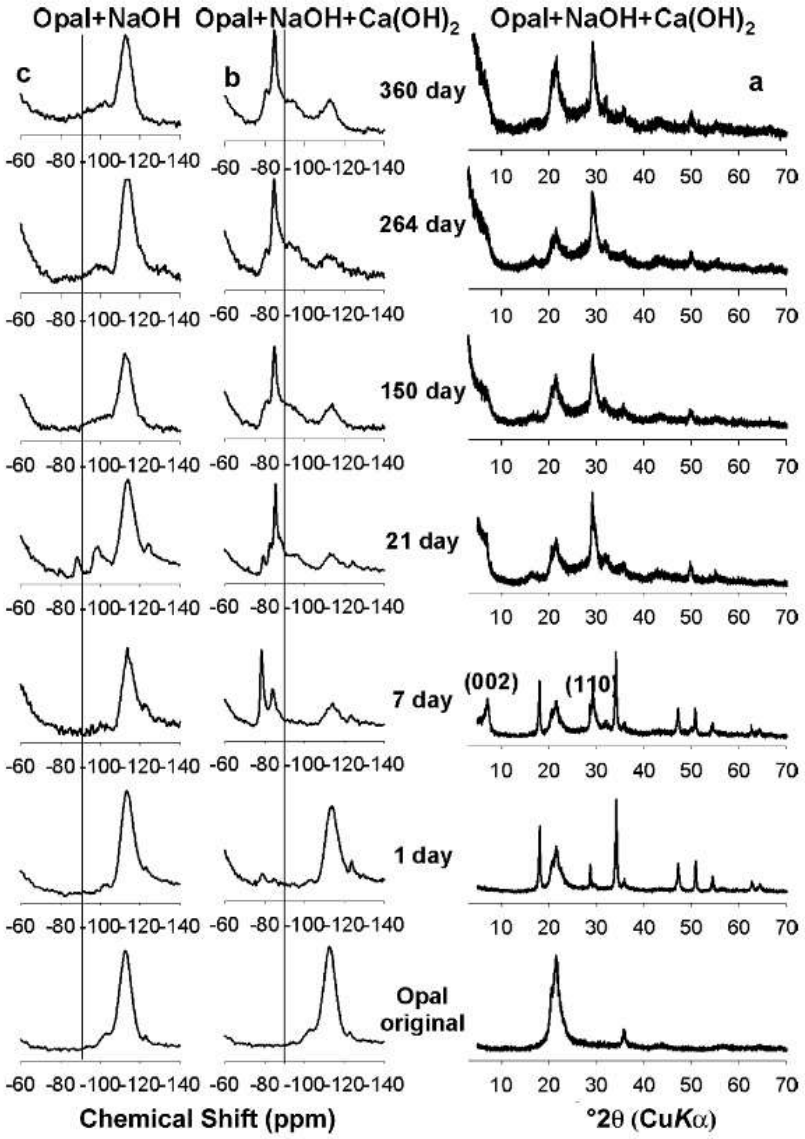

Fig. 2.13 (a) Powder XRD patterns of starting opal and selected reaction mixtures with $Ca(OH)_2$ and NaOH solution at the indicated reaction times (b) ^{29}Si MAS NMR spectra of starting opal and selected reaction mixtures with $Ca(OH)_2$ and NaOH solution at the indicated reaction times, and (c) ^{29}Si MAS NMR spectra of reaction mixtures of opal with NaOH solution at the indicated reaction times

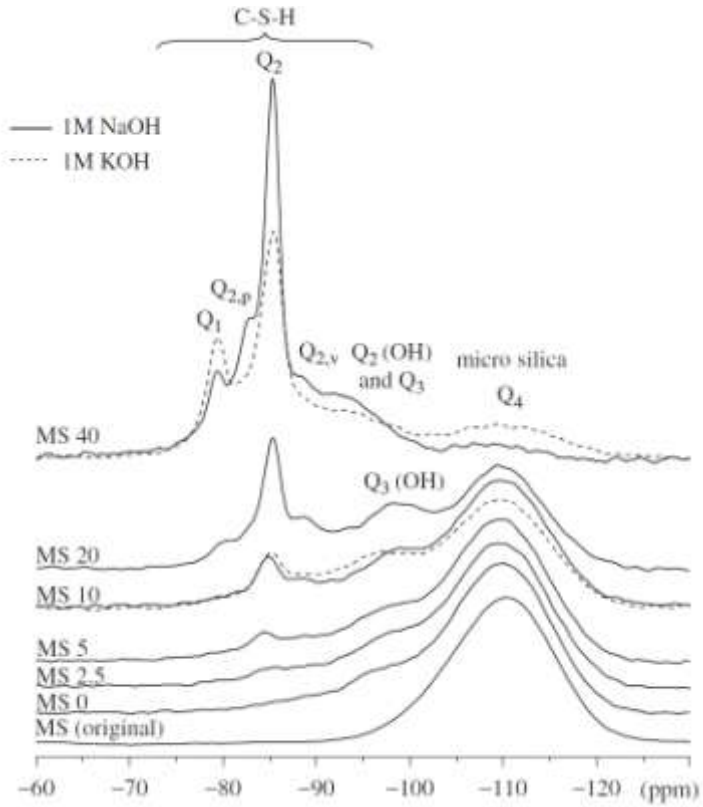

Fig. 2.14 ^{29}Si nuclear magnetic resonance spectra of MS with different portlandite contents after a reaction time of 96 h (MS0-MS10) and 144 h (MS20 and MS40) in 1M NaOH (plain lines) and KOH (dotted lines) "MS original" refers to the microsilica not exposed to alkaline solution.

2.4 REACTIVE MINERALS OF ASR

2.4.1 Reactive forms of silica in aggregates

Reactive aggregates exposed to a highly alkaline pore solution tend to break down, which creates silica. Subsequently, the reaction between alkali hydroxides and available silica occurs to produce ASR. According to a variety of minerals of the silica group, Ponce and Batic [19] categorized the ASR aggregates into 2 groups based on the evolution rate of the reaction as a consequence of the rock origin. The first is composed of vitreous or amorphous species; volcanic glass and opal. The second group of rocks includes crystalline rocks, like quartz, that show a slow or delayed reaction after many years. Similar to Islam et al.[20], they proposed the highlights two groups of rocks, and their main differences in the crystalline structure of mineral constituents (**Table 2.1**). The first set of rocks has a lack of minerals with crystalline structure, in which these rocks are in disorder. The rocks of this category are extremely reactive. The second group contains minerals with crystalline structure. The level of ASR of this group are mind to very. Moreover, Bulteel et al., 2002 [21] conducted the experiment on the basis of Arrhenius law with temperature dependence (**Fig. 2.15**) and reported that the E_a value of reactive flint aggregate is 78 kJ/mol in a range of size distribution 0.16-0.63 mm.

Table 1 Minerals and rocks that are potentially deleteriously reactive with alkali [20]

Category (1)	Alkali-reactive poorly crystalline or metastable silica minerals, and volcanic or artificial glasses (Classical alkali-silica reaction)
Reactants	Opal, Tridymite, Cristobalite, volcanic glasses, artificial glasses, beekite
Rocks	Opal such as shale, sandstones, silicified carbonate rocks, some cherts, flints, and diatomite Volcanic rocks such as rhyolites, dacites, latites, andecites, and their tuffs, perlites, obsidians, some basalts
Category (2)	Alkali-reactive quartz-bearing rocks
Reactants	Chalcedony, cryptocrystalline to microcrystalline quartz, quartz with deformed crystal lattice, rich in inclusions, intensively fractured or granulated, poorly crystalline quartz at grain boundaries, quartz cement overgrowths (in sandstones)
Rocks	Chert, flints, quartz vein, quartzites, quartz-arenites, quartzitic sandstones which contain microcrystalline to cryptocrystalline quartz and/or chalcedony Volcanic rocks such as that in category (1) but with devitrified, cryptocrystalline to microcrystalline groundmass Micro-granular to macro-granular silicate rocks of various origins which contain microcrystalline to cryptocrystalline quartz: a) Metamorphic rocks: gneisses, quartz-mica schists, quartzites, hornfelses, phyllites, argillites, slates; b) Igneous rocks: granites, granodiorites, charnockites; c) Sedimentary rocks: sandstones, greywackes, siltstones, shales, siliceous, limestones, arenites, arkoses; Sedimentary rocks (sandstones) with epitax

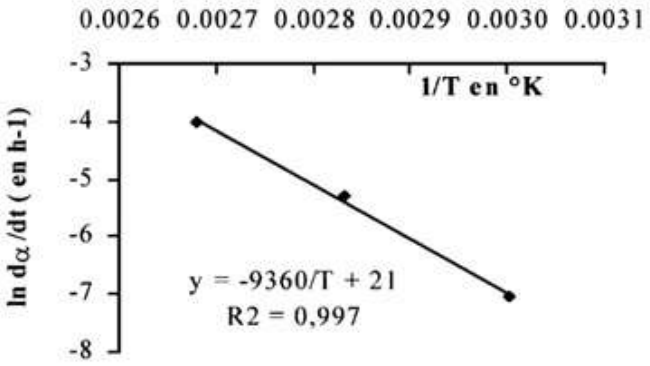

Fig. 2.15 ln(dα/dt) versus 1/T

2.4.2 American society for testing and materials (ASTM)

Concrete deterioration due to the ASR moderately takes place in a few years but is strongly aggressive. On the other hand, the accelerated test methods have become increasingly essential to be able to investigate ASR for a short time under the several conditions. Experiments have been carried out by accelerated test methods to estimate the potential reactivity of aggregates before their use in concrete in order to avoid later problems arising from ASR-affected structures [11][14] and there are investigations of the residual expansion of existing concrete structures damaged by ASR [22-24]. There are a number of

standards for evaluating ASR reactivity, for instance the ASTM codes, which include the C289, C294, C1260, and C1293 standards [25-28]. Concerning new concrete structures, Chatterji [29] suggested guidelines to be able to mitigate ASR problems and that these can be used to evaluate the quality of aggregate. The basic test methods include a direct evaluation of the aggregates, so-called the chemical reactivity test such as ASTM C289, and an indirect evaluations of aggregates, such as mortar bar test according to ASTM C277 [30]. The mortar bars test is the most commonly used for evaluating ASR reactivity of aggregate. For instance, accelerated mortar bars tested by ASTM C1260 were made and tested with mixtures of chert blended with limestone, to study the ASR behavior of chert from Turkey [31]. With ten sets of mortar bars, it was shown that there was a great deal of expansion that increased to maximum values at 5-15% chert content. It was concluded that with reactive aggregates like Turkey chert, the expansion does not increase steadily with increasing chert contents but that there is a maximum expansion at some content ratio after which the volume of expansion decreases. This phenomenon of Turkey chert [31] is termed pessimum behavior of siliceous aggregate.

2.4.3 The use of reactive glass

As an alternative, some researcher [32-35] began to use the water glass as a concrete aggregate (a low cost and environmentally friendly cementitious material) because they believed that the mixtures between the glass aggregate and the supplementary cementitious materials may significantly decrease the expansive ASR reaction. The three approaches used in industry to access ASR reactivity of aggregate are (i) petrographic analysis of aggregate (ii) direct expansion measurement of mortar and concrete made with test aggregates and (iii) chemical test. According to reference [35], they compared the relative ASR reactivity of various colors of recycled glass aggregates using the ASTM C227 and C1260 methodologies. In **Fig. 2.16**, the results show that with limited exception the ASTM C1260 method does not cause glass aggregate to react by the end of the prescribed test period. In contrast, the ASTM C227 method causes all glass aggregate to react within 2 weeks, despite the test being designed for 12 months or even longer if necessary.

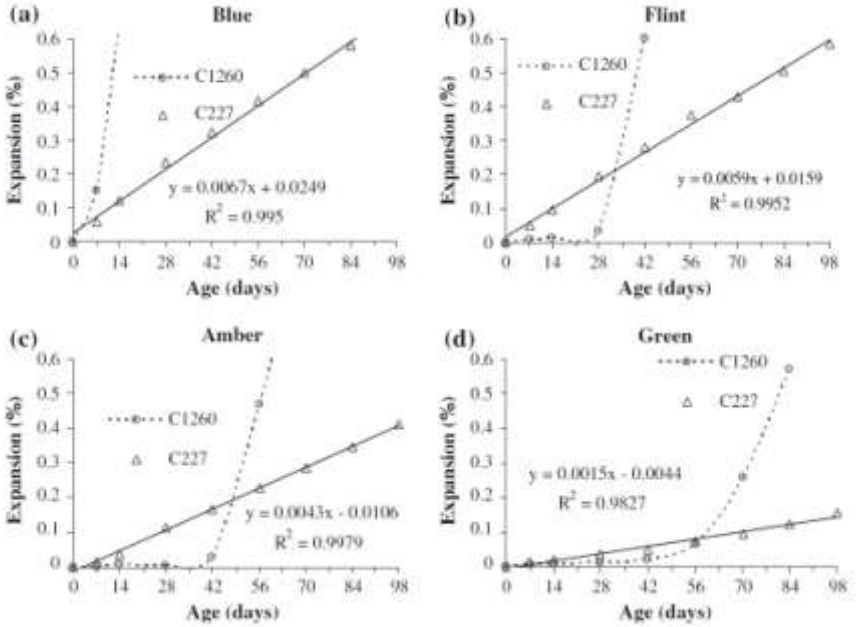

Fig. 2.16 Combination of ASTM C1260 and C227 results

REFERENCES

[1] T. Kim, J. Olek. Chemical Sequence and Kinetics of Alkali–Silica Reaction Part II. A Thermodynamic Model, J. Am. Ceram. Soc. 2014; 97(7) pp.2204–2212.

[2] E. Iwatsuki, K. Morino. Characteristics of alkali silica reaction of siliceous sedimentary rocks. JSMS 2008;57(10): 967-972.

[3] T.E. Stanton, Expansion of concrete through reaction between cement and aggregates, Proceedings of The American Society of Civil Eng, 1940.

[4] T. Katayama, A critical review of carbonate rock reactions-is their reactivity useful or harmful?, Proceedings of 9th International Conference on Alkali-Aggregate Reaction in Concrete, London, 1992, 508-518

[5] T. Mingshu, Classification of a alkali-aggregate reaction in concrete, Proceedings of 9th International Conference on Alkali-Aggregate Reaction in Concrete, London, 1992, 6348-6353

[6] J.W. Pan, Y.T. Feng, J.T. Wang, Q.C. Sun, C.H. Zhang, D.R.J. Owen (2012) Modeling of Alkali-Silica Reaction in Concrete: a Review, Front. Struct. Civ. Eng. 6(1), 1-18.

[7] H. Wang and J.E. Gillott (1991), MECHANISM OF ALKALI-SILICA REACTION AND THE SIGNIFICANT OF CALCIUM HYDROXIDE, Cement and Concrete Research. 21, 647-654

[8] W.C. Hansan (1944), "Studies Relating to the Mechanism by which the Alkali-Aggregate Reaction Produces Expansion in Concrete", ACI Journal, 40, 213-227.

[9] E.Garcia-Diaz, J.Riche, D.Bulteel and C. Vernet (2006), Mechanism of damage for the alkali-silica reaction, Cement and Concrete Research, 36, 395-400

[10] T. Ichikawa and M. Miura (2007), Modified model of alkali-silica reaction, Cement and Concrete Research, 37, 1291-1297.

[11] A. Shayan and J. Grimstad (2006), Deterioration of concrete in hydroelectric concrete gravity dam and its characterisation, Cement and Concrete Research, 36, 371-383

[12] I. Fernandes, F. Noronha, M. Teles (2004), Microscopic analysis of alkali-aggregate reaction products in a 50-year-old concrete, Materials Characterization, 53, 295-306

[13] N.W. Hollis, D.S Lane and P.E. Stutzman (2004), Petrographic Methods of Examining Hardened Concrete, A petrographic Manual Revised. Retrieved from March 10, 2013 http://nti.bts.gov/lib/2000/2500/2587/chapters/tbicont1.htm

[14] I. Fernandes (2009), Composition of alkali-silica reaction products at different locations within concrete structures, Material Characterization, 60, 655-668

[15] T. Katayama (2012), LATE-EXPANSIVE ASR IN A 30-YEAR OLD PC STRUCTURE IN EASTERN JAPAN, Proceedings of 14th ICAAR, Austin, Texas, USA.

[16] X. Hou, J.S. Leslie, R.J. Kirkpatrick (2004) "Formation of ASR and the C-S-H and Porlandite." *Cement and Concrete Research*, 34 (9), 1683-1696.

[17] Andreas L., Gwenn L.S., Frank W., Daniel R.and Barbara L. 2010; Alkali-Silica Reaction' the Influence of Calcium on Silica Dissolution and the Formation of Reaction Product. *American Ceramic Society*, 94(4), 1243-1249.

[18] T. Kim, J. Olek. Chemical sequence and kinetics of alkali-silica reaction part I Experiment. J Am Ceram Soc 2014; 97(7):2195-2203.

[19] J.M. Ponce, O.R. Batic (2006), "Different Manifestations of the Alkali-Silica Reaction in Concrete According to the Reaction Kinetics of the Reactive Aggregate." *Cement and Concrete Research*, 36, 1148-1156.

[20] M.S. Islam and S. Akhtar (2013), A Critical Assessment to the Performance of Alkali-Silica Reaction (ASR) in Concretem Canadians Chemical Transactions, 1 (4), 253-266

[21] D. Bulteel, E. Garcia-Diaz, C. Vernet, H. Zanni (2002) Alkali-silica Reaction A Method to Quantify the Reaction Degree. *Cement and Concrete Research*, 32, 1199-1206.

[22] D. Lu, L. Mei, Z. Xu, M. Tang, X. Mo, B. Fournier. Alteration of alkali reactive aggregates autoclaved in different alkali solutions and application to alkali–aggregate reaction in concrete: (I) Alteration of alkali reactive aggregates in alkali solutions. Cem Concr Res 2006;36(6):1176–1190.
[23] M. Kawamura, K. Iwahori. ASR gel composition and expansive pressure in mortars under restraint. Cem Concr Comp 2004;26(1): 47-56.
[24] Federal highway administration, Alkali-aggregate reactivity (AAR) workshops for engineers and practitioners. U.S. department of transportation 2012.
[25] Test method for potential alkali-silica reactivity of aggregates (chemical method). ASTM international 2007. Retrieved from http://www.astm.org/Standards/C289.htm.
[26] Test method for constituents of natural mineral aggregates. ASTM international. Retrieved from http://www.astm.org/Standards/C294.htm.
[27] Test method for potential alkali-silica reactivity of aggregates (mortar-bar method). ASTM international 2007. Retrieved from http://www.astm.org/Standards/C1260.htm.
[28] Test method for determination of length change of concrete due to alkali-silica reaction (concrete prisms test). ASTM international.
Retrieved from http://www.astm.org/Standards/C1293.htm.
[29] S. Chatterji. Chemistry of alkali-silica reaction and testing of aggregates. Cem Concr Res 2005;27(7):788-795.
[30] Test method for potential alkali reactivity of cement-aggregate combinations (mortar-bar method). ASTM international. Retrieved from http://www.astm.org/Standards/C277.htm.
[31] F. Bektas, T. Topal, M.C. Goncuoglu, L. Turanli. Evaluation of the alkali reactivity of cherts from Turkey. Constr Build Mater 2008;22:1183-1190
[32] E.A. Byars, B. Morales, H.Y. Zhu (2004), Waste Glass as Concrete Aggregate and Pozzolan-Laboratory and Industrial Projects. *Concrete,* 38 (1),41-44
[33] E.A. Byars, B. Morales, H.Y. Zhu (2003), Use of Waste Glass for Construction Products: Legislative and Technical Issues. *In proceedings of the international symposium on reclycling and reuse of waste materials*, Dundee, UK, 827-838.
[34] C. Meyer, Y. Xi (1999). Use of Recycled Glass and Fly Ash for Precast Concrete. Journal of Material Civil Engineering, 11:2(89), 89-90.
[35] H. Zhu, W. Chen, W. Zhou and E.A. Byars (2009), Expansion behavior of glass aggregates in different testing for alkali-silica reactivity, Material and Structures, 42, 485-494.

CHAPTER 3 MATERIALS AND EXPERIMENTS

We focus on four silica materials in this investigation. As reactive silica aggregates, two aggregates, Yoro-chert and Seto-chert aggregates were used. Both aggregates are composed of sedimentary rocks, which had be deposited in middle-paleozoic strata, produced from the Gifu Prefecture and Aichi Prefecture in Japan, respectively. Seto-chert aggregate includes some sandstone and slate except for chert. The values of reduction in alkalinity (R_c) and dissolved Si (S_c) of both cherts according to the JIS A1145 standard [1] are shown in **Table 3.1**. The results confirm that the cherts have the deleterious behavior of aggregates, as they are sedimentary rock composed of reactive minerals including chalcedony and cryptocrystalline quartz [2]. Pyrex glass (PG) produced by Iwaki Company and Silica sand (SS) was selected as highly reactive silica and non-reactive aggregate, respectively. **Table 3.2** presents the chemical compositions analyzed by XRF analysis. **Fig. 3.1** represents the outlines of this chapter.

Table 3.1 JIS A1145 results of the two chert aggregates here [1]

Chert	Prefectures	Minerals	Results of JIS A1145 (mmol/L)		S_c/R_c	Interpretation of chosen aggregates
			S_c	R_c		
Yo	Gifu	Chalcedony and Cryptocrystalline quartz	329	130	2.53	Deleterious
			391	88	4.44	
Se	Aichi	Chalcedony and Cryptocrystalline quartz	116	58	2.00	Deleterious
			316	128	2.47	

Table 3.2 Chemical compositions of materials by X-ray fluorescence

Oxides	Materials				
	PG	Yo	Se	SS	WPC
SiO_2	86.92	93.33	93.19	86.93	21.56
Al_2O_3	5.32	4.61	5.17	11.78	4.68
Fe_2O_3	0.21	0.65	0.34	0.06	2.98
CaO	-	0.10	0.09	-	65.63
MgO	1.02	0.71	0.54	-	1.3
Na_2O	5.07	0.10	0.07	-	0.33
K_2O	0.61	0.15	0.19	1.16	0.39
TiO_2	0.02	0.04	0.16	0.04	0.23
P_2O_5	0.73	0.25	0.25	-	0.27
MnO	-	0.05	0.01	-	0.14
SO_3	-	-	-	-	1.9
Density (g/cm^3)	-	-	-		3.16
Blaine (cm^2/g)	-	-	-		3310

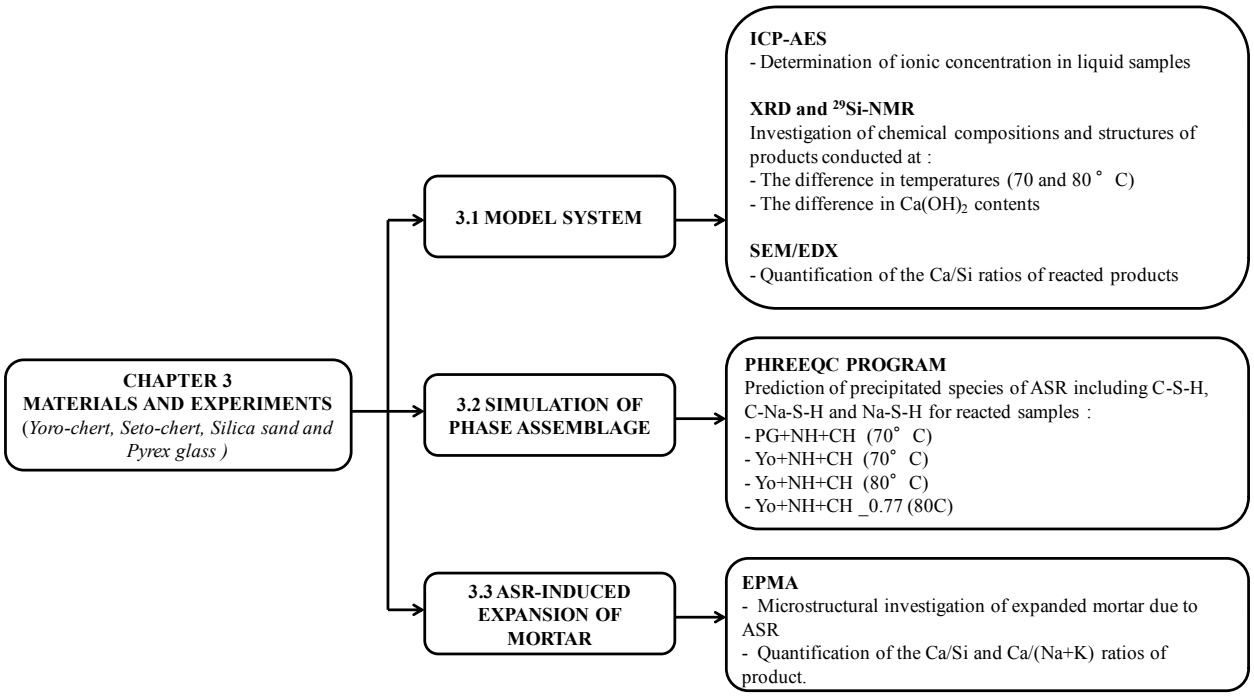

Fig. 3.1 Outline of chapter 3

3.1 MODEL SYSTEM

3.1.1 Sample preparation

The experimental procedure in a model system was adapted from previous work [3]. In a model system, the reaction of materials was observed using siliceous aggregates, portlandite (CH) and 1 M NaOH (NH). 1 M NH plays the role of the pore solution and CH acts as source for calcium in hardened mortar and concrete. The aggregates were primarily grounded and sieved to a range of particle sizes from 500 to 150 µm. When 1.54 g of CH was added, CH solid was mixed gently with the aggregate samples of 5.0 g. Then 1 M-NH solution was added to the samples in the aggregate/solution ratio of 0.25 and immediately mixed well for 3 h by magnetic stirrer. The samples were separated into several-30 mL polyethylene tubes and placed in an oven at high temperatures (60, 70 and 80°C) to accelerate reactions. The reaction was stopped at 24, 72, 120, 168, 240, 336, 480 and 576 h for the mixtures with 1 M-NH by filtration through a 0.45-µm filter and washing the solid with acetone to stop the reactions. In case of rapidly reactive glass, the reaction was shorten to stop at 3, 7, 14, 24, 72, 120 and 168 h for PG mixtures. Solids were placed in an oven at 40 °C until they were dehydrated.

In an attempt to seek the effect of Ca on ASR formation, the fine chert (a range of particle sizes from 300 to 150 µm) of 5.0 g was also mixed with small amounts of CH solid of 0.77 and 0.385 g. For the sake of simplicity, only the Yo-chert was selected (Yo+NH+CH_0.77 and Yo+NH+CH_0.385). By doing these mixtures, we were able to simulate the reaction environment that CH was almost consumed. After being placed in the oven at 80°C for 14 days, the samples were kept as the same method as mentioned previously.

3.1.2 Ionic concentration in liquid samples determined by ICP-AES analysis

All samples were filtrated by 0.45 μm filter at 24, 72, 120, 168, 240, 336, 480 and 576 h for Se, Yo and SS, and at 3, 7, 14, 24, 72, 120 and 168 h for PG and washing the solid with acetone solution to stop the reactions. Liquid samples were diluted to the range from 10 ppb to 10 ppm of the Si concentration and then the dissolved Si content in the liquid samples was quantified by ICP-AES. The activation energy (E_a) of soluble silica from each material can be calculated on the basis of Arrhenius equation. **Table 3.3** presents test samples and exposures parameters used in this part

3.1.3 Identification of insoluble product

The chemical compositions and structures of hydrated products under 70 and 80°C was investigated by XRD ^{29}Si-NMR and SEM/EDX. The summary information regarding the test samples and exposure parameters used in this model for 70 and 80°C is listed in **Table 3.4 and Table 3.5**, respectively.

- **XRD**

The fine powders for the XRD showed the compositions and phases of the samples. A rigaku X-Ray diffractometer was used with CuK_α radiation at a scanning rate of 1°2θ per min, and a step size of 0.02°2θ the ranging from 5 to 70°2θ in the XRD analysis. In addition to the quantitative phase analysis by XRD, the Siroquant-Rietveld program was used to quantify the phases generated in the reacted solids under 80°C. The quantitative phase analysis by XRD is abbreviated as Q-XRD used in this paper. Based on the Q-XRD combined with the weight loss on ignition measurements, the weight of the ASR, like C-S-H product, in percentage can be changed to mass in the unit of grams (g). Loss on ignition was conducted by heating reacted solids to 950°C for 2 hours, and the weight loss of the solids due to heating was calculated. Before heating the solids to 950°C, they were placed in an oven at 105°C to eliminate the moisture content. **Table 3.6** provides the weight loss of solids at 105 and 950°C for ignition loss calculation. Loss on ignition is calculated by using Eq. (3.1).

$$H_x = \left(\frac{W_{105°C} - W_{950°C}}{W_{105°C}} \right) \times 100 \qquad (3.1)$$

where H_x is the percentage of total water in C-S-H calculated from the loss on ignition
$W_{105°C}$ is the weight of solids at 105°C in gram, g
$W_{950°C}$ is the weight of solids at 950°C in gram, g

- **^{29}Si-NMR**

The ^{29}Si-NMR was executed and recorded from a MSL 400 9.4 T BRUKER operating with frequencies of 79.486 MHz for ^{29}Si at room temperature to show the structure of produced ASR in the solids. The conditions were as follows: a 90° pulse length of 5 μs with ^{29}Si recycling delay of 60 seconds and 480 scans for Se, Yo and SS, and 30 seconds and 1920 scans for PG. The Q_8M_8 ($Si(CH_3)8Si_8O_2$) at 12.4 ppm was used as an external standard for the ^{29}Si-NMR chemical shifts. The NMR data were transferred to a PC and further explored by NUTS [4]. The data were manually phased and baseline corrected.

- **SEM/EDX**

Furthermore, a change in micro-texture of quartz before and after reaction was observed by SEM. Before tested with accelerated condition, Yo-chert was gentle mixed with CH solid, represented by Yo+CH. To estimate the Ca/Si ratio of generated ASR product, the observation by SEM/EDX was made on both

Yo+NH+CH and Se+NH+CH at 14 days of reaction. For SEM/EDX analysis, the powder samples were coated with Platinum (Pt). The SEM model Superscan SSX-550 combined system with EDX was conducted at room temperature using the accelerating voltage at 15.0 kV for SEM and 20.0 kV for EDX analysis.

Table 3.3 Test samples and exposures parameters used in liquid sample of model experiment at different temperatures

Reacted samples	**1M-NH solution, mL**	**CH solid, g**	**The total mass ratios (aggregate : CH solid)**	**Exposure conditions**
PG+NH	20			60,70 and 80°C
PG+NH+CH	20	1.54	0.77: 0.23	
Yo+NH	20	-	-	60,70 and 80°C
Se+NH	20	-	-	
Yo+NH+CH	20	1.54	0.77: 0.23	60,70 and 80°C
Se+NH+CH	20	1.54	0.77: 0.23	
SS+NH	20	-	-	60,70 and 80°C

Table 3.4 Test samples and exposure parameters used in model experiment under temperature of 70°C and solid measurements

Reacted samples	**1M-NH solution, mL**	**CH solid, g**	**The total mass ratios (aggregate : CH solid)**	**Measurements of the solid samples**
PG+NH (70°C)	20			XRD, ^{29}Si-NMR
PG+NH+CH (70°C)	20	1.54	0.77: 0.23	
Yo+NH (70°C)	20	-	-	XRD, ^{29}Si-NMR
Yo+NH+CH (70°C)	20	1.54	0.77: 0.23	

Table 3.5 Test samples and exposure parameters used in model experiment under temperature of 80°C and solid measurements

Reacted samples	**1M-NH solution, mL**	**CH solid, g**	**The total mass ratios (aggregate : CH solid)**	**Measurements of the solid samples**
Yo+CH (No reaction)	-	20	0.77:0.23	SEM
Yo+NH	20	-	-	XRD, ^{29}Si-NMR
Se+NH	20	-	-	
Yo+NH+CH	20	1.54	0.77: 0.23	XRD, ^{29}Si-NMR , SEM/EDX
Se+NH+CH	20	1.54	0.77: 0.23	
Yo+NH+CH_0.77	20	0.77	0.87: 0.13	XRD, ^{29}Si-NMR
Yo+NH+CH_0.385	20	0.385	0.93: 0.07	

Note: Each sample was prepared by placing a fine aggregate of Yo- or Se- chert of 5.0 g.; Yo+CH represents the pure aggregate before reaction, providing for SEM observation.

Table 3.6 The weight loss of solids at 105 and 950°C for ignition loss calculation

Reacted samples	Reaction time, day	$W_{105°C}$, g	$W_{950°C}$, g
Yo+NH+CH (80°C)	1	0.9760	0.8810
	3	0.9750	0.8815
	5	0.9787	0.9142
	7	0.9722	0.8756
	10	0.9648	0.8666
	14	0.9761	0.8995
Se+NH+CH (80°C)	1	0.9871	0.9123
	3	0.9772	0.8998
	5	0.9775	0.8890
	7	0.9752	0.8919
	10	0.9720	0.8757
	14	0.9784	0.8848
Yo+NH+CH (70°C)	3	0.9836	0.8866
	7	0.9889	0.9004
	10	1.0026	0.9004
	14	0.9983	0.9151
	20	0.9938	0.8856
	24	0.9914	0.8838

3.2 SIMULATION OF PHASE ASSEMBLAGE

The PHREEQC [5-6] is used for calculations of hydrogeochemistry and is a useful tool for modeling data. The results of geochemical evaluations depend on factors like the quality of the input data and the sequence of the calculations. For the simulations, the phase-equilibrium were built in the program and the input data were followed by ion concentrations to determine the ion activities and the relevant states for the involved minerals to precipitate as ASR product, including tobermorite type C-S-H, in this investigation. ASR phase is defined by chemical reactions, an equilibrium constant. These thermodynamic properties are used in this paper (**Table 3.7**) as reported in the BRGM database, Thermoddem [7-8] and the equilibrium constants of the solids at 70 and 80°C estimated by T. Kim et al [9]. The basic equations (Eqs. (3.2) and (3.3)) of the phase-equilibrium model used are shown as below [10];

The mass-action equations in PHREEQC is given by

$$K_p = \Pi_i (\gamma_i c_i)^{n_{i,p}} \tag{3.2}$$

where K_p is the thermodynamic equilibrium constant for the phase *p* [-]
γ_i is the activity coefficient of ion *i* [-]
c_i is the concentration of ion *i* in mol
ni,p is the stoichiometric coefficient of ion *i* in the phase *p* [-]

The extended Debye-Huckel activity model

$$\log \gamma_i = -\frac{A z_i^2 \sqrt{I}}{1 + B a_i \sqrt{I}} + b_i I \tag{3.3}$$

where A[-] and B [-] are the temperature-dependent coefficients
a_i and b_i are the ion-specific fitting parameters.

Table 3.7
Thermodynamic data for the simulations [11]

Name	Formula	log K (70°C)	log K (80°C)
Amorphous silica	SiO_2	-2.929	-2.710
Portlandite	$Ca(OH)_2$	19.960	22.810
C-S-H_0.83	$Ca_5SiO_6H_{21}O_{27.5}$	58.219	57.046
C-S-H_1.66	$(CaO)1.667(SiO_2)2.1H_2O$	28.63	-
C-Na-S-H	$Na_2Ca_4Si_6H_{21}O_{27.5}$	63.119	62.115
Na-S-H	$NaHSi_2O_53H_2O$	4.5157	4.539
Basis solution			
Water (kg)		0.98	
Concentration of Na (mmol/L)		1000	

3.3 ASR-INDUCE EXPANSION OF MORTAR

3.3.1 Preparation of mortar-bar

Pyrex glass (PG) and silica sand (SS) were crushed to the obtain particle sizes specified in ASTM C227 [11] except for the size of the mortar bar, as detailed in **Table 3.8**. A white Portland cement with an equivalent Na_2O content of 3.94 kg/m^3 (0.6%) was used for the mixture of mortar bar test. The alkali contents (equivalent Na_2O) in the mortar were adjusted to 7.27 kg of alkali per m^3 (1.2%) for PG and SS by adding NaOH in the mixing water. The mortars were prepared in prismatic specimens of 2.8x2.8x18.0 cm for PG and SS. The water-cement (w/c) ratio of the mortar was 0.50 and the sand to cement ratio 2.25. After demolding, the mortar prisms were kept in a sealed container at 40°C. At each measurement (at 7, 14, 21, 28 56 and 91 days), the sizes of the mortars were determined using a length comparator with the scale millimeter method. **Fig. 3.2** presents the procedure of ASTM C227.

Table 3.8

Sieve Size		Mass (%)
Passing	Retained on	
4.75mm (No.4)	2.36mm (No.8)	10
2.36mm (No.8)	1.18mm (No.16)	25
1.18mm (No.16)	0.60 mm (No.30)	25
0.60 mm (No.30)	0.30 mm (No.50)	25
0.30 mm (No.50)	0.15 mm (No.100)	15

Fig. 3.2 The procedure of ASTM C227

3.3.2 The relation of ASR gel formation to expansion of mortar: using the Elakneswaran' s model with PHREEQC

In Elaneswaran's model [12], the chemical thermodynamic calculations were carried out to predict the solid-phase assemblages and pore solution composition of hydrating Portland cement and slag as a function of hydration time. In present work, the integrated model that combined PHREEQC with empirical expression for dissolution of clinker minerals and reaction degree of reactive materials was developed. As illustrated in **Fig. 3.3**, the parameters such as mix proportion and detail of cement composition were input in model. To simulate the ASR formation of PG100 and Yo100 mortars, the rate of silica dissolution at 40°C was selected to be the degree of reaction compared between Yo-chert and Pyrex glass instead of the slag reaction degree in here. **Table 3.9** shows the equilibrium phases of solids precipitation.

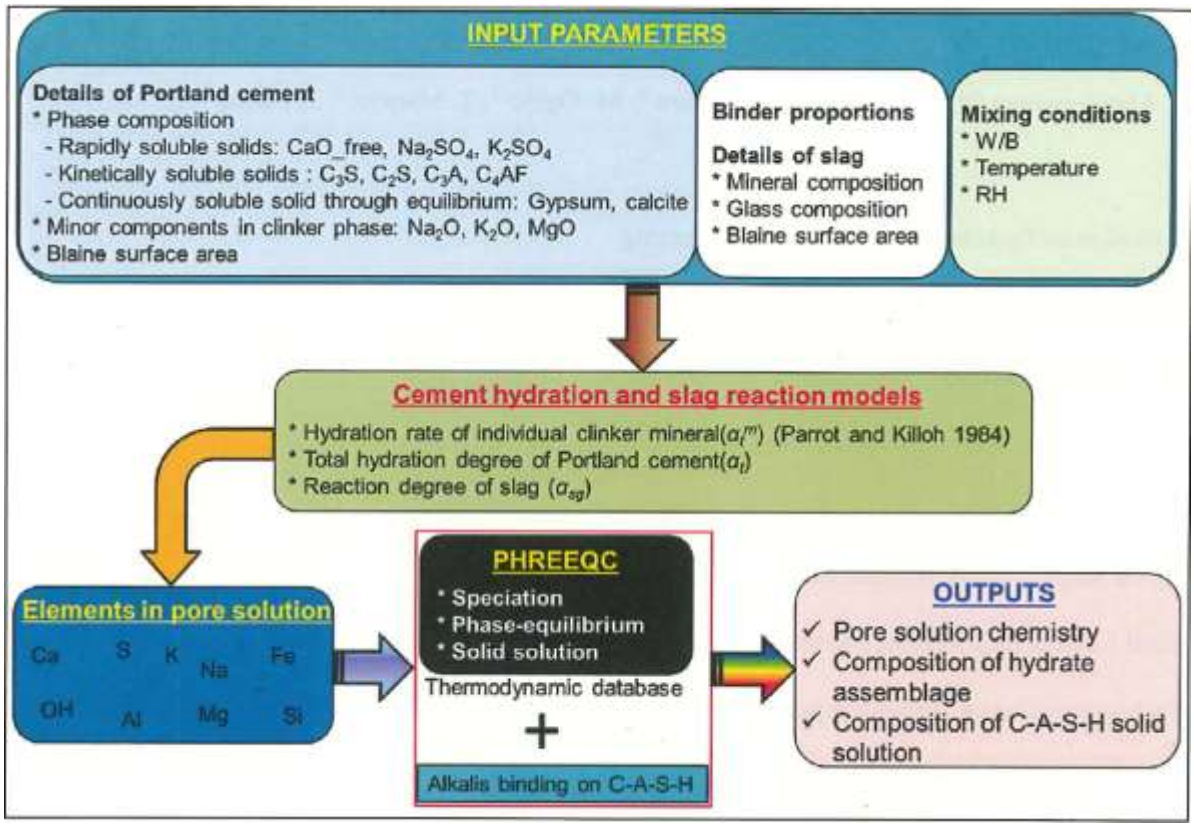

Fig. 3.3 The outline of Elaneswaran's model

Table 3.9 Thermodynamic properties of phases at 25℃ used in calculation

Name	Formula	log K	ΔH
C-S-H_1.0	$(CaO)_{1.25}(SiO_2)_{1.25}$ $2.5H_2O$	18.74	-83.46
C-S-H_1.66	$(CaO)_{1.667}(SiO_2)_{2.1}H_2O$	29.60	-148.44
C-Na-S-H	$CaO_{1.0}(Na_2O)_{0.3125}(SiO_2)_{1.5}1.1875(H_2O)$	19.236	-101.2075
Na-S-H	$NaHSi_2O_5 3H_2O$	4.5157	4.539
Basis solution			
Water (kg)		0.98	
Concentration of Na (mmol/L)		1000	

3.3.3 EPMA analysis of mortar-bar

In microstructure examination, the EPMA was chosen to perform on our mortar prisms. With EPMA analysis, the Ca/Si ratio of ASR product can be identified. The mortars of SS100 and PG100 with 1.2% alkali were selected and cut into a small size of 1.0x1.0 cm. Samples were arranged in the mold and then molded with Specifix-20 resin. After demolding, the samples were placed in an oven at 40°C for 3 days. **Fig. 3.4** shows the sample preparation provided for EPMA analysis. Especially for high magnification, the samples were polished with sand paper and diamond slurry to be a smooth surface and then coated with carbon. Field Emission Probe Micro Analysis, EPMA with a model of JXA-8530F (JEOL manufacture, Japan), was conducted with an acceleration voltage of 15.0 kV [13].

Fig. 3.4 Sample preparation for EPMA

REFERENCES

[1] Method of test for alkali-silica reactivity of aggregates by chemical method (JIS A1145). Japan Concrete Institute (JCI) 2007.

[2] E. Iwatsuki, K. Morino (2008). Characteristics of alkali silica reaction of siliceous sedimentary rocks. *Society of Materials Science Japan*, 57(10): 967-972.

[3] X. Hou, J.S. Leslie, R.J. Kirkpatrick (2004) "Formation of ASR and the C-S-H and Porlandite." *Cement and Concrete Research*, 34 (9), 1683-1696.

[4] Acorn, NUTS—NMR utility transform software 1D versión (1997), 19970721, Livermore, CA.

[5] D.L. Parkhurst, C.A.J. Appelo, User's Guide to PhreeqC (Version 2) —A Computer Program for Speciation, Batch-Reaction, One-Dimensional Transport, and Inverse Geochemical Calculations, U.S. Geological Survey, Water-Resources Investigations

[6] O.P. Kari, Y. Elakneswaran, T. Nawa, J. Puttonen. Modelling approach for long-term diffusion behavior of multispecies in concrete on the basis of ion-cement-hydrate interaction. J. Mater. Sci 2013; 48(12):4243-4259.

[7] P. Blanc, X. Bourbon, A. Lassin, E.C. Gaucher. Chemical model for cement-based materials: Temperature dependence of thermodynamic functions for nanocrystalline and crystalline C-S-H phases. Cem Concr Res 2010; 40(6):851-866.

[8] P. Blanc, X. Bourbon, A. Lassin, E.C. Gaucher. Chemical model for cement-based materials: Temperature dependence of thermodynamic functions for phases other than C-S-H. Cem Concr Res 2010; 40(9):1360-1374.

[9] T. Kim, J. Olek. Chemical Sequence and Kinetics of Alkali–Silica Reaction Part II. A Thermodynamic Model, J. Am. Ceram. Soc. 2014; 97(7) pp.2204–2212.

[10] O.P. Kari, Y. Elakneswaran, T. Nawa, J. Puttonen. Modelling approach for long-term diffusion behavior of multispecies in concrete on the basis of ion-cement-hydrate interaction. J. Mater. Sci 2013; 48(12):4243-4259.

[11] Test method for potential alkali reactivity of cement-aggregate combinations (mortar-bar method). ASTM international. Retrieved from http://www.astm.org/Standards/C277.htm.

[12] Y. Elakneswaran, E. Qwaki, S. Miyahara, M. Ogino, T. Maruya and T. Nawa. (2016) "Hydration study of slag-blended cement based on thermodynamic considerations. *Construction and Building Material*.

[13] K. Tanaka, K. Kurumisawa (2002) "Development of Technique for Observing Pores in Harded Cement Paste." Cem Concr Res, 32, 1435-1441.

CHAPTER 4 MODEL SYSTEM

The results and discussion of products through the ASR model system were presented in this chapter. The ASR product was generated by the reaction between siliceous materials, portlandite (CH) and 1 M NaOH (NH). Reacted samples can be classed into 2 phases: liquid and solid. The ionic concentration in liquid samples after conducting under temperature of 60, 70 and 80°C was determined by ICP-AES. The chemical compositions and structures of hydrated products under 70 and 80°C was investigated by XRD and ^{29}Si-NMR. For SEM/EDX analysis, this method is subjected to verify the texture and the Ca/Si ratio of reacted products.

4.1 IONIC CONCENTRATION IN LIQUID SAMPLES DETERMINED BY ICP-AES ANALYSIS

The considerable contents of soluble silica (SiO_2) in the four samples up to 24 days are shown in **Figs 4.1-4.4.** The PG suggests that this kind of rapidly acting active glass is sensitive to hydroxide in the solution, and that this contributes to the presence of the very high content of soluble silica in the liquid sample within a short period of the start of the process.

Figs 4.2-4.4 also show the content of SiO_2 in the presence of CH for 3 temperatures (60, 70 and 80°C). With CH, there were low contents of SiO_2 in all three samples, quite different from the dissolved Si of liquid samples without CH. **Figs 4.2-4.3** show that the curves of SiO_2 started to increase significantly after 168 h with the Se and Yo samples, while the content of SiO_2 with the PG sample was significant after 72 h (**Fig. 4.4**). These changes suggest that the rate of Si dissolution may be related to the available Ca ions. At the initial stage, dissolved hydrous silicate ions such as $Si(OH)_2^{2-}$ may react with Ca ions and result in the formation of calcium silicate hydrate, C-S-H, which does not have a constant composition but rather that the composition depends on the activity of the Ca ions. These results suggest that after most of the Ca ions are consumed the rate of Si dissolution increases [1]. According to kinetic rate law of silica dissolution, three parameters including surface area, activity of OH^- and the ionic strength were assumed to be constant. The rate of silica dissolution (k) can be calculated by Arrhenius equation. Consequently, the rate of silica dissolution at 40°C is also presented in **Table 4.1**.

Table 4.1 Calculation parameters of siliceous materials

Materials (150 to 500 µm)	**Arrhenius constants (A)**	**$E_a$values (kJ/mol)**	**Dissolution rate at 40°C, $k_{40°C}$ (mol/h)**
Silica sand (SS)	$3.188x10^{-3}$	112.52	5.42x10-22
Cher-seto (Se)	$2.340x10^{-3}$	41.40	2.91x10-10
Chert-yoro (Yo)	$1.874x10^{-3}$	19.81	2.92x10-7
Pyrex-glass (PG)	$3.015x10^{-3}$	12.82	2.19x10-5

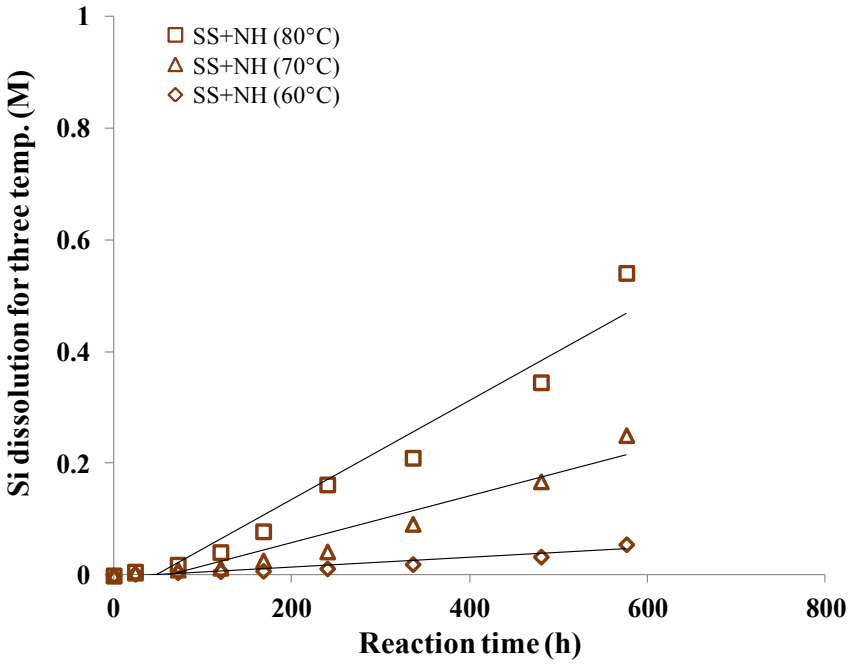

Fig. 4.1 The soluble silica contents of the Silica sand sample (SS). SS+NH (60°C), SS+NH (70°C) and SS+NH (80°C) stand for the liquid samples decanted from the reaction between SS and NH exposed in temperature of 60, 70, and 80°C, respectively

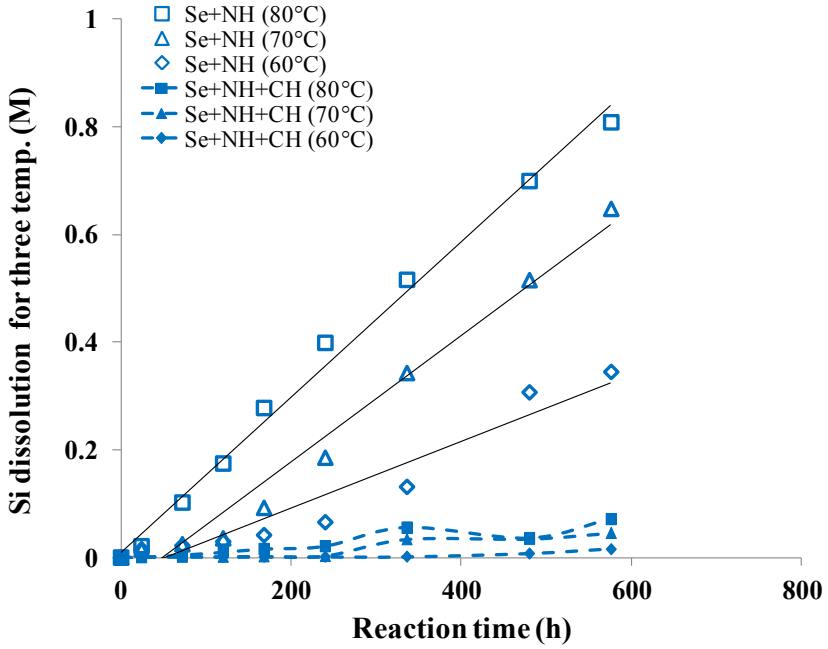

Fig. 4.2 The soluble silica contents of the Seto-chert sample (Se). Se+NH (60°C), Se+NH (70°C) and Se+NH (80°C) stand for the liquid samples decanted from the reaction between Se and NH exposed in temperature of 60, 70, and 80°C, respectively. While the mixtures between Se, NH and CH at different temperatures are represented by Se+NH+CH (60°C), Se+NH+CH (70°C) and Se+NH+CH (80°C)

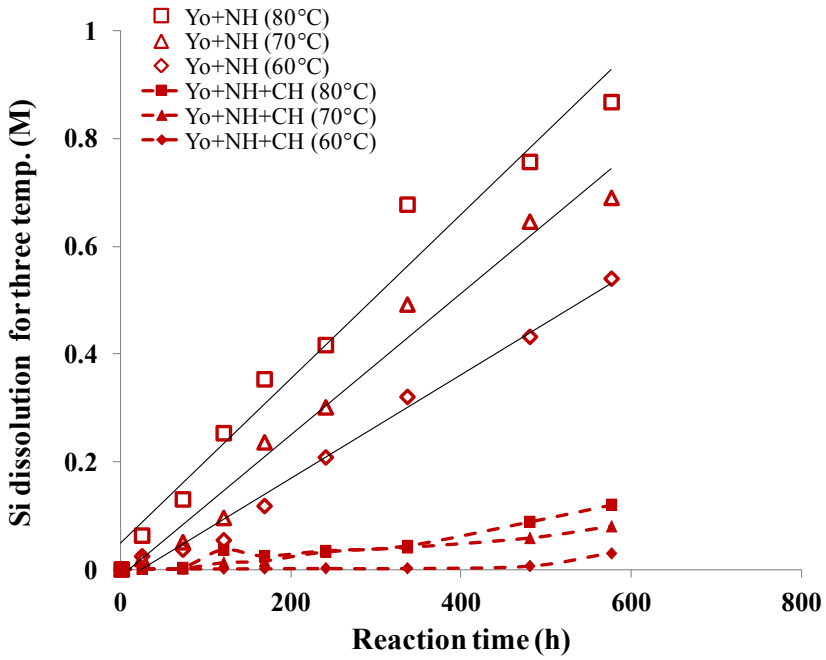

Fig. 4.3 The soluble silica contents of the Yoro-chert sample (Yo). Yo+NH (60°C), Yo+NH (70°C) and Yo+NH (80°C) stand for the liquid samples decanted from the reaction between Yo and NH exposed in temperature of 60, 70, and 80°C, respectively. While the mixtures between Yo, NH and CH at different temperatures are represented by Yo+NH+CH (60°C), Yo+NH+CH (70°C) and Yo+NH+CH (80°C)

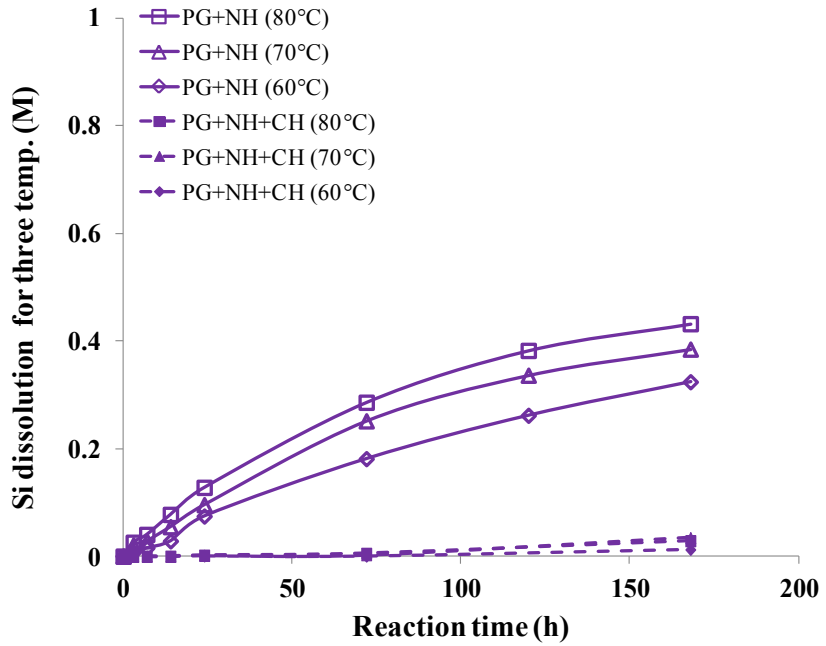

Fig. 4.4 The soluble silica contents of the Pyrex glass sample (PG). PG+NH (60°C), PG+NH (70°C) and PG+NH (80°C) stand for the liquid samples decanted from the reaction between PG and NH exposed in temperature of 60, 70, and 80°C, respectively. While the mixtures between PG, NH and CH at different temperatures are represented by PG+NH+CH (60°C), PG+NH+CH (70°C) and PG+NH+CH (80°C)

4.2 XRD, ^{29}Si-NMR AND SEM/EDX RESULTS OF INSOLUBLE PRODUCT (MODEL SYSTEM AT 80°C)

This part aims to describe the reacted products from the model system with accelerating conditions at constant temperature of 80°C using two-chert aggregates, Yo and Se aggregates. The experiments present the results of ASR generated through a reactive system conducted to gain a more comprehensive understanding of the ASR mechanism of formation by an analysis of XRD, ^{29}Si-NMR, and SEM/EDX results. This comprehensive effort has been developed to take understanding of the mechanism of ASR-affected structures and the role of Ca on ASR formation. Correlating these experimental data with previous studies [1-5] leads to insight into the sequence of reaction, particularly the ASR formation in the presence of CH. The Q-XRD has been developed in this part in order to estimate the ASR product like C-S-H_0.83 in the unit of gram. As mentioned earlier, the Ca ion may effect on ASR formation, the fine chert (a range of particle sizes from 300 to 150 μm) of 5.0 g was also mixed with small amounts of CH solid of 0.77 and 0.385 g. For the sake of simplicity, only the reacted sample of Yo-chert (Yo+NH+CH_0.77 and Yo+NH+CH_0.385) was selected to analyze by XRD, ^{29}Si-NMR in this section.

4.2.1 Model experiment results of Yo and Se for ASR formation

- **XRD analysis**

The XRD patterns of the Yo+NH and Se+NH powders appear in **Fig. 4.5**. There are no broad peaks for amorphous and poorly-ordered crystalline silicate in the powder samples of Yo+NH and Se+NH. The peak patterns at 20.64 and 26.3°2θ observed here are the crystalline phases of Quartz [6]. There are peak patterns at 32.3°2θ and 37.92°2θ in both samples which may be assigned to thermonatrite (Na_2CO_3). This thermonatrite comes from carbonation due to the high Na content remaining in the liquid samples. In the presence of CH (**Fig. 4.6**), the XRD patterns of both Yo+NH+CH and Se+NH+CH show peak patterns at 7.14°2θ and 29.34°2θ which changes with reaction time, indicating ASR product incorporation with Ca. The broad peaks at 7.14°2θ in the XRD patterns suggests an amorphous phase in the solids. The diffraction peaks at 7.14°2θ and 29.34°2θ became dominant at 3 days of reaction, and these two peaks are readily identified as tobermorite type C-S-H [1-4]. After 10 days, the relative intensity of these two peaks has increased significantly. The intensity of the portlandite peaks (CH marked in **Fig. 4.6**) at 18.06°2θ and 34.06°2θ were substantially diminished as an effect of A-S-R precipitation associated with the portandite peaks (CH). The greater CH consumption supports the idea that Ca ions play an important role in accelerating the ASR reaction, with ASR formation of chemical compositions similar to tobermorite type C-S-H at low Ca/Si ratios [1-4].

According to **Fig. 4.6**, the broad peak patterns of ASR products like tobermorite type C-S-H, at 7.14°2θ and 29.34°2θ, appears to be an amorphous phase. In order to quantify amorphous phases in the Q-XRD analysis, corundum is commonly used as an internal standard in XRD patterns. The content of amorphous product in the samples determined by adding corundum is illustrated in **Fig. 4.7** at the various reaction times. The amorphous content at 14 days of Se+NH+CH was 43.92 %, which was less than that 49.94% of Yo+NH+CH. Quartz content decreased gradually from the initial content (77%). At 14 days of the experiments the quartz contents in Yo+NH+CH and Se+NH+CH solid samples were 41.65% and 48%, respectively. The considerable reduction of residual quartz provides strong evidence that Si was dissolved from the aggregate by OH^-, and then precipitated as ASR products such as C-S-H. This is also able to explain a reason why the content of dissolved Si was low when CH is present, as shown in **Figs. 4.2-4.3**. The amount of C-S-H existed in Yo+NH+CH and Se+NH+CH, as shown in **Fig. 4. 7**, can be expressed in term of mass percent. Combining the Q-XRD data with the loss on ignition data (H_x) from Eq. (3.1), the content of C-S-H can be converted into mass based on the interpolation from the initial mass of reactant.

The formula is shown in Eq. (4.1). The change in mass of C-S-H with time is presented in **Table 4.2**. It can be seen that the amount of C-S-H in the Yo-chert samples can be seen to be higher than that in the Se-chert samples.

$$W_x = \frac{100}{(100 - H_x)} \times T_x \times M_q \tag{4.1}$$

where W_x is the mass of C-S-H in g**,** H_x is the percentage of total water in C-S-H calculated from loss on ignition**,** T_x is the percentage of tobermorite C-S-H calculated from XRD quantitatively, M_q is the initial mass ratio of the aggregate (5/77)**,** X is the Yo or Se sample.

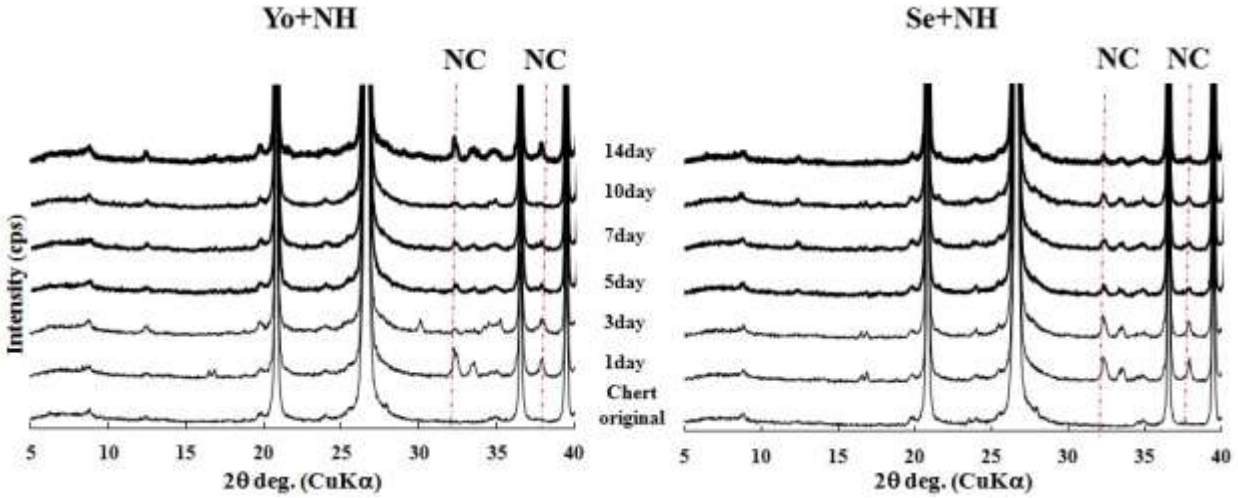

Fig. 4.5 XRD patterns of Yo+NH and Se+NH solids. The notation "NC" is for the Na_2CO_3 phase.

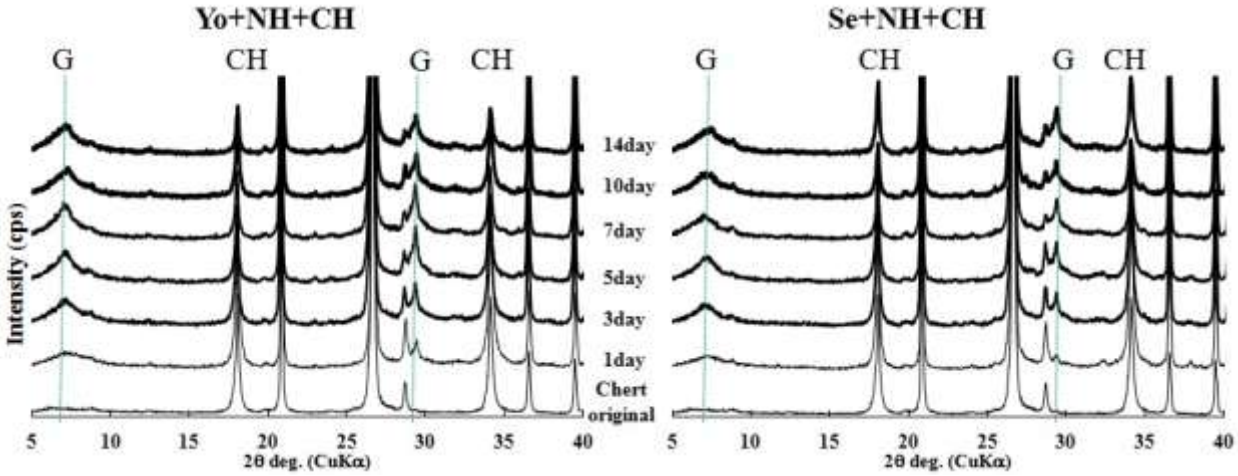

Fig. 4.6 XRD patterns of Yo+NH+CH and Se+NH+CH solids. The notations "G" and "CH" are the ASR phase and the portlandite phase.

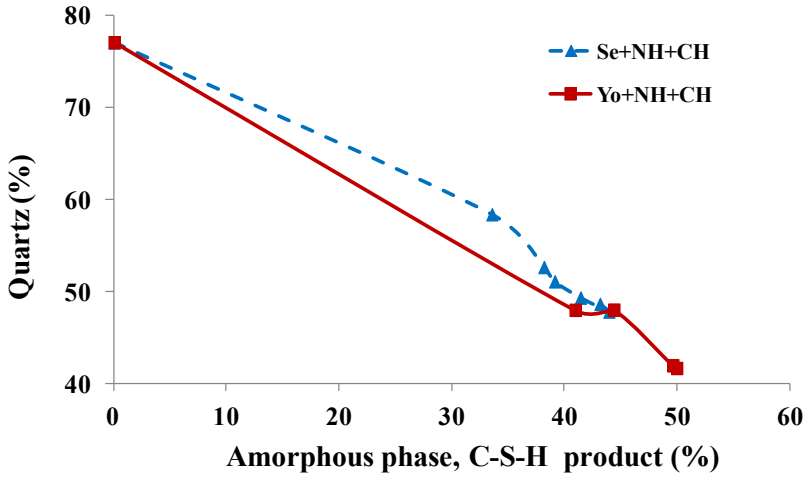

Fig. 4.7 The amorphous and Quartz content (%) in the solid samples at the different reaction times.

Table 4.2 Mass of C-S-H_0.83

Reaction time (day)	Yo-samples		Se-samples	
	Loss on ignition, H_X (%)	Mass of C-S-H, W_X (g)	Loss on ignition, H_X (%)	Mass of C-S-H, W_X (g)
1	9.7336	2.9648	7.5778	2.3729
3	9.5897	3.2091	7.9206	2.7097
5	6.5904	2.9595	9.0537	2.8123
7	9.9362	3.6017	8.5418	2.9601
10	10.1783	3.6362	8.9074	3.1886
14	7.8476	3.3682	9.5666	3.1186

- **^{29}Si-NMR analysis**

The chemical structure of the synthesized ASR product, was analyzed by ^{29}Si-NMR, and in the results Q^n is commonly referred to, here the Q stands for a particular tetrahedron and the exponent n is for the number of bonded bridging oxygens. Starting components of aggregates represented by Q^4 describes the state of fully-cross-linked silica. **Table 4.3** illustrates ^{29}Si-NMR chemical shift data for silicates with Q^1 to Q^4 from [5].

The original Yo and Se cherts yielded peaks at -108, with respect of the Q^4 site of quartz, as shown in **Fig. 4.8**. There were no observations identical to the other peaks (Q^1, Q^2 and Q^3) in the Yo+NH but a sole peak at -98 implying Q^3(1OH^- site in the chert: **Table 4.3**) was found in the Se+NH sample at 10 days of reaction. After 14 days of reaction, the relative intensity of both samples yielded a peak at -98 (Q^3). In the ^{29}Si-NMR spectra, Q^3 sites (with 1OH^-) suggest that the Si site tetrahedron has three bridging oxygens and one non-bridging oxygen. It may be surmised that the non-bridging oxygen could be bonded to either OH^- or other low-charge cations, like in the Na group, which has been suggested in some types of ASR gel, like kanemite (Na/K-S-H) [5].

In **Fig. 4.9**, the ^{29}Si-NMR peaks at -79 and -85 ppm in the solids of Yo+NH+CH and Se+NH+CH at 3 days of reaction, represent Q^1 and Q^2 sites, respectively (**Fig. 4.9**). The relative intensity of the -85 ppm (Q^2) peak increased until 14 days of reaction in support of a process of polymerization of ASR product.

With CH present, the peaks at -79 (Q^1) and -85 (Q^2) ppm of ASR are associated with the chemical structure of C-S-H which is dominated by Q^1 and Q^2 sites in the ^{29}Si-NMR spectra [2-3]. In agreement with the XRD analysis of solids mixed with CH (**Fig. 4.6**), the reaction proceeds toward CH consumption and the ASR product could be assigned to tobermorite type C-S-H. The relative intensity of the -79 ppm (Q^1sites) peak decreased and the -85 ppm (Q^2) peak increased with the progress of the reaction, implying a Ca/Si ratio difference in the C-S-H. The change of C-S-H structure from Q^1 to Q^2 dominant may be attributed to the conclusion previously reported by X. Hou et al. [3].

- **A change in micro-texture of quartz observed by SEM/EDX analysis**

Fig. 4.10 shows the SEM images for three solid samples of Yo+CH, Yo+NH+CH, and Se+NH+CH. In **Fig. 4.10**, SEM images of unreacted sample of Yo+CH (A and B) show a clear fracture surface of grains; those of reacted samples at 14 days of Yo+NH+CH (C and D) and Se+NH+CH (E and F) show a rough surface of grains due to Si dissolution. It is evident that the SEM images of reacted samples at 14 days (C, D, E and F) are in good agreement with Q-XRD results (see **Fig. 4.7**), in which the contents of quartz gradually decreased with an increase of reaction time. Dissolution of quartz is almost identical in both analysis (Q-XRD and SEM). It is therefore speculated that during reaction all samples contains grains with dissolution effect of hydroxide radical attack. Addition to the SEM with EDX analysis (SEM/EDX), the value of Ca/Si ratios can be roughly estimated: 0.74 for Yo+NH+CH and 0.81 for Se+NH+CH. The value is similar to Ca/Si ratio of 0.83 for tobermorite type C-S-H. Taking into account that a value of Ca/Si ratio of produced C-S-H was not a define value but distributed, SEM/EDX observations confirms that reacted samples at 14 days of Yo+NH+CH and Se+NH+CH include tobermorite type C-S-H.

Table 4.3 ^{29}Si MAS NMR chemical shift data for silicate material [5]

For Al-free silicate (Q^n)	The range of chemical shift, ppm
Q^4	-103 to-115
Q^3	-98 to -103 for a single OH^- in amorphous silica -91 to -98 for alkali-containing system
Q^2	-79 to -85
Q^1	-62 to -83

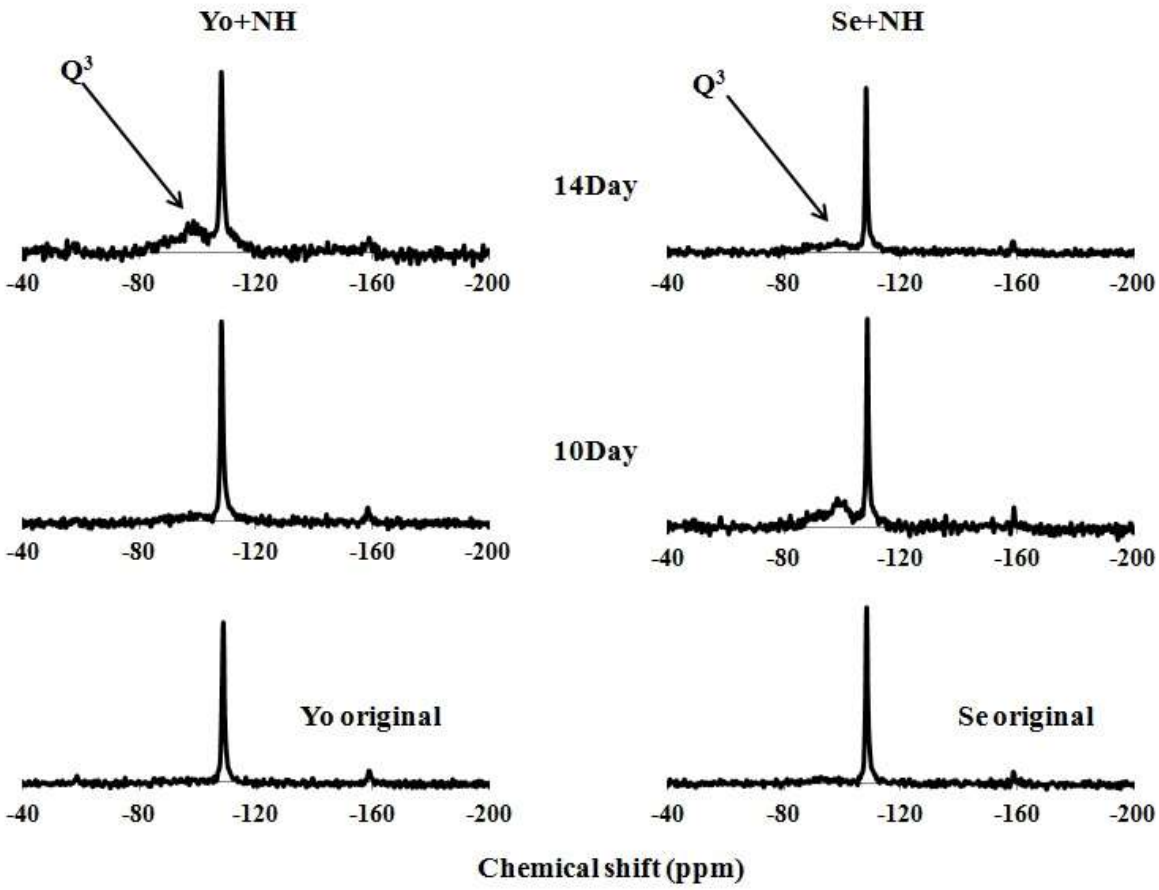

Fig. 4.8 ^{29}Si-NMR spectra of Yo+NH and Se+NH powder after reactions at 10 and 14 days without CH solid

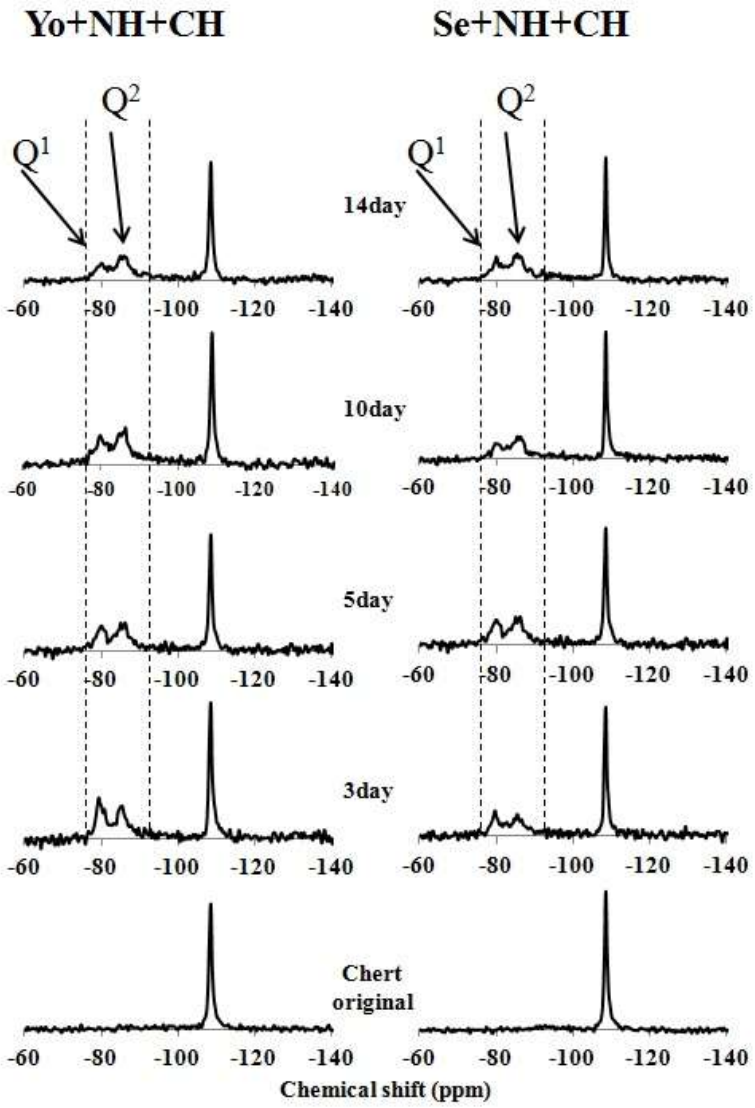

Fig. 4.9 ^{29}Si-NMR spectra of Yo+NH+CH and Se+NH+CH powder after reaction with NH solution and CH solid

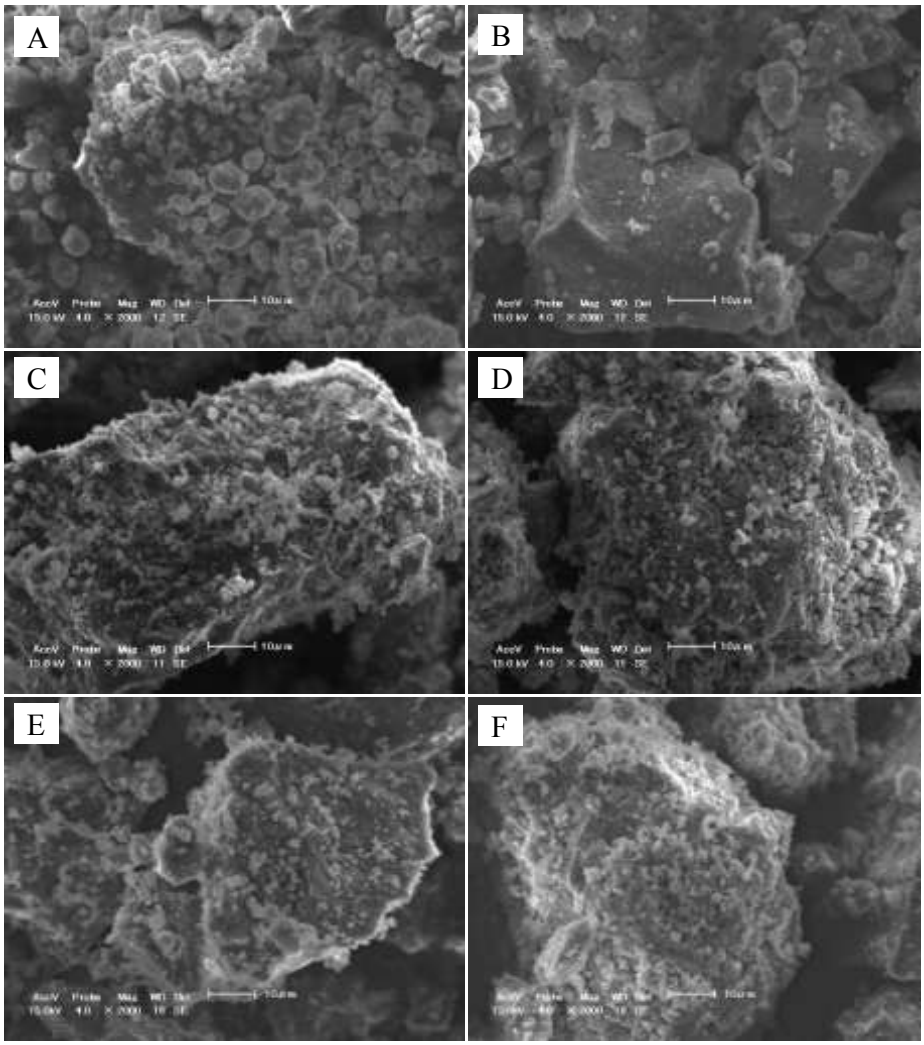

Fig. 4.10 SEM images of quartz from the fine solids: A and B, quartz grains of Yo+CH (No reaction) showing a clear fracture surface of grains with CH solid; C and D, reacted sample at 14 days of Yo+NH+CH showing grains with a rough surface due to dissolution; E and F, reacted sample at 14 days of Se+NH+CH showing grains with a rough surface due to dissolution.

4.2.2 The role of Ca on ASR formation

It was reported that Ca ions play an important role in accelerating the ASR reaction. According to X. Hou et al. [2], ASR gel does not form until the available CH has reacted with dissolved Si from the aggregate and produced C-S-H. This implies that the presence of CH is crucial. Hence, the effect of CH on ASR formation was investigated experimentally by varying the addition of CH. The amounts of CH of 0.77 g and 0.385 g was mixed with Yo-chert samples.

- **XRD analysis**

As illustrated by **Fig. 4.11**, typical XRD peaks located at 7.14°2θ and 30°2θ were observed. As comparing among Yo+NH+CH, Yo+NH+CH_0.77, and Yo+NH+CH_0.385, it was noticeable that by the addition of small content of CH, the XRD peaks of C-S-H peaks located 29.3° 2θ shift to 30°2θ and became broader. This broadening of XRD peaks agrees with the observation by Hou et al. [2], which

indicates an increase in the degree of polymerization of C-S-H, that is the conversion of the tobermorite type C-S-H to C-Na/K-S-H [1][4].

- **^{29}Si-NMR analysis**

As discussed previously, the XRD results of Yo+NH+CH_0.77 and Yo+NH+CH_0.385 displayed the significantly broadened peak located 30°2θ (**Fig. 4.11**). ^{29}Si-NMR data in **Fig. 4.12** reveals that not only the Q^1 (-79 ppm) and Q^2 (-85 ppm) sites were detected, the relative intensity of -95 ppm (Q^3 sites in the range from -91 to -98 ppm was expected in OH^- and Na^+ containing system [5]) was apparently observed in both Yo+NH+CH_0.77 and Yo+NH+CH_0.385 at 14 days of reaction. This is consistent with results obtained in [1][2]. It is believed that excessive alkali ions might be incorporated into the re-polymerization of tobermorite type C-S-H to produce ASR, such as C-Na-S-H.

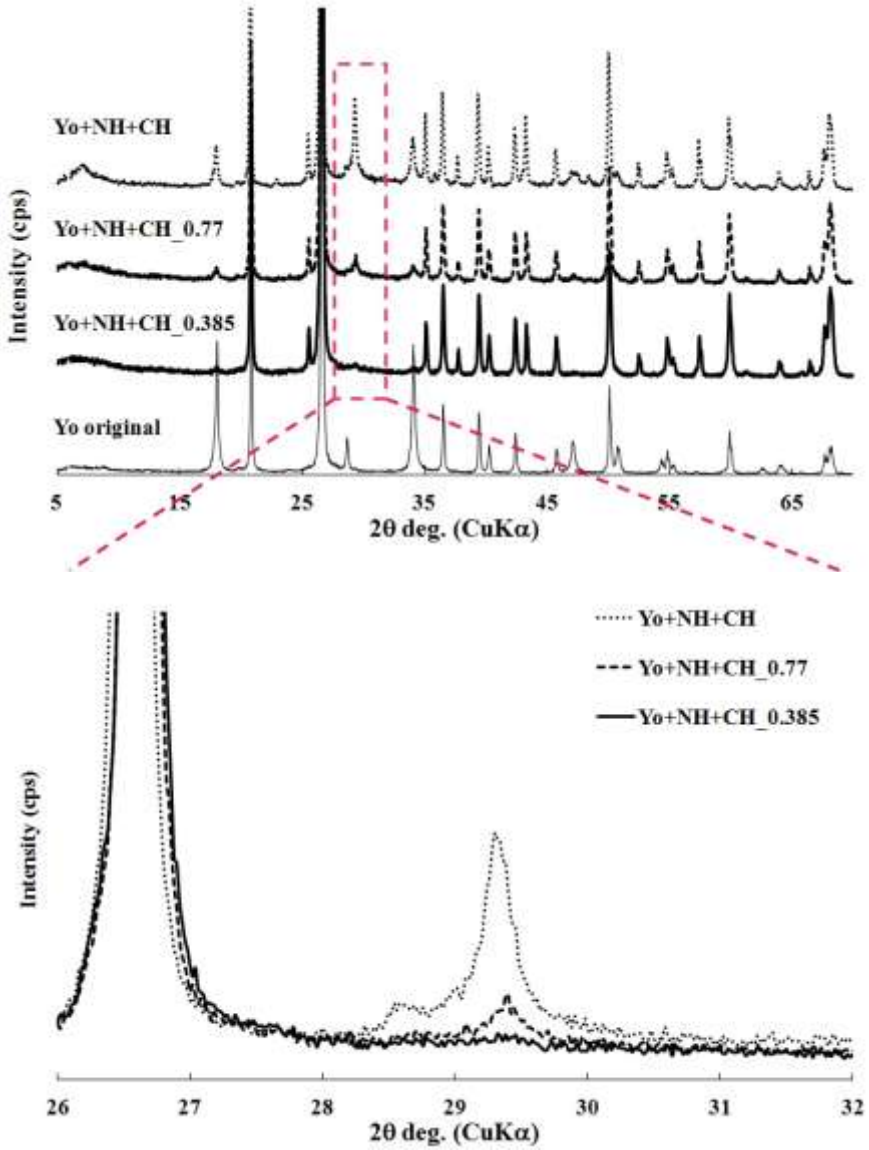

Fig. 4.11 XRD patterns of Yo-mixtures with various contents of CH for 14 days of reaction time (Yo+NH+CH, Yo+NH+CH-0.77,and Se+NH+CH-0.385 solids), showing tobermorite type C-S-H located at 7.14°2θ and nearly 30°2θ

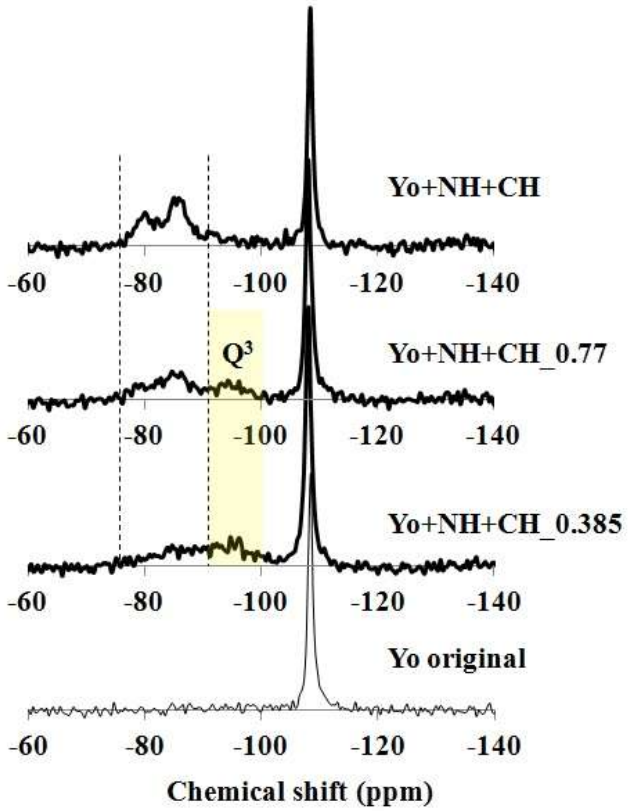

Fig. 4.12 ^{29}Si-NMR spectra of Yo+NH+CH_0.77, and Se+NH+CH_0.385 powder after reaction with NH solution and CH solid at 14 days, showing the appearance of the Q^3 sites (-95 ppm)

4.3 XRD AND ^{29}Si-NMR RESULTS OF INSOLUBLE PRODUCT (MODEL SYSTEM AT 70°C)

This study aims to describe the reacted products from the model system with accelerating conditions at constant temperature of 70°C using two-siliceous materials, Yo and PG. The experiments present the results of ASR generated through a reactive system conducted to gain a more comprehensive understanding of the ASR mechanism of formation by an analysis of XRD, and ^{29}Si-NMR results. This comprehensive effort has been developed to take understanding of the mechanism of ASR-affected structures when glass used as aggregate. Correlating these experimental data of PG with Yo leads to suggesting that the sequence of reaction of PG, particularly the ASR formation in the presence of CH, is similar to reactive chert aggregate (Yo).

4.3.1 Model experiment results of Yo for ASR formation

- **XRD analysis**

In model system, it was suggested that the C-S-H formation was attributed to the ASR reaction between available SiO_2 and Ca ions. For simplicity, Yo+NH (70 °C) and Yo+NH+CH (70°C) was selected to detect the insoluble product. There are no broad peaks for amorphous and poorly-ordered crystalline silicate in the powder samples of Yo+NH (70 °C), as shown in **Fig. 4.13 (A)**. Whereas the XRD peaks of Yo+NH+CH (70°C) at 29.4°2θ became sharper with the progress of the experiments (see in **Fig. 4.13(B)**). The peaks also exhibited the diffraction at 7.2°2θ that is ordinarily observed with amorphous or disordered crystalline silicate. These peak locations are related to the basic peak patterns of a layer

structured clay mineral, tobermorite and alkali disilicates, suggesting ASR, by the presence of C-S-H, when Ca ions are available for reaction [2-3]. The intensities of the portlandite peaks at 18.0°2θ and 34.2°2θ decrease with increasing reaction time.

- **NMR analysis**

^{29}Si-NMR spectra of Yo+NH (70°C), the peaks of Q^3 was solely detected at reaction time of 576 h (**Fig. 4.6**). The spectra of Q^3 site (with 1 OH^-) suggest that the Si site tetrahedron has three bridging oxygen and one non-bridging oxygen, in which the non-bridging oxygen could be bonded to either OH- or other low-charge cations, like in the Na group. This has been suggested in some types of ASR gel. In addition to CH condition, the ^{29}Si-NMR spectra of Yo+NH+CH (70°C), there are main peaks at -78.8 ppm (the end chain tetrahedral Q^1) and -84.1 ppm (non-bridging tetrahedral Q^2) in **Fig. 4.14**. At 336 h, the intensity of Q^2 has increased and become dominant (the Q^1/Q^2 ratio < 0.50 as listed in **Table 4.1**). At the end of the experiments at 576 h there were Q^1, Q^2, and Q^3 sites, and it appears that the chemical shift of the signal was initially dominated by Q^1 when there were Ca ions present in the solution. This observed spectrum of Q^1 can be related to a previous study by Lothenbach and Nonat [12], suggesting the incorporation of the alkalis into the gel structure, like in calcium alkali silicate hydrate (C-K-S-H or C-Na-S-H). Later in the experiments the intensity of Q^2 became dominant (the Q^1/Q^2 ratio decreased as shown in **Table 4.1**) due to the action of available Ca ions which could be assigned to a more polymerized structure of C-S-H. Considering the spectra at -95.1 ppm of the Q^3 site (as detailed in **Fig. 4.14** and **Table 4.1**), this probably shows links between two silicate chains of two adjacent layers. The Q^3 site is a defect when compared with the tobermorite structure at a low Ca/Si ratio [13-15].

With XRD and ^{29}Si-NMR results, this current finding expands prior work about the sequence of ASR from model experiment at 80°C. Alkali silicate hydrate, Na/K-S-H, may be supposed to be the first product in the sequence of the ASR. It is commonly accepted that prior to the completed C-S-H formation, C-Na/K-S-H (the Q^1 site dominantly) could be formed by the incorporation of Ca^{2+} ions into Na/K-S-H. Later, excess Ca^{2+} ions are closely involved in the precipitation of ASR gel, likely to form a more polymerized structure of C-S-H (dominated by the Q^2 site). With lower amounts of Ca ions, the Q^3 site becomes detectable and finally, the presence of C-Na/K-S-H and Na/K-S-H may be attributed to the complete consumption of CH.

4.3.2 Model experiment results of PG for ASR formation

With XRD and ^{29}Si-NMR results of PG+NH (70°C) (**Figs. 4.15(A)** and **4.16**), it can be deduced that there were no observations identical to the formation of ASR. This is because the structure of PG is disorder structure, which is difficult detected by XRD and ^{29}Si-NMR.

- **XRD analysis**

In **Fig. 4.15**, the XRD peaks at 29.4 °2θ and 7.2 °2θ were present in PG+NH+CH (70°C). This result demonstrates that when CH is present the Si dissolved by hydroxide would have reacted with Ca ions to precipitate ASR.

- **NMR analysis**

Generally, original PG has the fully polymerized Q^4 and Q^3 site in structure. To study the formation of ASR product of PG, it is necessary to consider the peak area of Q^3 and Q^4 by NUT program. At 24 h of reaction, the peaks at -79.9 ppm (the end chain tetrahedral Q^1) and -84.1 ppm (non-bridging tetrahedral Q^2) presented (**Fig. 4.16**). It was also observed the peak area of Q^4 decreased due to dissolution but the

intensity of Q^3 increased, as shown in **Table 4.4**. The presence of Q^1, Q^2, and Q^3 may be related to the formation of C-S-H and C-Na-S-H formed in solid samples. At 72 and 168 h, the major peak of the Q^2 site was alone corresponding with the increase in the peak area of Q^3, suggesting the formation of additional Na-rich product. It is believed that the XRD peaks at 29.4 °2θ can be assigned to either C-Na-S-H (Ca-Kanemite) or Na-S-H (Kanemite). Supporting by the ^{29}Si-NMR spectra, it can be deduced that the final product of PG sample seem to be C-Na-S-H and Na-S-H, accordingly.

■ Quartz ▲ Portlandite ★ ASR product ● Corrundum ◆ Pyrex glass

(A)

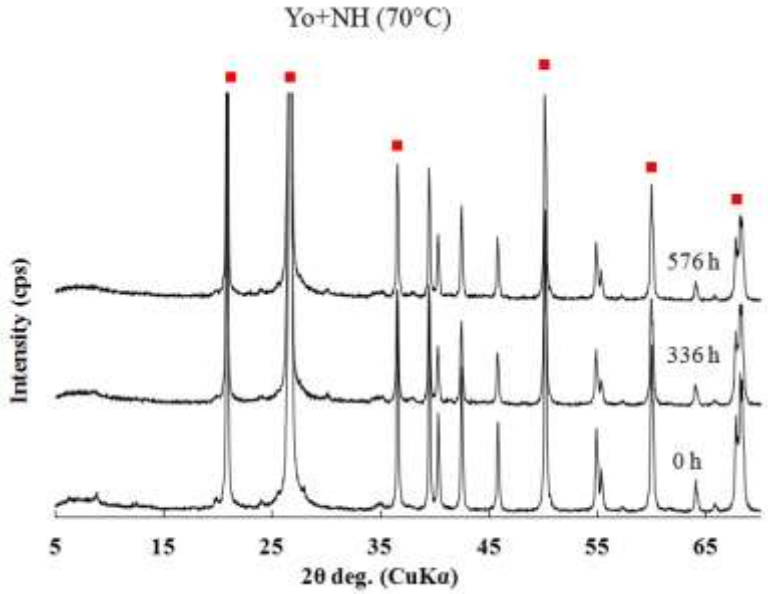

(B)

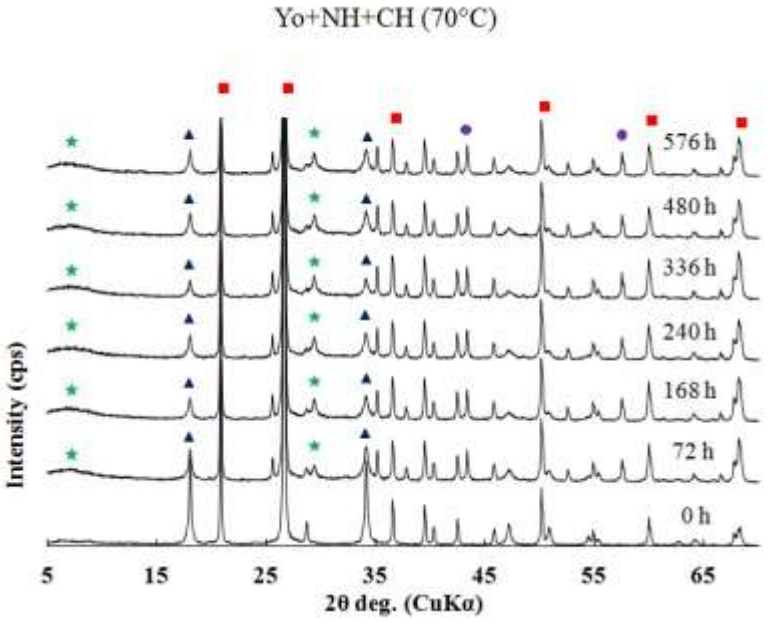

Fig. 4.13 The XRD results: (A) Yo+NH (70°C) and (B) Yo+NH+CH (70°C)

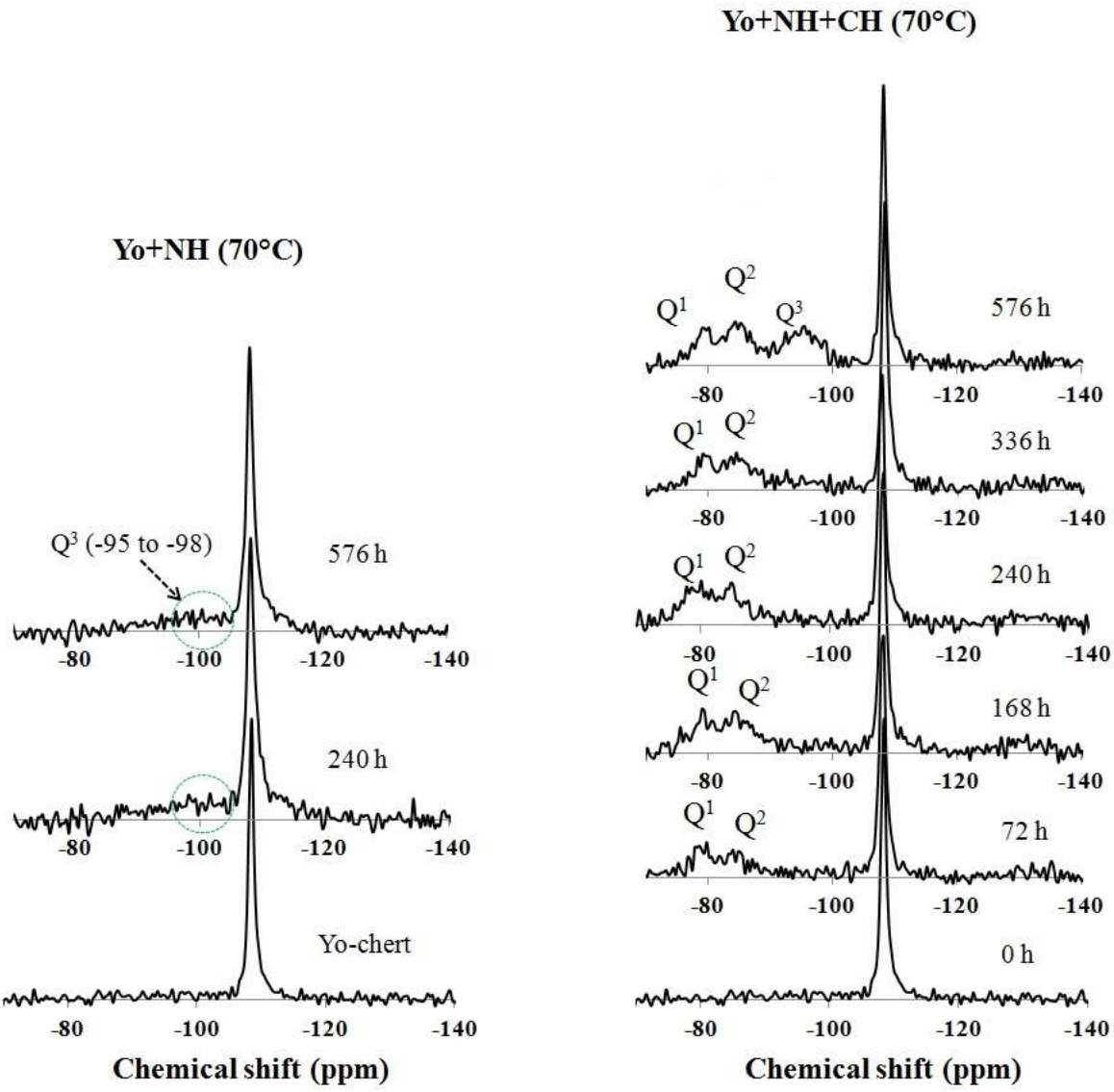

Fig. 4.14 The ^{29}Si-NMR results of Yo+NH (70°C) and Yo+NH+CH (70°C)

Table 4.4 Calculated output of the Nuts program from the ^{29}Si-NMR spectra

Reaction	**Yo+NH+CH (70°C)**				**PG+NH+CH (70°C)**			
time	**72 h**	**168 h**	**336 h**	**576 h**	**0 h**	**24 h**	**72 h**	**168 h**
Q^4	-107.9 63.48%	-107.9 54.17%	-108 54.28%	-108.1 36.51%	-109.5 92.242	-109.5 84.53%	-109.5 82.47%	-109.5 81.74%
Q^3	0	0	0	-95.1 25.76%	-96.5 7.758	-96.5 10.498	-96.5 11.364	-96.5 11.087
Q^2	-84.1 18.15%	-84.4 29.197%	-84.4 32.36%	-84.7 27.03		-84.1 2.741%	-84.0 6.168%	-84.3 7.174%
Q^1	-78.8 17.91%	-78.8 16.63%	-79.1 13.35%	-79.2 10.69%		-79.9 2.233%	0	0
Q^2/Q^1 ratio	0.99	0.57	0.41	0.39		0.11	N/A	N/A

Note: N/A means to not available.

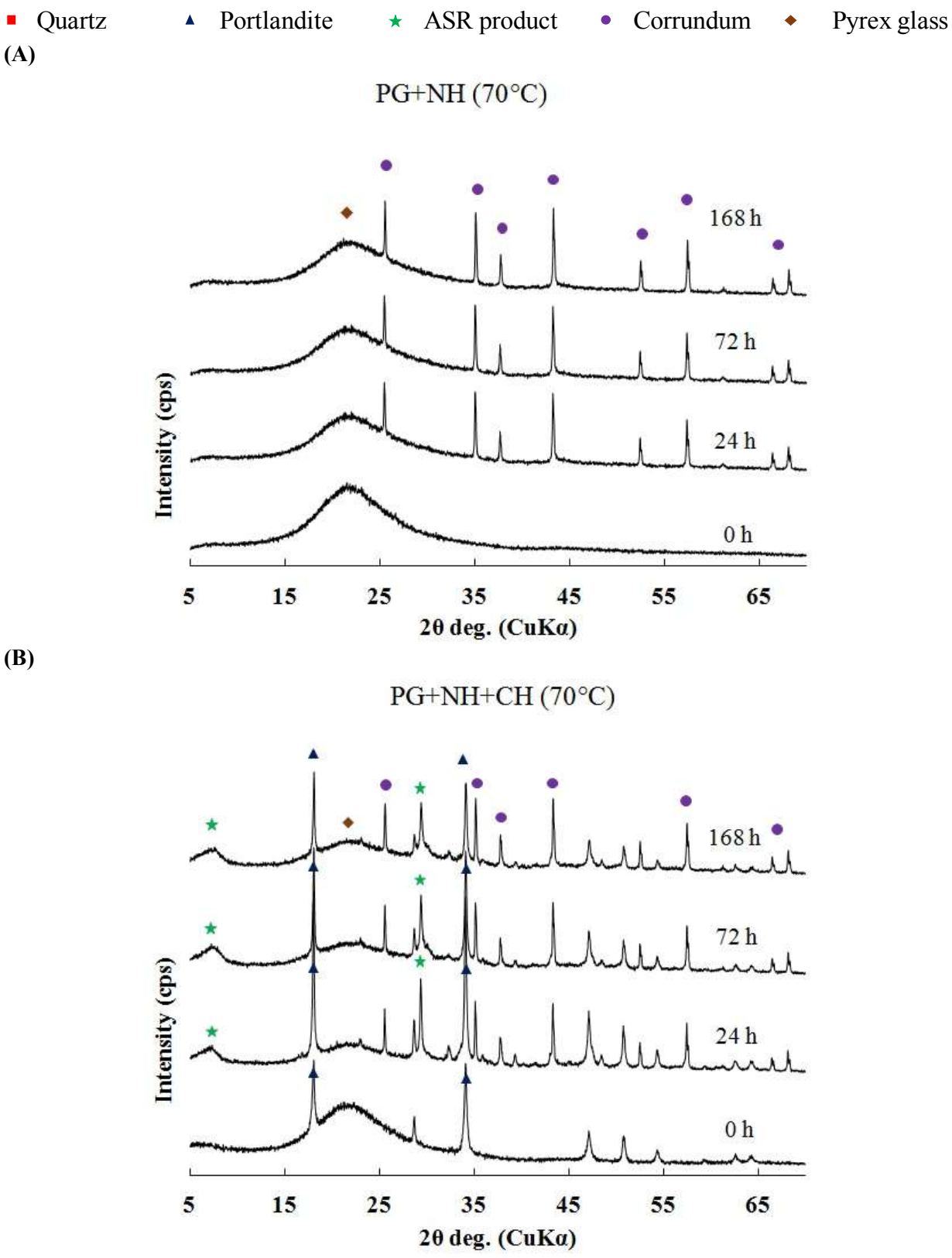

Fig. 4.15 The XRD results: (A) PG+NH (70°C) and (B) PG+NH+CH (70°C)

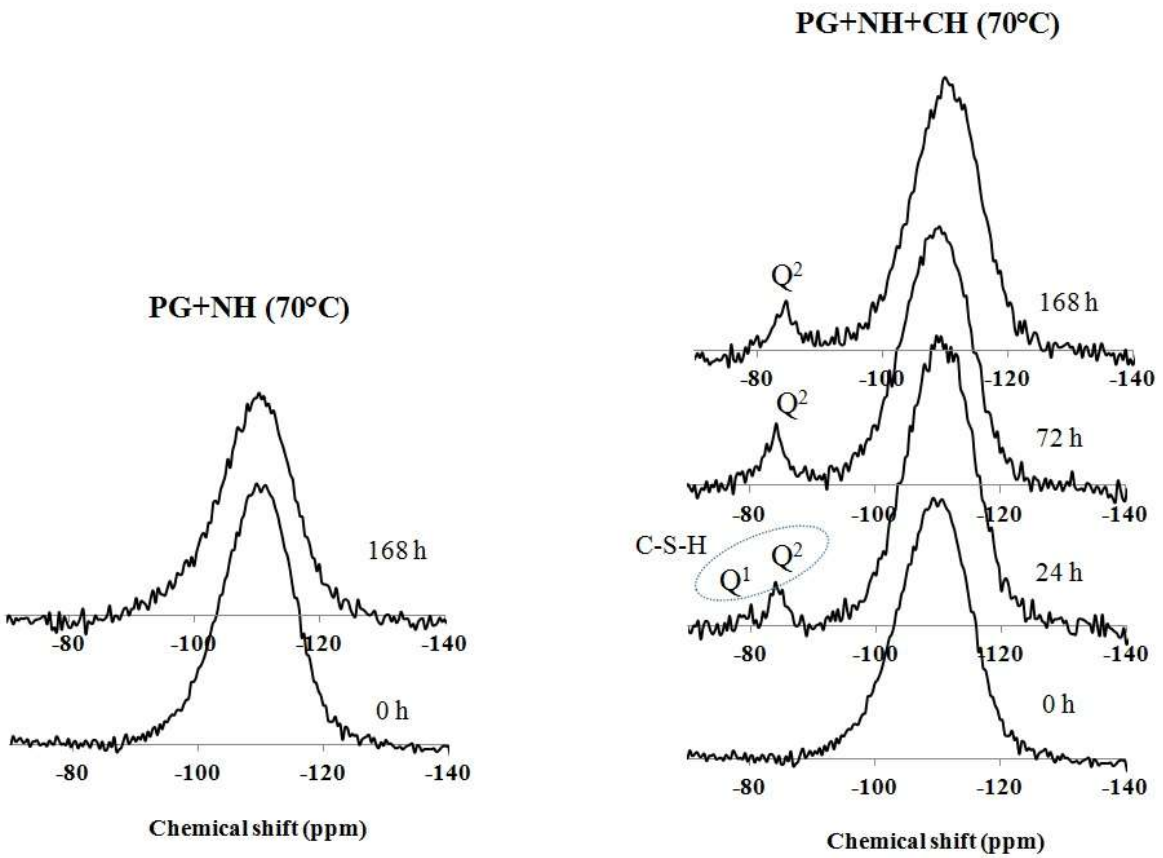

Fig. 4.16 The ^{29}Si-NMR results of PG+NH (70°C) and PG+NH+CH (70°C)

- **A change in micro-texture of pyrex glass observed by SEM/EDX analysis**

The SEM images for solid samples of PG+NH+CH (70°C) at 24 h show a rough surface of grains due to Si dissolution (**Fig. 4.17**). It is therefore speculated that during reaction all samples contains grains with dissolution effect of hydroxide radical attack. Addition to the SEM with EDX analysis (SEM/EDX), the value of Ca/Si ratios can be roughly estimated 1.69 for PG+NH+CH (70°C). The value is similar to Ca/Si ratio of 1.66 for jennite type C-S-H. Taking into account that a value of Ca/Si ratio of produced C-S-H was not a define value but distributed, SEM/EDX observations confirms that reacted samples at 24 h of Yo+NH+CH including jennite type C-S-H. When reaction increased, the Ca/Si ratio of ASR gel was gradually decreased due to the adsorption of Na in structure.

4.4 SUMMARY

With ICP-AES analysis, the dissolution rate of soluble silica of each material at different temperature can be determined. It was found that the dissolution rate of PG was very rapid, which it is significantly different from SS. In the presence of CH, it can be noticed that the content of dissolved Si was observed a little in all liquid samples. Surprisingly, we detected the amount of soluble silica started to increase when CH was almost consumed by the reaction. For insoluble product investigated by XRD ^{29}Si-NMR and SEM/EDX, the results showed that Ca ions were initially involved in the ASR precipitation to form tobermorite type C-S-H (Ca/Si of 0.83) for chert sample and jennite type C-S-H (Ca/Si of 1.66) for pyrex glass sample. Almost the exhaustion of Ca ions, this contributed to the onset of calcium alkali silicate hydrate (C-Na-S-H) due to alkali ions being incorporated in the existing C-S-H structure by binding with

OH^-. Analysis of the solid samples by XRD and ^{29}Si-NMR, the distinction in chemical structures between C-S-H and C-Na-S-H is explicit. This demonstrated that, for the samples mixed with small contents of $Ca(OH)_2$, the XRD peaks of C-S-H located at 29.3 °2θ shift to 30.0 °2θ and the spectra of ^{29}Si-NMR displayed the peaks at -79 ppm (Q^1 sites), -85 ppm (Q^2 sites) and -95 ppm (Q^3 sites). These results indicated the formation of ASR becomes C-Na-S-H at Q^3 dominantly. The Q^3 site is link to for a single OH^- in amorphous silica or alkali-containing system [10].

From above results of ICP-AES, XRD ^{29}Si-NMR and SEM/EDX, the studies on insoluble product of ASR suggests that when $Ca(OH)_2$ initially exists in the reacting system such as actual concrete structure, the chemical sequence of ASR process is initiated by the dissolution of silica due to an attack by the hydroxyl ions; subsequently to form a C-S-H by the reaction between dissolved silica and Ca ions because the electrostatic charge of the Ca-O is higher than that of the Na-O bond [11]; after complete consumption of available $Ca(OH)_2$, dissolved silica reacts with existing tobermorite-type C-S-H, producing C-Na-S-H gel; more continuously increasing the concentration of silica ions in the solution and high Na-ion concentration promotes the formation of ASR gel, like Na-S-H. These findings extend those results of Kim et al [1] and Hou et al [3]. Katayama [12] described the location of ASR deposits in concrete. ASR gel with increased Ca mostly found in the vicinity of reactive site, such as in the gap between aggregate and cement paste, in the cracks of cement paste, and within the air voids. In contrast, the cracking inside the reactive aggregate is filled by the rich alkali-ASR gel, like Na/K-S-H or C-Na/K-S-H. Based on the results mentioned above and previous studies [1-3][9][13], the composition and location of ASR products can be summarized as follows. With highly alkali and moisture condition, the siloxane bond (Si-O-Si) on the surface of aggregate is broken and Si ions are dissolved into the solution at adjacent surface reacted site. In the presence of Ca ions, Ca ions react with Si ions, resulting in the formation of C-S-H. Once available Ca ions are completely consumed, existing C-S-H reacts with Si ions and Na/K ions to form C-Na/K-S-H. These ASR products might be filled within the air voids or deposited in the rim between reactive site and cement paste, acting as the reaction rim. In case of reaction rim, not only the diffusion of ionic species (Na, K and OH) into reactive aggregate but also it would induce the pressure to crack to the surrounding paste but also the more penetration of alkali and OH, generating Na/K-S-H, which causes aggregate to crack. Simultaneously, the existing Na/K-S-H can be extruded from the inside aggregate into the cement paste along the cracks of aggregate. Crack-filling in cement paste and air voids also contains the ASR gel being incorporated with Ca content, such as C-Na/K-S-H and C-S-H gel.

C-Na-S-H and Na-S-H gel consists of layered structure identified by Q^2 or Q^3 forms, respectively and can hold an interlayer water [9], resulting in remarkable swelling. In contrast, C-S-H also has the layered structure, but shows a little swelling. These results and discussions supported T. Ichigawa's model of ASR expansion [13] that a rigid reaction rim is tightly packed around reactive sites due to the reaction between dissolved Si and Ca ions; the stable rigid rim consisted of C-S-H around reactive sites prevents the formation of C-Na/K-S-H and acts as a porous zone, which allows the invasion of alkali (Na or K) and OH but prevent the penetration of Ca ions. When CH is completely consumed, the stable C-S-H might be reacted with alkali ions to promote the formation of C-Na/K-S-H, and then highly reactive of alkali induces the OH passing trough the reaction rim generates the accumulated pressure over the tolerance of aggregate, causing the cracking of aggregates and the surrounding cement paste [14]. The accumulated pressure due to swelling of gel exerts the cracks, expansion and loss of strength on concrete structure. It is believed that the C-Na/K-S-H gel with low Ca/Si ratio has a potential for swelling [15]. Concerning the swelling of gel to cause cracks and expansion of concrete, it is necessary to study additional information and eventually lead to the identification of swelling mechanisms of the ASR gel incorporated with Ca.

(A)

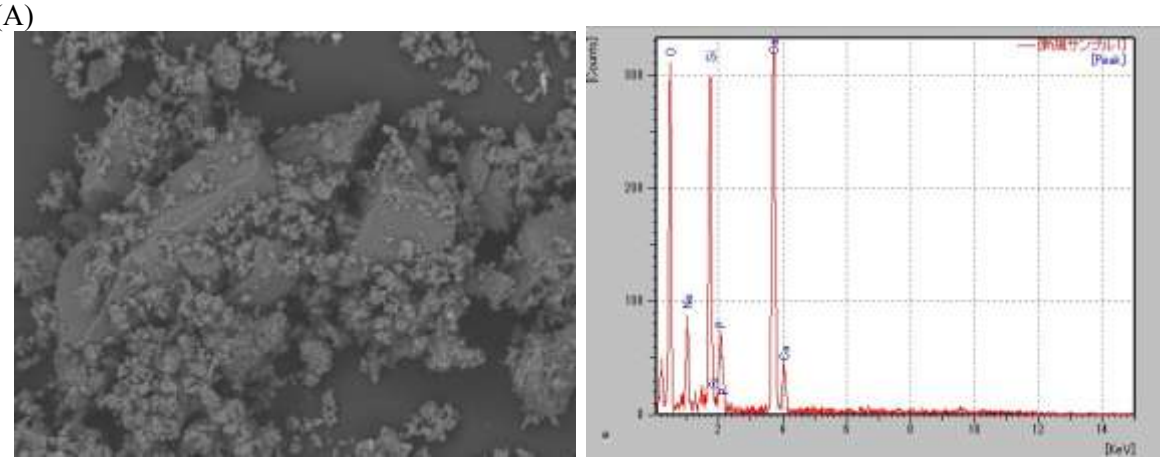

(B)

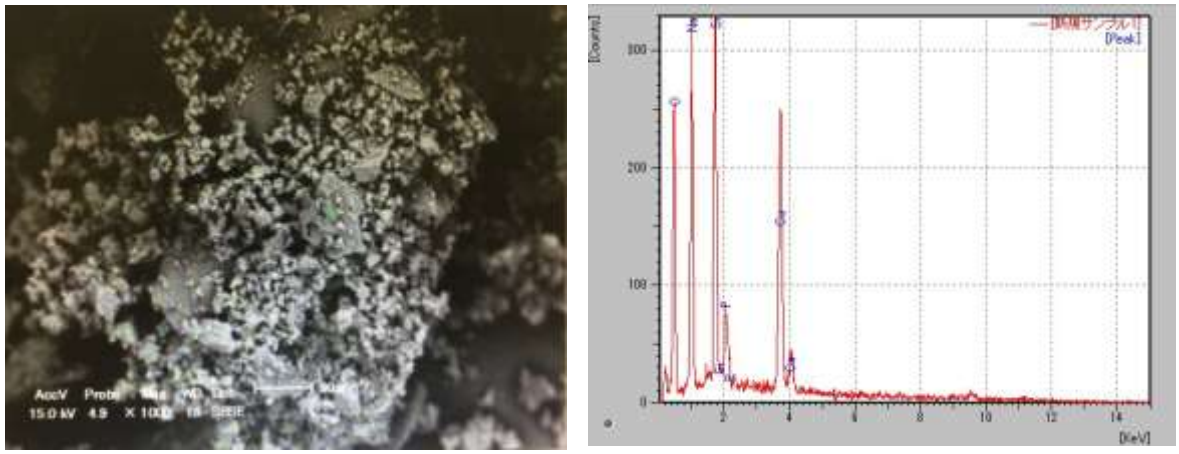

(C)

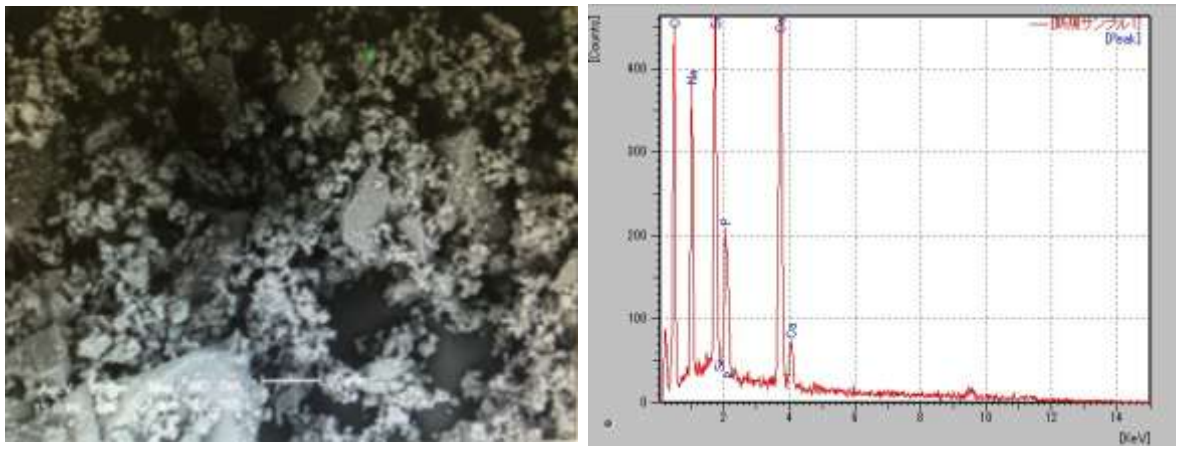

Fig. 4.17 SEM images of pyrex glass from the fine solids of PG+NH+CH (70°C): (A) at 24 h, (B) at 72 h and (C) at 168 h.

REFERENCES

[1] T. Kim, J. Olek. Chemical sequence and kinetics of alkali-silica reaction part I Experiment. J Am Ceram Soc, 97(7) (2014, 2195-2203.

[2] X. Hou, R J. Kirkpatrick. Structural investigation of alkali silicate gels. J Am Ceram Soc 2005; 88 (4): 943-949.

[3] X. Hou, L.J. Struble, R.J. Kirkpatrick. Formation of ASR gel and the roles of C-S-H and portlandite. Cem Concr Res 2004;34(9):1683-1696.

[4] T. Kim, J. Olek. Chemical Sequence and Kinetics of Alkali–Silica Reaction Part II. A Thermodynamic Model, J. Am. Ceram. Soc. 2014; 97(7) pp.2204–2212.

[5] X.D. Cong, R.J. Kirkpatrick. 29Si MAS NMR spectroscopic investigation of alkali silica reaction product gels. Cem Concr Res 1993 ; 23(4):811-823.

[6] M.C. Morris, H.F. Mcmurdie, E.H. Evans, B. Paretzkin, H.S. Parker., N.C. Panagiotopoulos. Standard x-ray diffraction powder patterns section 18-data for 58 substances. JCPDS, National Bureau of Standards, Washington DC 1981; 61-62.

[7] H. Wang, J.E. Gillott. Mechanism of alkali-silica reaction and the significance of calcium hydroxide. Cem Concr Res 1991;21:647-654.

[8] T. Katayama. Late-expansive ASR in a 30-year old PC structure in eastern Japan.14th ICAAR 030411-KATA-05. Austin;Texas: USA:2012.

[9] T. Ichikawa, M. Miura. Modified model of alkali-silica reaction. Cem Concr Res. 2007;37(9):1291–1297.

[10] S. Multon, A. Sellier, M. Cyr. Chemo-mechanical modeling for prediction of alkali silica reaction (ASR) expansion. Cem Concr Res 2009;39:490-500.

[11] X.Cong. Silicon-29 and oxygen-17 nuclear magnetic resonance investigation of the structure of calcium-silicate-hydrate (cement), University of Illinois at Urbana-Champaign 1994.

[12] B. Lothenbach, A. Nonat "Calcium Silicate Hydrate: Solid and Liquid Phase Composition." Cem Concr Res, 78 (2015), 57-70.

[13] F. Brunet, Ph. Bertani, Th. Charpentier, A. N.onat, J. Virlet (2004) "Application of ^{29}Si Homonuclear NMR Correlation to Structure Studies of Calcium Silicate Hydrate, Physical Chemistry B., 108, 15494-15502.

[14] Andreas L., Gwenn L.S., Frank W., Daniel R.and Barbara L. 2010; Alkali-Silica Reaction' the Influence of Calcium on Silica Dissolution and the Formation of Reaction Product. *American Ceramic Society*, 94(4), 1243-1249.

[15] John L.P., Angel P., Caijun S. Advances in Understanding Alkali-activated Materials, Cem Concr Res, 78 (2015), 110-125.

CHAPTER 5 SIMULATION OF PHASE ASSEMBLAGE

According to the previous study by Kim and Olek [1], they described the manuscript to predict the chemical sequence of ASR process by development the thermodynamic model, closed to reacting system. The application of the commercial geochemical modeling software, Geochemist's Work-bence (GWB) was used to simulate. In their method, the ASR process was assumed to be surface-controlled. This was because the activation energy of the surface-controlled reaction (i.e. 96,78 and 42-44 kJ/mol) is higher than that of the diffusion-controlled reaction (21 kJ/mol). Refer to dissolution of silica minerals is influenced by many factors, including specific surface are of mineral, reaction temperature, the pH value of the solution, the type and concentration of ionic species present, and the degree of saturation with respect to the dissolving mineral or to the secondary minerals. Therefore, they presented main silica dissolution and the formation of kinetic rate law for the dissolution of silica mineral. In thermodynamic modeling of chemical kinetics of the ASR process, this involves the chemical equilibrium of any species of solid. Therefore, the equilibrium constants for the reactant and the solid products used in their model illustrated in **Table. 5.1**.

In present work, the same concept with reference of [1] was used in order to demonstrate the ASR sequence for reactive siliceous materials such as chert aggregats and pyrex glass. the chemical sequence of ASR is verified by a thermodynamic model for the mixture of reactive silica mineral, calcium hydroxide and alkali hydroxide solution. Using their thermodynamic model, the prediction of precipitated species by the mass action equation with equilibrium constants at 70 and 80°C for several ASR products should also be simulated using PHREEC program. Firstly, due to SEM/EDX results described in Section 4.3, the $Ca_5SiO_6H_{21}O_{27.5}$ (Ca/Si ratio equal to 0.83) was selected as chemical compounds of C-S-H to simulate the phase assemblage of ASR formed in the presence of CH under temperature of 80°C for Yo+NH+CH compared to Se+NH+CH. The prediction of its precipitation was made using PHREEQC program at the initial concentrations of Ca and Si as shown in **Table 5.2**. Secondly, the prediction of precipitated species by the mass action equation with equilibrium constants at 80°C for several ASR products of Yo+NH+CH should also be simulated using PHREEC program. With less content of CH in ASR model system as described in section 4.2.2, we observed the dissolution rate of Yo+NH+CH at different CH contents. It was found that high contents of dissolved Si was determined in liquid sample with decreasing the CH contents in system (See **Fig. 5.1**). Therefore, the simulation of Yo+NH+CH_0.77 was conducted to estimate the formation of ASR by considering the estimated ions concentration of Si and Ca from XRD. Finally, the presence of precipitated species compared between Yo+NH+CH and PG+NH+CH under temperature of 70°C was simulated using their thermodynamic model. The initial concentrations of Ca and Si for simulation of Yo and PG samples at temperature 70°C show in **Table 5.3** and **Table 5.4**, respectively

Table 5.1 The equilibrium constants for the reactant and the solid products used in model [1]

	Temperature		
Equilibrium constant	38°C	55°C	80°C
log K_1 (cristobalite)	−3.276	−3.072	−2.827
log K_2 (C–S–H)	62.166	59.933	57.046
log K_3 (C–K–S–H)	66.230 < log K_3 < 66.761 average: 66.496	64.211 < log K_3 < 65.300 average: 64.756	61.573 < log K_3 < 62.489 average: 62.031
log K_3 (C–Na–S–H)	65.946 < log K_3 < 67.163 average: 66.555	64.086 < log K_3 < 65.051 average: 64.569	61.495 < log K_3 < 62.735 average: 62.115
log K_4 (K–S–H)	log K_4 < 5.005 95% value: 4.755	log K_4 < 5.028 95% value: 4.777	log K_4 < 5.014 95% value: 4.763
log K_4 (Na–S–H)	log K_4 < 4.600 95% value: 4.370	log K_4 < 4.488 95% value: 4.489	log K_4 < 4.778 95% value: 4.539

Table 5.2 Ions concentration of Yo+NH+CH and Se+NH+CH

Reaction time (day)	Yo+NH+CH		Se+NH+CH	
	Free Si ions	Free Ca ions	Free Si ions	Free Ca ions
1	92.92	10.97	74.405	12.72
3	92.88	14.03	84.63	12.63
5	81.61	13.33	87.40	12.10
7	103.68	13.31	90.56	12.56
10	104.2	13.36	93.25	13.46
14	93.80	16.3	91.77	13.48

Note: Values of free ions (mmol/L) computed using Q-XRD data.

Table 5.3 Ion concentrations of Yo+NH+CH (70°C)

Reaction time (day)	Free Si ions	Free Ca ions
3	60.34	13.10
7	58.34	15.12
10	68.41	14.20
14	54.72	16.89
20	76.17	14.20
24	76.19	15.15

Note: Values of free ions (mmol/L) computed using Q-XRD data.

Table 5.4 Ions concentration of PG+NH+CH (70°C)

Reaction time (h)	Free Si ions	Free Ca ions
3	7.36	4.08
7	8.90	6.61
10	10.40	7.20
14	11.20	8.76
24	13.77	10.47
72	17.45	14.07
168	31.4	15.3

Note: Values of free ions (mmol/L) computed using ^{29}Si-NMR (Si ions) and Q-XRD data at 70°C (Ca ions)

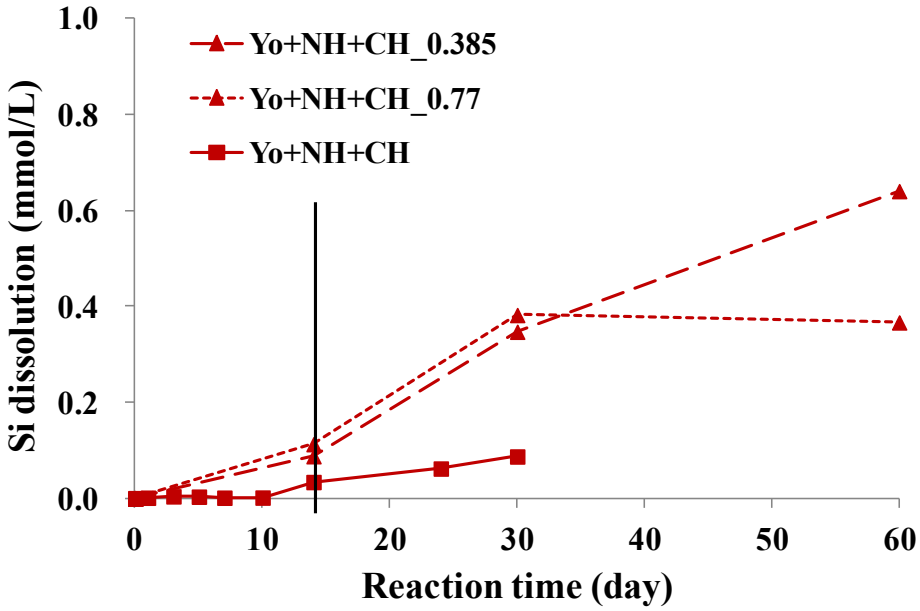

Fig. 5.1 The content of dissolved Si under temperature of 80°C for Yo+NH+CH at varying CH contents

5.1 ESTIMATION OF ASR PRODUCT OF REACTIVE CHERT

In the previous section, XRD, SEM/EDX and ^{29}Si-NMR results show that the formation of ASR is compatible to tobermorite type C-S-H. Kim et al. [2] reported the similar results, and strongly suggested that the reaction product obtained in the presence of CH was identical to tobermorite type C-S-H with Ca/Si ratio approximately 0.833. According to their evidence and our SEM/EDX results, we selected $Ca_5SiO_6H_{21}O_{27.5}$ (Ca/Si ratio equal to 0.83) as chemical compounds of C-S-H to simulate the phase assemblage of ASR formed in the presence of CH. The prediction of its precipitation was made using PHREEQC program at the initial concentrations of Ca and Si as shown in **Table 5.2**. After the simulation at 80°C, mole values of $Ca_5SiO_6H_{21}O_{27.5}$ were computed from 0.0022 to 0.0032 for both the Yo and Se samples. From simulation data, one can confirm the precipitation of C-S-H with the Ca/Si 0.83 ratio. The results were in good agreement with the experimental data. As the equilibrium condition, the calculations (Q-XRD combined with the loss by ignition measurements) and simulation (PHREEQC program) of the phase assemblage are shown as plots, with straight connecting lines in **Fig. 5.2**. It must be noted that the calculated data (Tobermorite type C-S-H) is double of the simulated data (assumed to be $Ca_5SiO_6H_{21}O_{27.5}$). The calculated and simulated data showed similar trends, indicating that the samples were close to or at the condition of ASR precipitated as C-S-H with a Ca/Si ratio of 0.83.

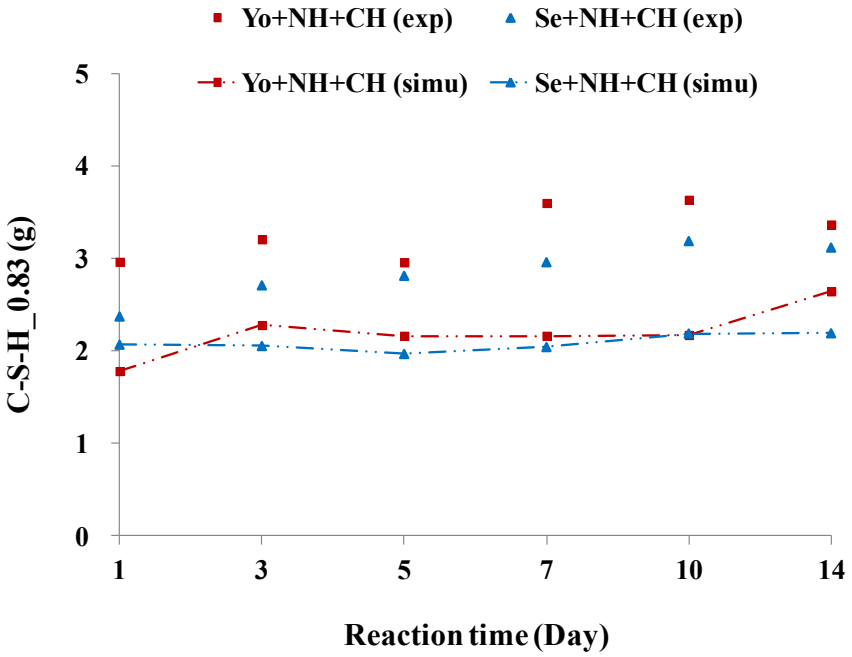

Fig. 5.2 Plot of experimental and simulated data in mass of C-S-H_0.83: experimental data, exp (individual points), simulated data by PHREEQC, simu (dash-line).

5.2 CHEMICAL SEQUENCE OF ASR PRODUCTS FOR DIFFERENT SILICEOUS MATERIALS

5.2.1 Phase assemblage simulation at 80°C for reactive Yo-chert

As mentioned in above, the chemical sequence of ASR is verified by a thermodynamic model for the mixture of reactive silica mineral, calcium hydroxide and alkali hydroxide solution [1,2]. Using their thermodynamic model, the prediction of precipitated species by the mass action equation with equilibrium constants at 80°C for several ASR products should also be simulated using PHREEC program. **Fig. 5.3 (A)** demonstrates the predicted species of ASR including C-S-H_0.83, C-N-S-H, and N-S-H and the ions concentration remained in the solution of Yo+NH+CH. It should be noted that the sequence in the simulated process of ASR can be divided into 3 steps. In addition to this, as shown in **Fig. 5.3 (B)**, there is another step for ASR sequence. Refer to **Fig. 5.1**, the experimental results clearly capture the increase in dissolved Si concentration in solution of Yo-samples mixed with small contents of CH. This existence is similar to those of earlier simulation by T. Kim and J. Olek [1]. It is believed that when the supply of CH is depleted, the silica concentration in the solution starts to increase during the formation of C-Na-S-H. Following that, it eventually decreases due to the formation of ASR gel, like Na-S-H. In particular, the overall steps of ASR process for chert-aggregate are simulated and can be divided into 4 steps: (i) formation of a stable C-S-H_0.83 by reaction between dissolved Si ions from cherts and Ca ions; (ii) after complete consumption of CH, formation of C-Na-S-H by reaction between existing C-S-H, Na ions and dissolved Si ions; (iii) during the conversion of C-S-H to C-Na-S-H, Si concentration in solution keeps increasing; (iv) after that formation of Na-S-H by reaction between dissolved Si ions from chert and alkali ions (**see Fig. 5.3 (B)**). We see that the simulation model tends to give predictions of C-Na-S-H that are

parallel to the experimental data from corresponding test, as mentioned previously in XRD and ^{29}Si-NMR results. Our simulation strongly confirm previous research of the sequence of ASR [2-4].

5.2.2 Phase assemblages simulation at 70°C for reactive Yo-aggregate

The prediction of precipitated species by the mass action equation with equilibrium constants at 70°C for several ASR products should also be simulated using PHREEC program. **Fig. 5.4 (A)** it was noticed that during the formation of Na-S-H, soluble Si and Na ions seem to decrease. **Fig. 5.4 (B)**, demonstrates the predicted species of ASR including C-S-H_0.83, C-Na-S-H, and Na-S-H and the ions concentration remained in the solution of Yo+NH+CH (70°C). The overall steps of ASR process for chert-aggregate are simulated and can be divided into 4 steps as mentioned above. Addition to the remained ions in system

5.2.3 Phase assemblages simulation at 70°C for reactive PG-glass

In a previous study, the results confirmed that the formation of ASR is congruent to C-S-H_1.66, C-Na-S-H, and Na-S-H, which were observed in the insoluble products of PG solids (**Chapter 4**). However, the ^{29}Si-NMR result of PG did not clearly demonstrate the sequence of the formation with the ASR because the reactions among reactive silica mineral, calcium hydroxide, and alkali hydroxide solution occur with great rapidity. According to the thermodynamic model by Kim and Olek [1], predictions of the kinds of precipitated species by mass action equations with equilibrium constants at 70 °C for several ASR products could be estimated by using the PHREEQC program to verify the sequence of reactions for ASR of PG. **Fig. 5.5 (B)** presents the species predicted to be involved in ASR including C-S-H_1.66, C-N-S-H, and Na-S-H. The sequence of the ASR formation can be separated into 4 steps: *(i)* the formation of C-S-H_0.83 during the first 1 to 24 h; *(ii)* after 24 h, the C-N-S-H is preferentially formed with consumption of CH; *(iii)* during the conversion of the different phases, the Si content increases steadily; *(iv)* finally leading to the formation of N-S-H by the available Si and Na ions. Here phases *(ii)* and *(iii)* proceed concurrently. This was established as the ICP results after 72 h clearly capture the increase in dissolved Si in the PG+NH+CH (70°C) solution (**Fig. 5.5 (A)**) and the ^{29}Si-NMR results confirmed that the structure of the insoluble product is compatible to N-S-H (Q^2 dominant as shown in **Fig. 4.16**).

5.3 SUMMARY

From a petrographic evaluation Katayama [5] considers that ASR proceeds in the following stages: (i) formation of a reaction rim, exudation (ii) exudation of sol/gel on the reacting aggregate partially filling microporosities in reacting cement paste, (iii) cracking in the reacting aggregate accompanied by gel-filling, (iv) propagation of radial gel-filled expansion cracks from the reacting aggregate into the surrounding cement paste, and (v) precipitation of ASR gel into air voids along cracks distant from the reacting aggregate. Katayama [5] also points out that a clear reaction rim develops in early-expanding aggregate such as opaline shale, andesite, and glassy rhyolite, whereas late-expanding aggregate such as schist, gneiss, quartzite, and limestone has a rim that can also can be seen on the fracture surface but that it is less marked. The reaction rim consists of ASR gel or crystalline ASR gel products. Ichikawa and Miura [6] proposed that when reactive silica is in contact with strong alkali ions including K, Na, and Ca ions, the ASR reaction occurs spontaneously, generating an ASR gel, acting like a phase that may be congruent to Ca-rich ASR gel, at the outer surface of the reactive aggregate. Hou et al. [3] reported that dissolved silica initially reacts with CH to produce more strongly depolymerized C–S–H, similar to a pozzolanic reaction, and when Ca^{2+} is depleted, dissolved silica starts to react with existing C–S–H and forms a silica-rich polymerized C–S–H. Consequently, they also stress that finally the amount of silica dissolved in the active site further increases until starting of gelation of ASR product. Kim and Olek [2] and the authors here have also found a very similar reaction sequence.

In this chapter, the sequence of ASR of chert-aggregate can be demonstrated on the basis of thermodynamic equilibrium model using XRD ^{29}Si-NMR and SEM/EDX data. The overall stages of the ASR process for chert-aggregate can be divided into 4 steps:

(i) formation of a stable C–S–H by reaction between dissolved Si ions from chert and Ca ions;
(ii) after complete consumption of CH, formation of C–N–S–H by reaction between existing C–S–H, Na ions, and dissolved Si ions;
(iii) during the conversion of C–S–H to C–N–S–H, the Si concentration in the solution keeps increasing;
(iv) following (iii) there is formation of N–S–H by reaction between dissolved Si ions from chert and alkali ions.

For reactive glass material, the predicted species of ASR including C–S–H_1.66, C–N–S–H, and N–S–H and the ion concentrations remaining in the solution of PG +NH +CH (70°C). The sequence in the simulated process of ASR can be divided into 4 steps and the simulation model tends to give predictions of C-S-H, C–N–S–H, and N-S-H that are in agreement with the experimental data from the corresponding tests, as mentioned previously in the XRD and ^{29}Si-NMR results. Our simulation strongly confirms that the ASR sequence of PG can be divided into 4 steps same as the chert-aggregate. This also suggests that the ASR examination using PG can be used for and would be effective to understand the chemical and physical behavior of the ASR induced expansion of mortar and concrete. However, the product formation of C-S-H with high Ca/Si ratios of PG indicated the greater consumption of Ca ions as initial stage. Less Ca ion available in the system attributes to the greater content of C-Na-S-H and Na-S-H formation. This phenomena supports the significant expansion of mortar containing PG that is strongly higher than that of mortars containing Yo or Se (further information in Chapter 6).

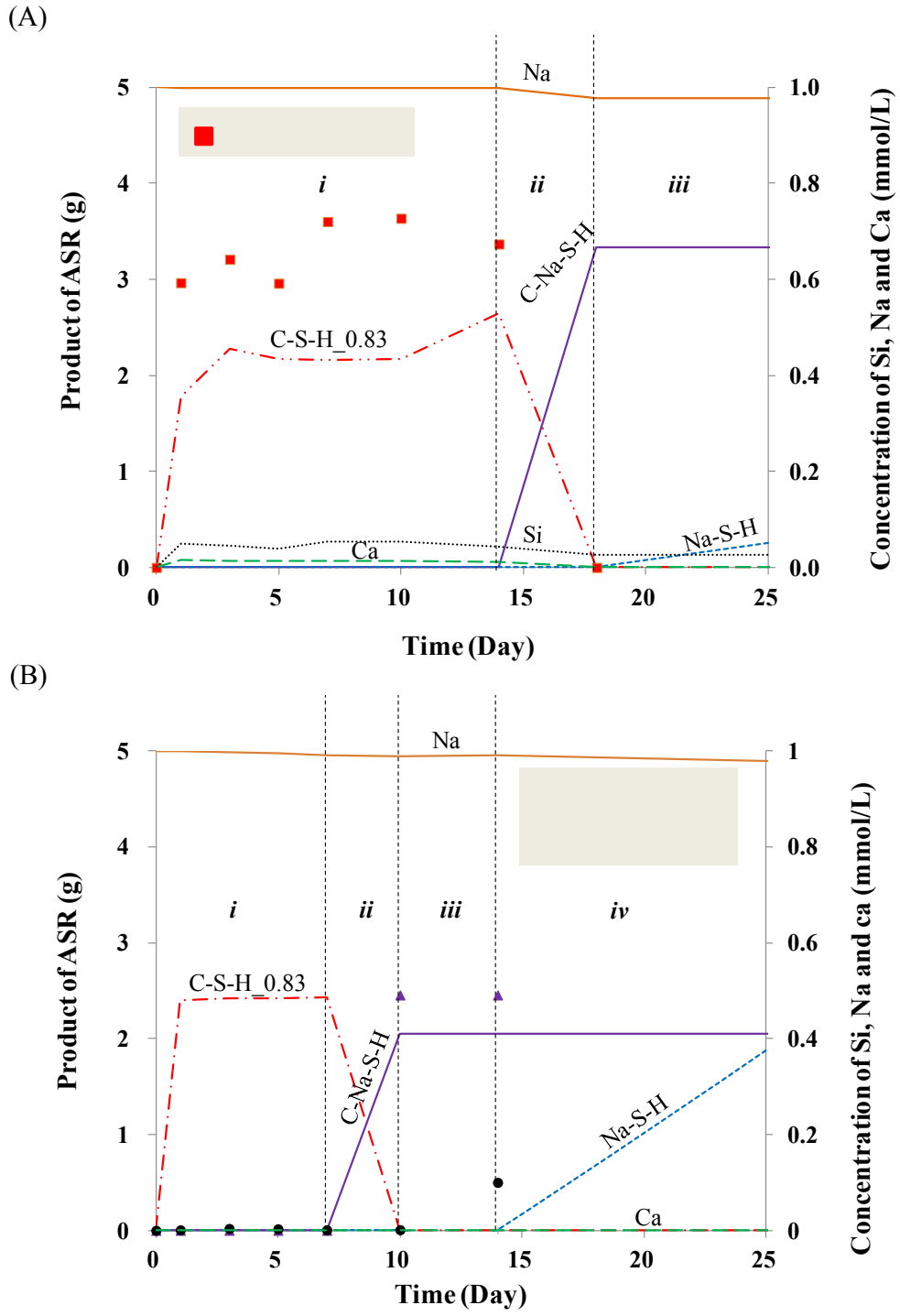

Fig. 5.3 Plot of experimental and simulated data: line-simulated results and individual points-experimental data. (A) The simulation of ASR products including C-S-H,C-Na-S-H and N-S-H) and ions concentration remained in the solution of Yo+NH+CH by PHREEQC; (B) The observed data (C-Na-S-H, dissolved Si and Ca ions remained in solution) and simulated data (C-Na-S-H, N-S-H and C-S-H_0.83) of Yo+NH+CH_0.77.

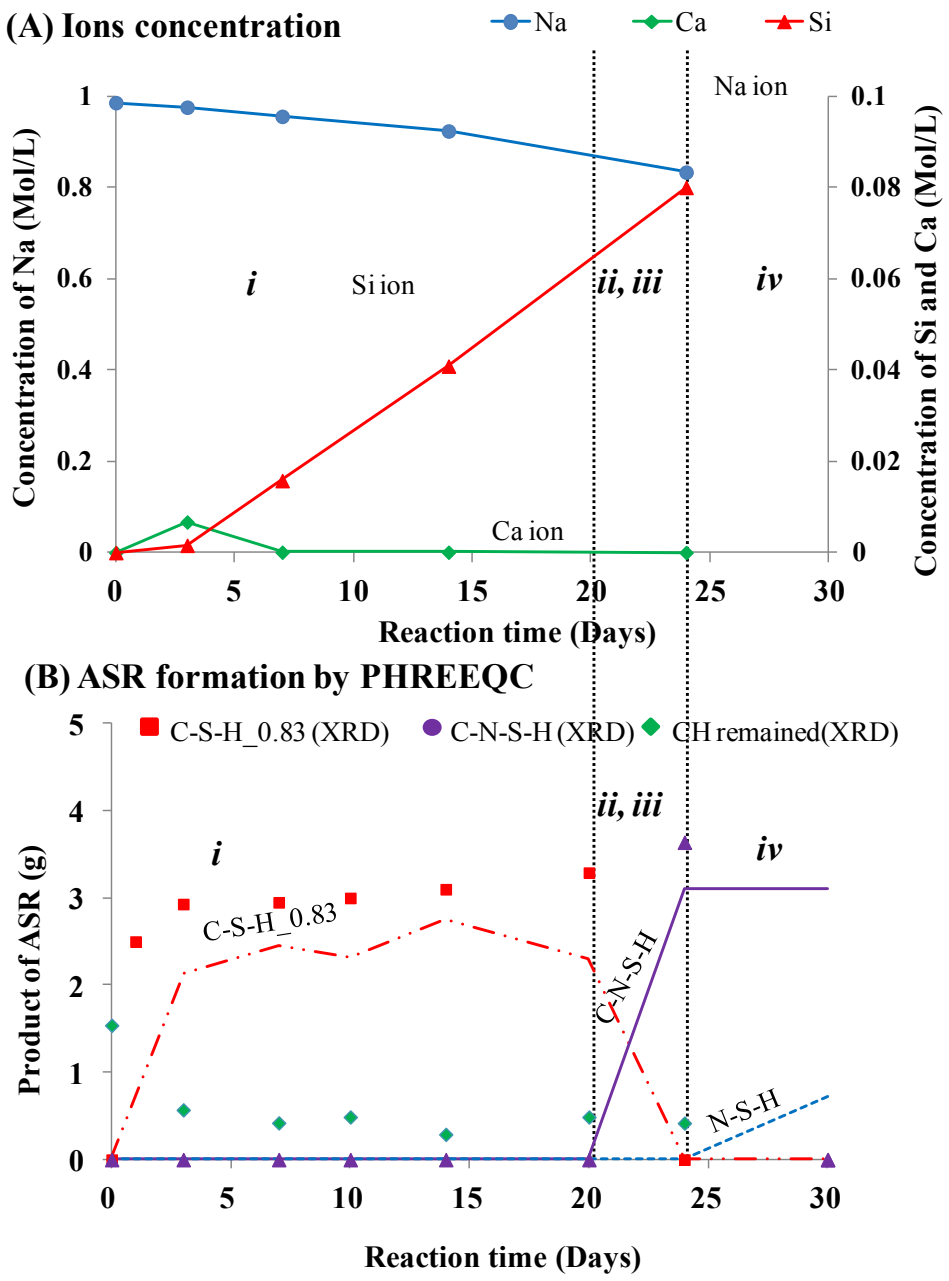

Fig. 5.4 Plot of experimental and simulated data: (A) ion concentrations remaining in the solution of Yo+NH+CH (70°C). (B) The simulation of the ASR products include C-S-H_0.83,C-N-S-H, and N-S-H by PHREEQC

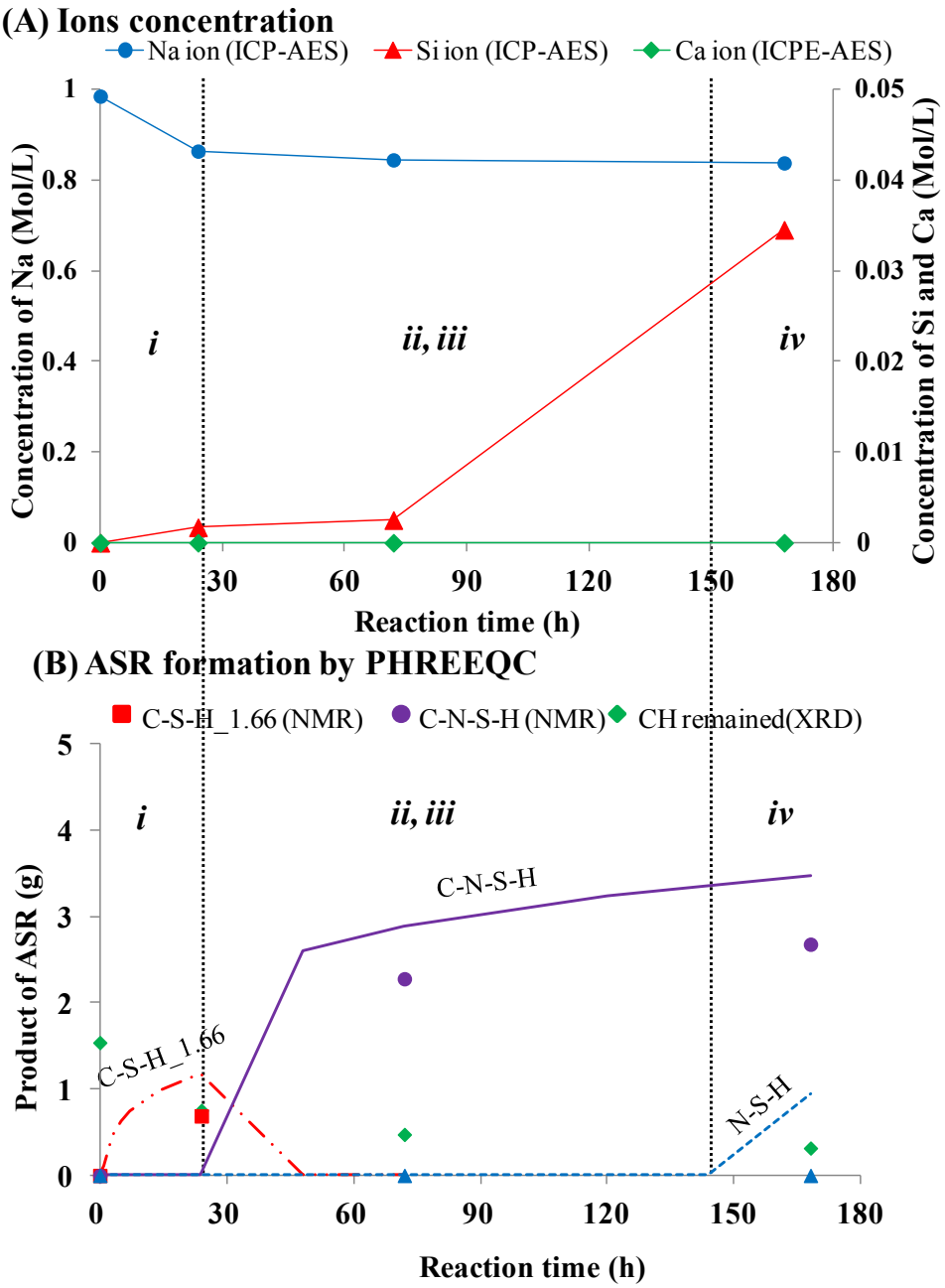

Fig. 5.5 Plot of experimental and simulated data: (A) ion concentrations remaining in the solution of PG+NH+CH (70°C). Si (Exp.) (B) The simulation of the ASR products include C-S-H_1.66,C-N-S-H, and N-S-H by PHREEQC

REFERENCES

[1] T. Kim, J. Olek. Chemical Sequence and Kinetics of Alkali–Silica Reaction Part II. A Thermodynamic Model, J. Am. Ceram. Soc. 2014; 97(7) pp.2204–2212.
[2] T. Kim, J. Olek. Chemical sequence and kinetics of alkali-silica reaction part I Experiment. J Am Ceram Soc 2014; 97(7):2195-2203.
[3] X. Hou, J.S. Leslie, R.J. Kirkpatrick (2004) "Formation of ASR and the C-S-H and Porlandite." *Cement and Concrete Research*, 34 (9), 1683-1696.
[4] X. Hou, R J. Kirkpatrick. Structural investigation of alkali silicate gels. J Am Ceram Soc 2005; 88 (4): 943-949.
[5] T. Katayama. Late-expansive ASR in a 30-year old PC structure in eastern Japan. Proceedings of 14th ICAAR 030411-KATA-05. Austin;Texas: USA:2012.
[6] T. Ichikawa, M. Miura. Modified model of alkali-silica reaction. Cem Concr Res, 37(9) (2007), 1291–1297.

CHAPTER 6 ASE-INDUCED EXPANSION OF MORTAR

According to Iwatsuki and Morino [1], they examined the expansion of mortar bar with chert aggregates according to JIS A1146. Chert aggregates including Yo and Se were crushed to obtain the particle sizes as specified in JIS A1146 [2], which is the same as ASTM C227 [3] except for size of mortar bar. Ordinary Portland cement having an equivalent Na_2O content of 3.94 kg/m^3 (0.51%) were used for mortar bars test. The alkali contents (equivalent Na_2O) in mortar were adjusted to 7.27 kg of alkali per m^3 (1.2 %) for Se and Yo, by adding NaOH in the mixing water. Mortars were prepared in prismatic specimens with sizes of4x4x16 cm. A water-cement (w/c) ratio of mortar is 0.50 and sand to cement ratio is 2.25. After demolding, the mortar prisms were kept in a sealed container at 40°C. At each measurement day (7, 14, 21, 28, 56 days and until 500 days), the expansion was measured on the mortars using a length comparator in the scale millimeter method. The mortars containing Yo or Se cherts with the alkali content of 1.2%. **Fig. 6.1 (A)** presents the expansion data of mixtures gradually increased with increasing the content of reactive chert aggregates. The highest expansion of 0.22% was observed in Yo (scattered plot), while the expansion of Se increased to 0.17 % (scattered plot with line) at the reaction time of 91 days, especially for long reaction time till 500 days **Fig. 6.1 (B)**. For this result, it was noted that Yo and Se are the same type of reactive chert but the expansion-time relationship between Yo and Se was significantly different. In the model system, the same chert (Yo and Se) as reference [1] were used. As described in **Chapter 4,** the change of concentrations of dissolved Si with time (**Figs. 4.2-4.3**), the highest amount of dissolved Si was also observed in solution of Yo-sample. Our results of the dissolution rate of silica supported the data of expansion found in [1]. It can be deduced from both studies that, for the aggregate used, Yo-chert has a higher potential ASR reactivity than Se-chert. This is because the high rate of dissolution contributes to the greater ASR product, in which the ASR induced cracking caused by the swelling of ASR gel by water absorption when the tensile stress due to swelling is beyond the tensile strength of aggregate or cement paste. Thus, the ASR reactivity of reactive aggregate might be related to the ASR-induced expansion.

The main task of this chapter is to associate the dissolution rate of soluble silica from certain aggregates in this model system associated with ASR-induced expansion. Based on Arrhenius law, three parameters including the constant rate at 40°C (k), the dissolution rate of soluble silica at 40°C and the activation energy (E_a) could be determined by considering the dissolution rate of soluble silica at different temperatures. The rate of dissolution at high temperatures (60, 70 and 80°C) in model system can be extrapolated to low temperature at 40 °C. These results will help us to explain the different in mortar expansion between Yo-and Se-cherts that observed by [1]. Additionally, for other siliceous materials, we selected Pyrex glass (PG) and Silica sand (SS) represents the highly reactive materials and the non-reactive aggregate, accordingly. PG and SS were prepared conforming to the method of ASTM C277 as described in **Chapter 3**. Expansion measurement made at constant temperatures of 40°C, using two alkali constants (0.6 and 1.2%), allows the ASR reactivity of PG to be investigated. Firstly, the role that alkali contents has on ASR expansion rates of mortar bars at 40°C will be shown. After that a quantitative consideration was given to the damage of mortar from a point of view of the relationships among the expanded mortar, the dissolution rate of soluble silica, and the gel composition of each reactive-siliceous materials. Subsequently, the activation energy of the dissolution reaction may provide an avenue to estimate the ASR reactivity of each siliceous compounds. Ultimately is the EPMA analysis to investigate the microstructure of affected mortar due to ASR.

(A)

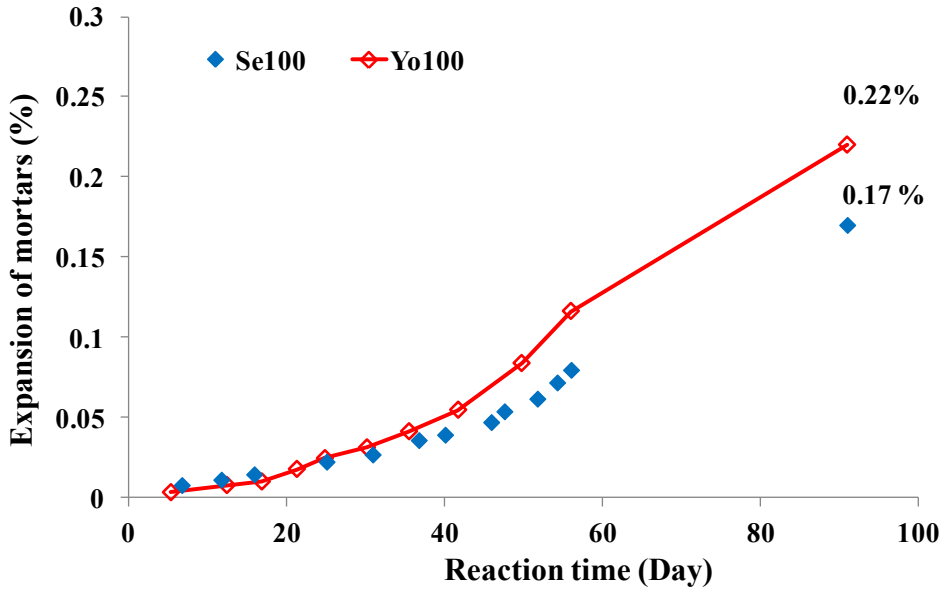

(B)

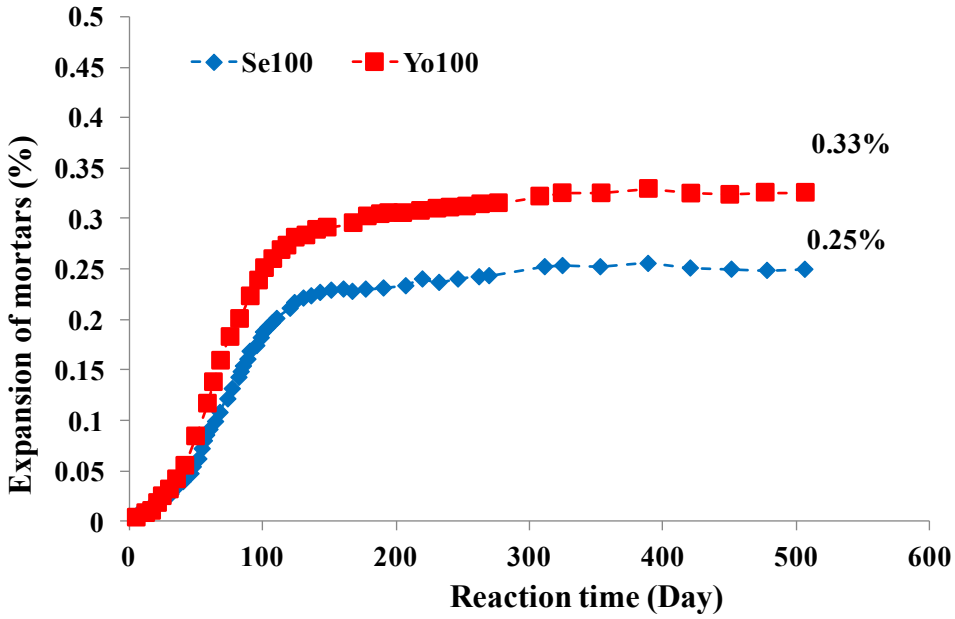

Fig. 6.1 Expansion of mortar bars with 1.2% alkali containing reactive cherts (Yo or Se) (A) until 91 days; (B) until 500 days, percentages over the symbols are the rates of expansion at final reaction time [1]

6.1 ASR EXPANSION MEASUREMENTS

As the previous section showed the alkali content of the mortar mixtures has a significant effect on ASR, and mortars with two alkali contents (equivalent Na_2O) of 3.94 (0.6%) and 7.27 kg/m^3 (1.2%) were investigated. With the low alkali content of 0.6%, there is no appreciable expansion in either of SS100 or PG100 (marks with solid lines). In **Fig. 6.2**, the notations of mortars containing SS and PG mixed with 1.2% alkali are represented by SS100 (circle marks with dash line) and PG100 (triangle marks with dash line), accordingly. With the alkali content adjusted to 1.2%, the SS100 still showed only a low expansion of 0.016%. Only the expansion of the PG100 showed significant expansion. At 91 days of exposure, the expansion of PG100 had increased to 0.56%. These results allow the conclusion that PG is a highly reactive compound inducing expansion due to ASR.

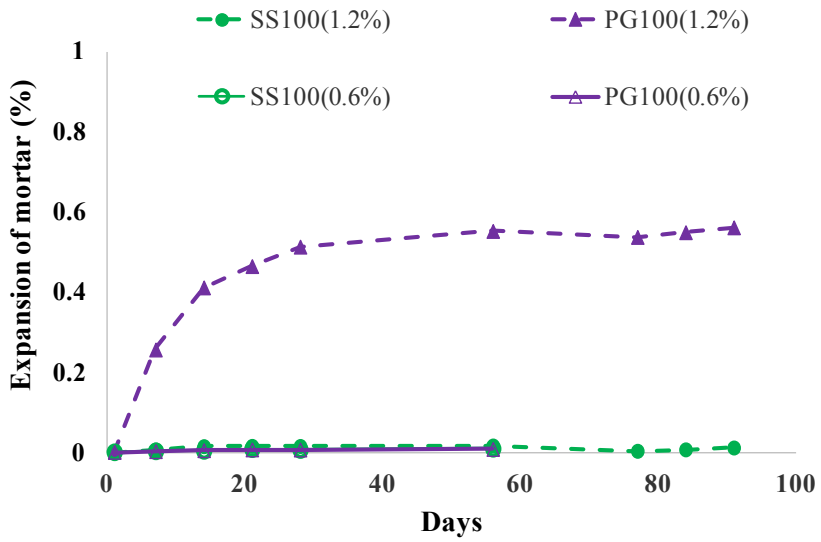

Fig.6.2 Expansion of mortar bars containing PG or SS, with two alkali contents, until 56 for 0.6% alkali and 91days for 1.2% alkali

6.2 RATE CONATANT AT 40°C CALCULATION OF SILICEOUS MATERIAL

Generally, the mechanism of ASR induced expansion can be divided into two processes: (1) Dissolved silica due to reaction between reactive silica and alkalis in pore solution cross-links, coagulates and forms ASR gel; and (2) ASR gel absorbs water molecules and expands, leading to internal stress increases and cracking of concrete. For actual concrete, there are also other chemical and physical mechanisms that have to be considered [4]: (1) alkali diffusion into the aggregate particles; (2) production of ASR gel with the increase of alkali concentration in the aggregate particles; (3) decreases in the alkali concentration of the cement paste with the progress of the alkali consumption by the ASR gel; (4) displacement of a part of the ASR gels in the cement paste porous zone surrounding the reactive aggregate particles.

Glasser and Kataoka [5] reported that formed ASR gels permeate through a part of the connected porous volume between aggregate and cement paste and fills a part of the connected porosities [6]. If the volume of gel exceeds the volume of the connected porosity, swelling occurs as the additionally formed ASR gel can no longer move into porosities. As a result gel exerts pressure on the cement paste, which could be a cause of cracking and expansion of the concrete. According to Multon and coworkes [7-9] an imposed gel pressure P_{gel} on the surrounding cement paste can be expressed by

$$P_{gel} = K_{gel} \left\langle V_a^{gel} - V_a^{poros} \right\rangle^{+}$$

$\langle X \rangle^{+}$ is equal to X if X>0 or equal to 0 if X≤0. The V_a^{gel} term is the volume of ASR gel formed in reactive aggregates, and V_a^{porosity} is the volume of the porosity where ASR gel can migrate without causing expansion. This suggests that the ASR induced expansion could be proportional to the bulk modulus and the volume of generated ASR gel. The bulk modulus of ASR gel depends mainly on the cross-link density of the network, which could be controlled by the $Ca(OH)_2$ concentration [10]. It can be hypothesized that the cross-link density of the network is closely related to the chemical composition of the components such as C-S-H, C-Na/K-S-H, and Na/K-S-H, and then the ASR induced expansion depends mainly on the ASR gel production when the chemical sequence of the ASR gel components remain unchanged. Kawamura and Iwahori [11] showed that the final expansive pressures increase with increasing volume fraction of ASR gels produced in the mortars. A great amount of alkalis is consumed in the first stage of the reaction (neutralization) of the alkali–silica reaction process on the then large internal and external reactive silica surface areas in the reactive aggregate; this surface reaction, not leading to the formation of ASR gels except in mortars with especially alkali-rich gels. Haha et al. [12] also found a strong correlation between mortar expansion and the degree of ASR, using a BSE image technique to quantify the reactivity of the aggregate.

Based on the ASR mechanisms detailed here, it is possible to propose a phase diagram for an ASR gel by using a thermodynamic model, when the amount of dissolved silica is known. Showing that the dissolution rate of silica from reactive aggregate is controlled by the amount of generated ASR gel. It is well-known that the dissolution process of minerals are closely related to the ambient temperature. In this study we consider the kinetics of the dissolution reaction to be of the first-order and the effect of temperature on the rate constants of the reactions may be expressed by the Arrhenius equation: where the parameter A is independent of, or varies little with, temperature and E_a is the apparent activation energy [kJ/mol]. The rate at a specific temperature can then calculated for the T corresponding to the temperature in K, T_0 to 293 K (20 °C) and $R_{t,T0}$ to the rate at a time t calculated at 20 °C. In the results here, it is apparent that the dissolution curves showed increases with higher temperatures. The temperature dependence, the E_a values of each sample here can be estimated using the Arrhenius equation. The results of the calculations are detailed in **Table 6.1**. Further, **Fig. 6.3** shows the correlation between the calculated E_a values and the rate constant of dissolution at 40°C of the four aggregates showing that the difference in E_a can explain the differences in the of rate constant of dissolution of the aggregates. The lowest E_a in this investigation resulted in the highest dissolution rate constant at 40°C for PG, as detailed in **Fig. 6.3**. Reported activation energies for cement hydration generally range from 35 to 50 kJ/mol [13-16]; and for example the activation energies of alite (C_3S) from 26 to 42 kJ/mol have been reported [15,17-20]. These activation energies for the dissolution of silica from reactive aggregate such as Se, Yo, and PG are comparable to those of cement compounds which are highly reactive despite the activation energies of cement hydration being due to the dissolution as well as to the growth of nuclei and crystals of hydrates such as C-S-H and calcium sulfate hydrates.

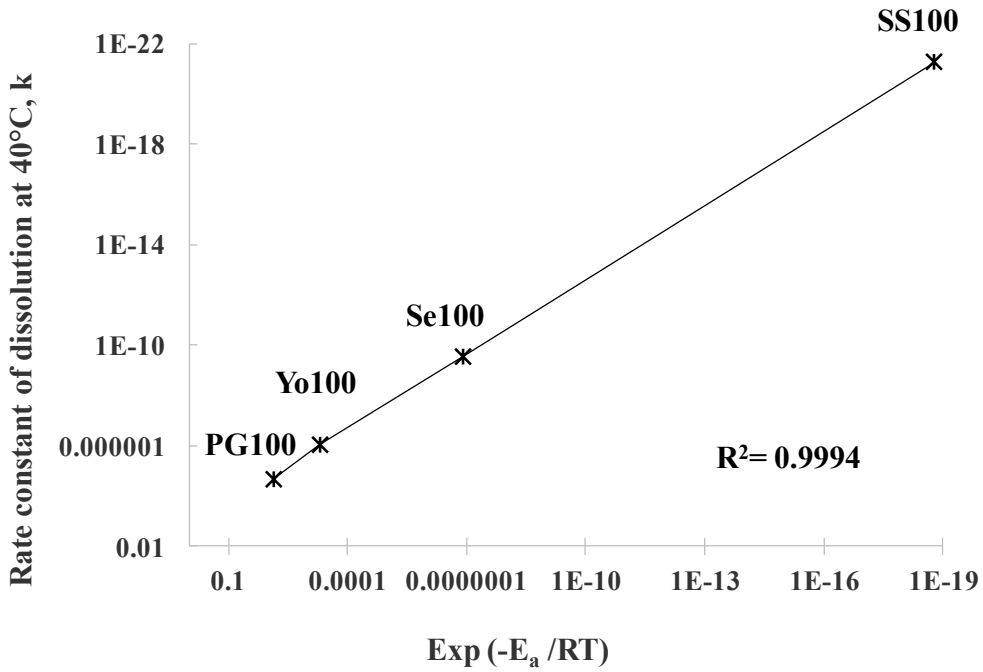

Fig. 6.3 Rate constants of dissolution at 40°C (k) versus the exponential ($-E_a/RT$) of all compounds investigated here

6.3 RELATIONSHIP BETWEEN MORTAR EXPANSION AND OBSERVED REACTIVITY ESTIMATED BY DISSOLUTION

The ASR reactivity of mortar samples at different time interval is given in **Figures 11 and 12.** When compared among 4 siliceous material at 91 day of exposure, the highest expansion due to ASR was observed in PG mortar. As expected in model system, the rate of soluble silica at various temperatures found in PG was occur rapidly. For this reason, the mortar expansion might be related to the observed reactivity estimated by dissolution rate of soluble silica (degree of reaction). The total dissolved Si at 40°C can be estimated using equation (1) from the data of the silica concentration in the liquid samples at 60, 70, and 80°C. Plots of the total amounts of dissolved Si (degree of reaction) and the expansion of mortars with 1.2% alkali for SS, Se, Yo, and PG at 40°C are plotted in **Fig. 6.4**. The result presents a good relationship between the mortar expansion and the degree of reaction. At wider non-linear domain of all data (Yo, Se and PG), it seem to belong the critical range of 0.2-0.5% of reaction degree, which corresponds to the reaction degree of reactive material determined by Haha et al. [12].

6.4 THE RELATIONSHIP OF ASR GEL FORMATION TO EXPANSION OF MORTAR USING ELAKNESWARAN'S MODEL WITH PHREEQC

In previous section, the degree of reaction for all reactive compound is in the range of 0.2 to 0.5 %. However, it was noticed that the mortar of PG did expand significantly and was totally different to mortar containing chert aggregates. As investigated in model system corresponding to simulation data, the C-S-H_1.66 existed in PG samples. With high consumption of Ca ions, available silica readily reacted with free alkali ions, producing the greater amount of C-N-S-H. This contributes to significant expansion by PG mortar. With simulation data, the weight fraction of ASR species is illustrated in **Figs. 6.5-6.6**. It is believed that high content of C-N-S-H found in PG sample seem to be metastable phase that is responsible for essential swelling of gel.

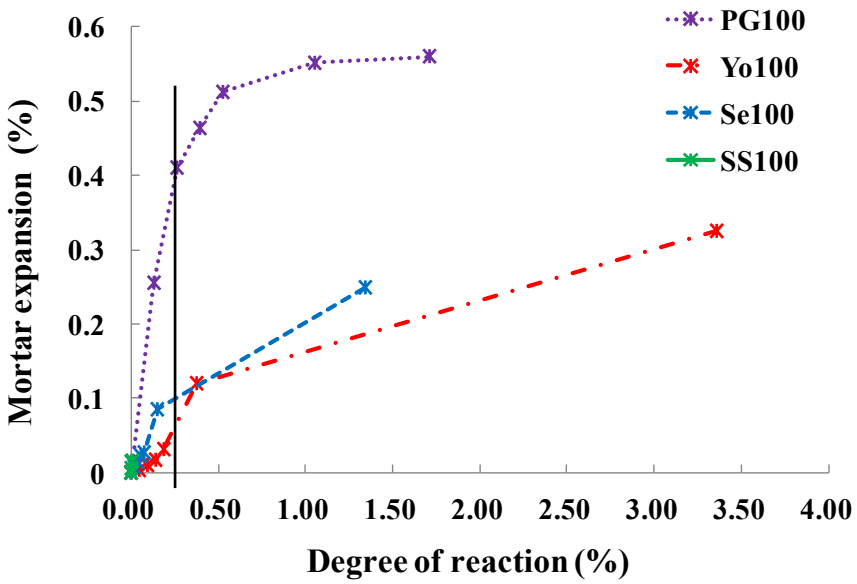

Fig. 6.4 Plot of mortar expansion (%) versus observed reactivity estimated by dissolved Si (% by weight) at 40°C and with 1.2% alkali addition at different time points

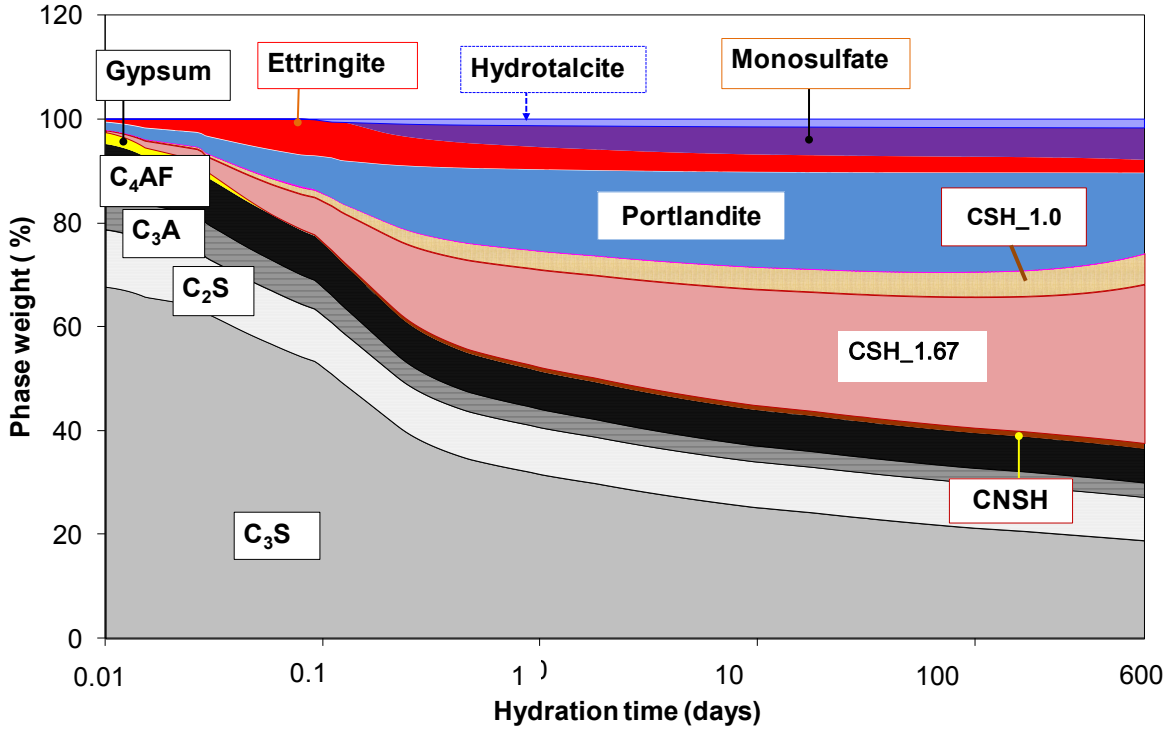

Fig. 6.4 Simulation result of Yo-100 mortar

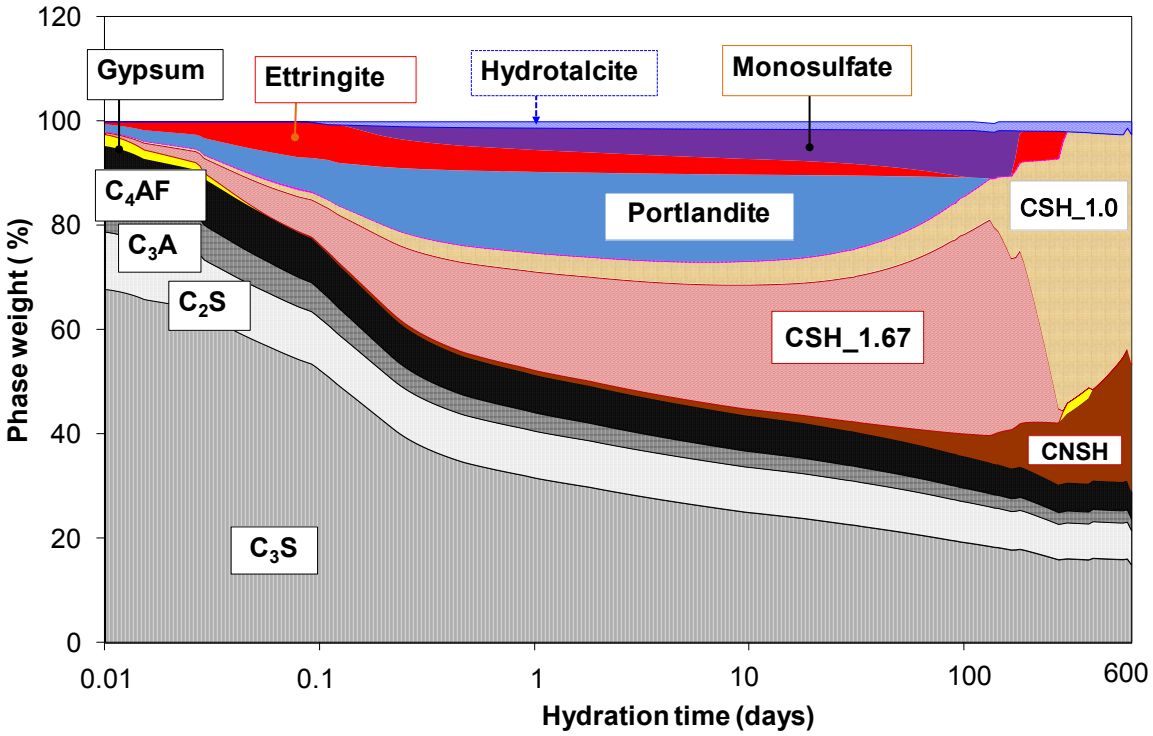

Fig. 6.6 Simulation result of PG-100 mortar

6.5 MICROSTRUCTURE OF MORTARS OBSERVED BY EPMA

Two mixtures including SS100, and PG100 were used to be investigated by EPMA. As it was described in the chapter 2, the location of ASR is inside or closed to the reactive sites such as in the cracked aggregate, in the rim between the aggregate and cement paste or in the voids of cement paste. For this reason, we randomly observed the formation of ASR in the vicinity area of reactive sites. With high powerful of EPMA analysis, not only we can identify whether the cause of expansion of mortar due to ASR reactivity or not, but also the chemical compositions of product can be estimated.

In EPMA analysis, the backscattered electron (BSE) image of the selected polished sections were shown. Backscattered electrons are primary electrons that are scattered by the specimen through more than 90 degree and re-emerge from the specimens surface. The BSE image shows atomic number contrast in the specimen because the proportion of primary electrons that are backscattered is strongly dependent on the atomic number of the specimen, which is called the backscatter coefficient. For example, in cements the calcium oxide is brighter that alite (alite is impure tricalcium silicate) and alite is brighter than belite (belite is impure dicalcium silicate) or silica or limestone. These different in brightness, or grey level (low atomic number. Therefore, the hydrated product (atomic number of Ca= 20) is brighter than the siliceous materials (atomic number of Si=14). This means to the reactive site or aggregate reflects the BSE image in grey level.

6.5.1 Microstructure results of SS100

Fig. 6.7 shows the BSE images of SS100. As detailed in **Fig. 6.7 (A)** the BSE image with x40 magnification contains the cement product due to hydration (brighter level) and the aggregate in term of grey level. When the specimen were observed with magnification of x200, as shown in Fig. 5.9 (B-C), the

formation of ASR deposited in the cracked aggregate or in the cement paste was not detected. With no ASR product, this is related to the results of SS100 with 1.2% alkali under temperature of 40°C (**Fig. 6.2**) which was extremely low lower than 0.01% of expansion. This implies that SS is non-reactive aggregate that does not cause ASR problem.

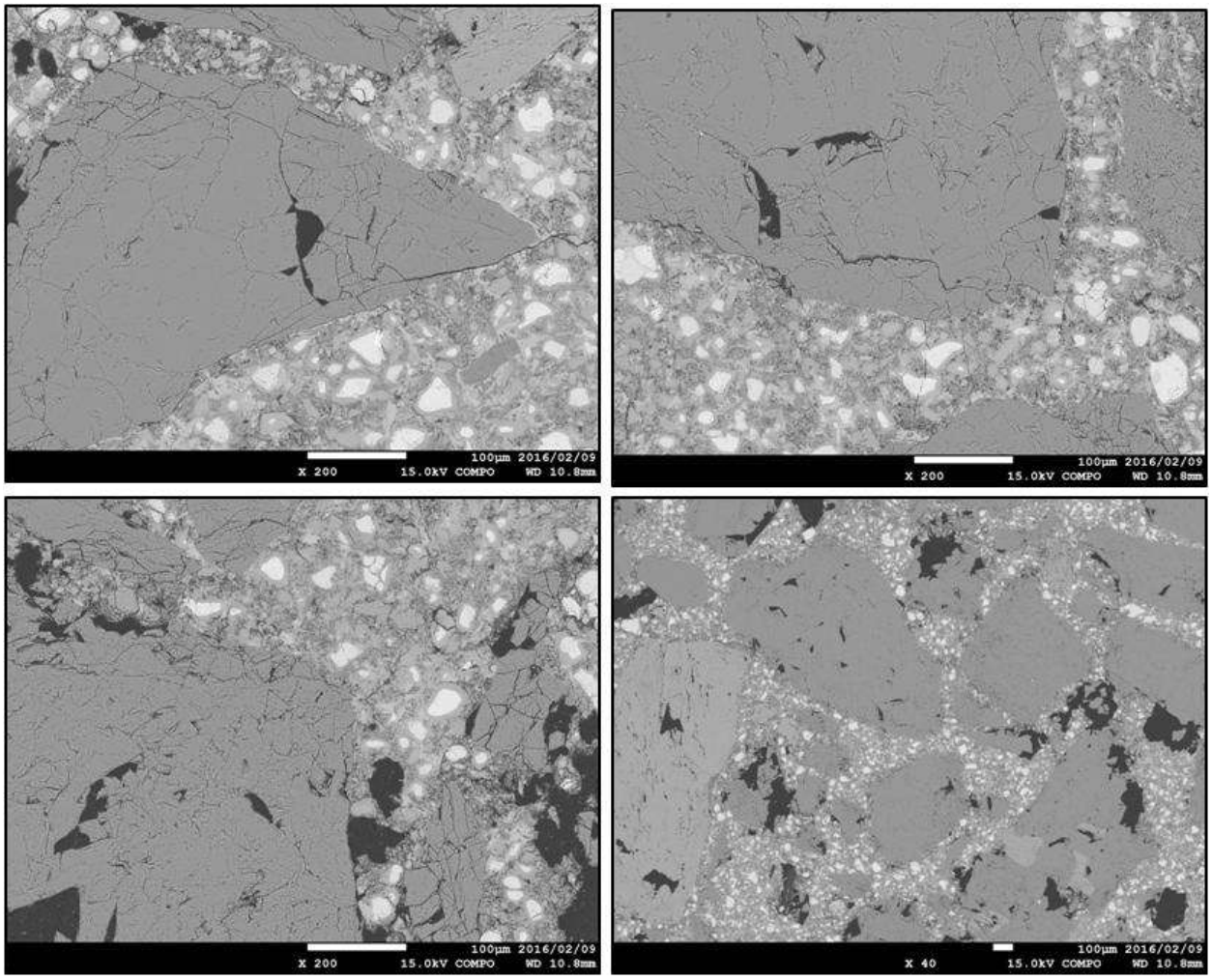

Fig. 6.7 BSE images of SS100 with alkali content of 1.2%

6.5.2 Microstructure results of PG100

The mortar sample of PG100 with alkali content of 1.2% were chosen to being observed by EPMA analysis into 2 aspects: the locations of ASR and; the chemical compositions of gel such as the Ca/Si or the Ca/(Na+K) ratios. The BSE images, as shown in **Fig. 6.8**, revealed the presence of ASR gel into the cracked PG (red cross). Moreover, it was noticed from BSE images that the ASR existed in the rim between reactive site (PG) and cement paste. An alternative, EPMA mapping method has been developed to analyze the element components such as hydration product and ASR product. **Fig. 6.9 (A)** presents the elements distribution of each material. The content of Si intensity can distinguish the SS (high intensity of Si, pink color) from PG (lower intensity of Si, red color). For ASR product, it was found that at inside the cracks of PG, high intensity of Si, Na and K with low Ca was investigated. **Fig. 6.9 (B)** revealed the chemical composition of ASR gel, which the Ca/Si ratio is lower 0.5 and the Ca/(Na+K) ratio is around

1.0. The graph in **Fig. 6.9 (B)** presents the chemical compositions by the Ca/Si ratio versus the Ca/(Na+K) of ASR and hydrated product.

Addition to **Fig. 6.10 (A)**, not only the formation of ASR appeared in cracked aggregate, but the gel deposited in the vicinity area of reactive site was also found. At this location, it was noticed that the high intensities of Si and Ca were detected with a little intensities of K and Na. As detailed in **Fig 6.10 (B)**, the Ca/Si ratio was in the range of 0.5 to 1.0 (blue cross).

6.6 SUMMARY

With equivalent Na_2O of 1.2%, this condition could produce some ASR product to cause mortar expansion. As described in chapter 2, the main factors that contribute to ASR problem are reactive aggregate, highly alkali conditions and the moisture content. It can be believed that at high temperature conditions, they accelerate the reaction of ASR, yielding the greater ASR gel in pore solution.

With ICP-AES, the rate of dissolved silica in the absence of Ca ions at different temperatures was used to estimate the constant rate of dissolution at 40°C, the dissolution rate of soluble silica at 40°C, and the activation energy (E_a) based on the Arrhenius law. With these results it can be deduced that the dissolution rate of soluble silica is related to the expansion behaviors of mortars subject to ASR, especially at the ambient temperature of 40°C. The result presents a good relationship between the mortar expansion and the degree of reaction. At wider non-linear domain of all data (Yo, Se and PG), it seem to belong the critical range of 0.2-0.5% of reaction degree of ASR. Ultimately, the activation energy of dissolution of reactive silica can also be used to evaluate the reactivity of ASR, suggesting that aggregate with activation energies below 95 kJ/mol may be sensitive to ASR.

In the EPMA analysis, the locations of ASR gel can be identified such as in the cracked aggregate or in the rim near the reactive site. This result is linked to Katayama [22] that ASR with Ca/Si ratios less than 1.00 mostly deposited in the cracked aggregate, while ASR in the cement paste has been found to be high Ca/Si ratios (0.50-1.50), as described in chapter 2 (**Fig. 2.12**). Although the reaction rim around reactive site was not observed in the present work. This was due to the less reaction time for reaction rim formation. In future, long term investigation should be taken.

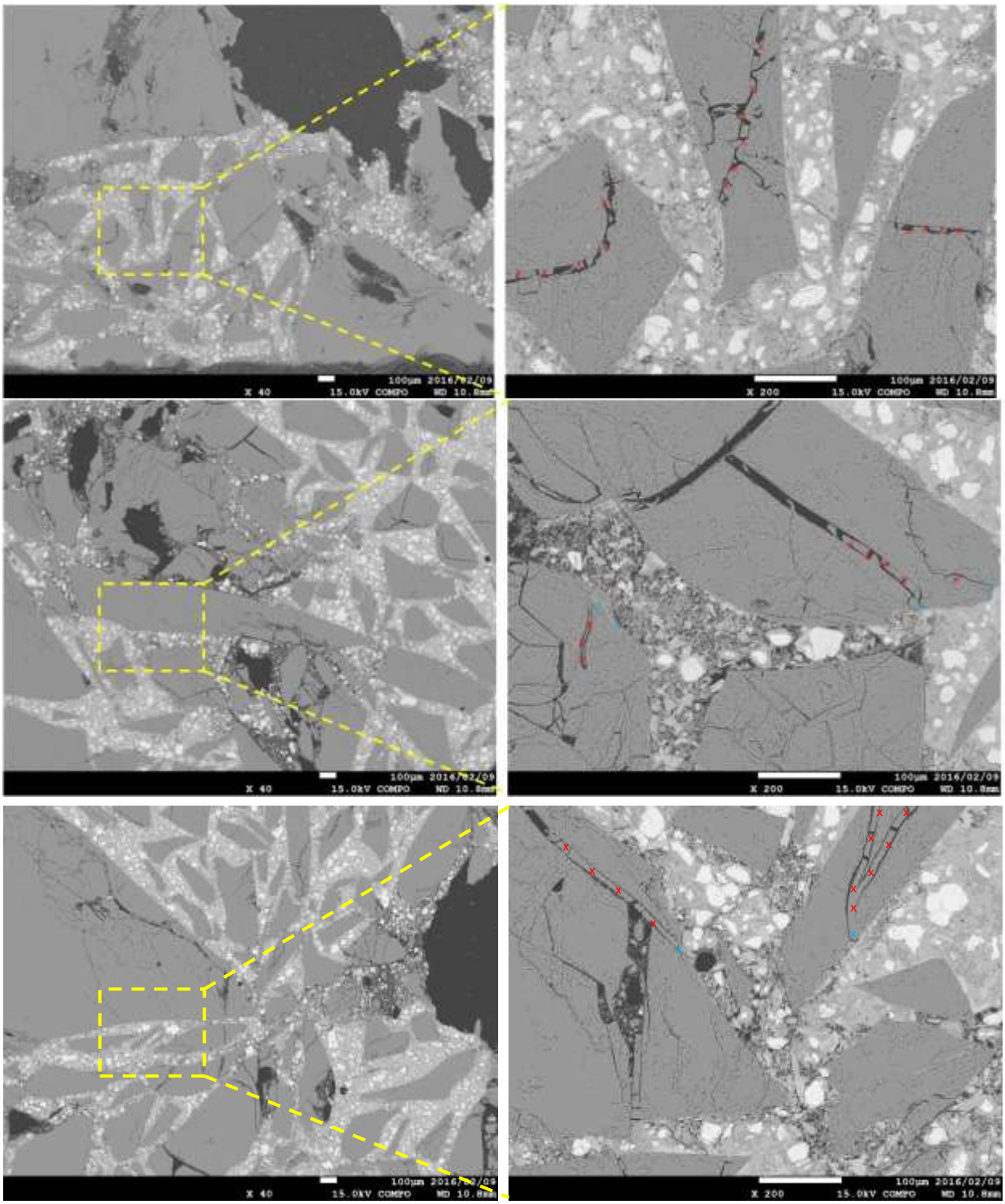

Fig. 6.8 BSE images of PG100 with alkali content of 1.2%: ASR deposited in the cracked aggregates (red cross); ASR deposited in the rim between aggregate and paste (blue cross).

(A)

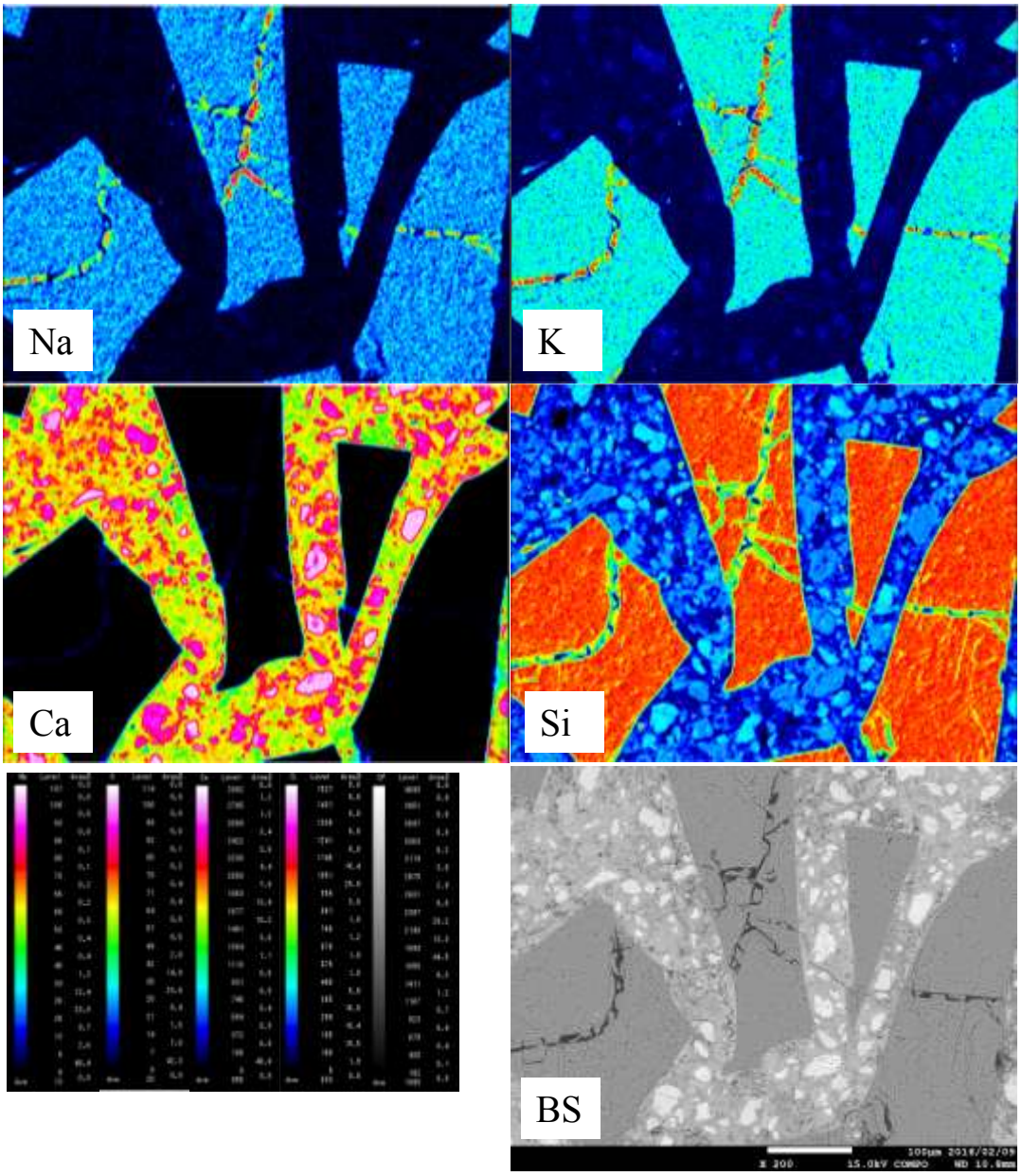

(B)

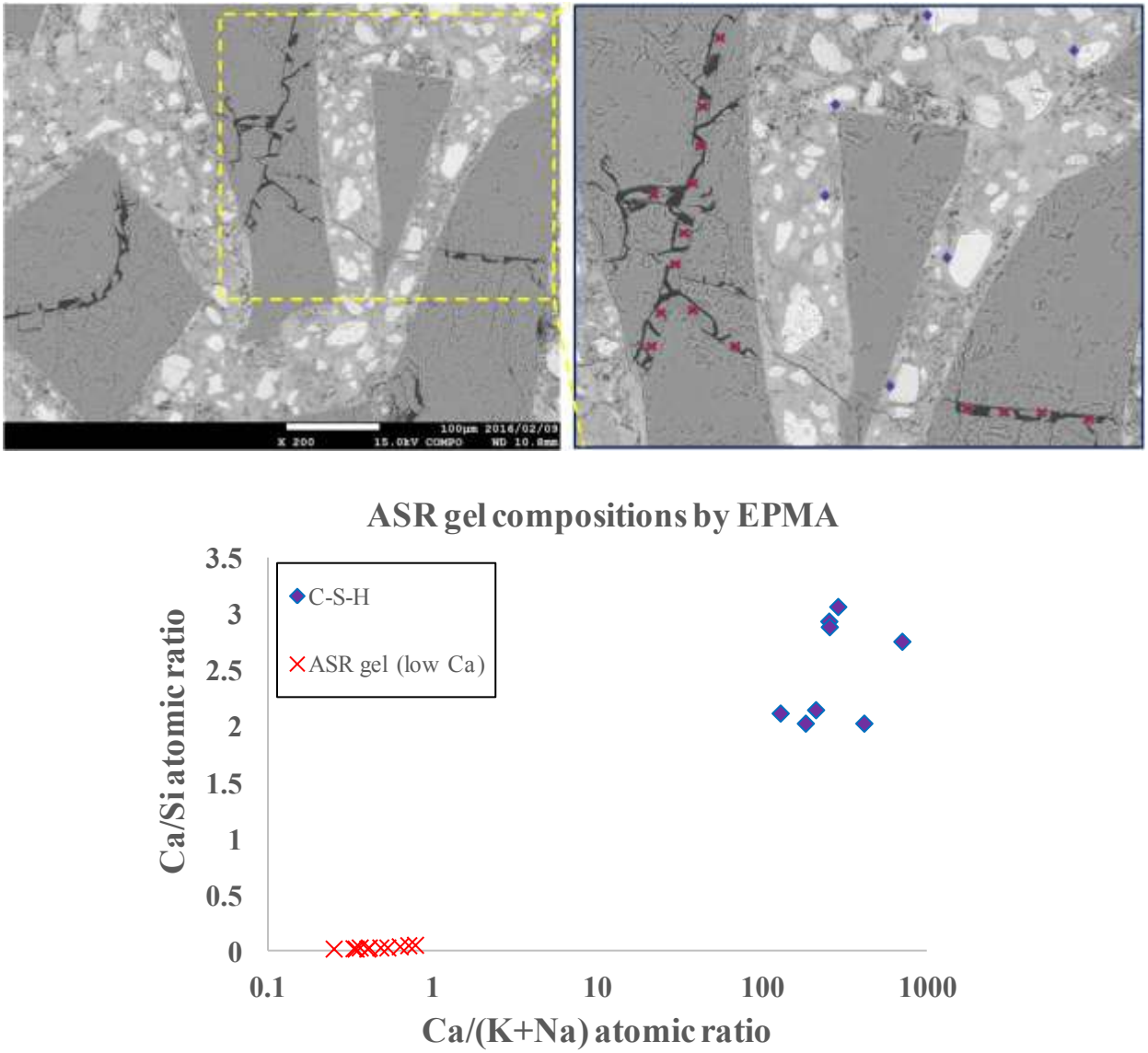

Fig. 6.9 BSE images of PG100 with alkali content of 1.2% : (A) EPMA with mapping method of; (B) Magnification of BSE images showing ASR deposited in the cracked aggregates (red cross), ASR deposited in the rim between aggregate and paste (blue cross) and the hydrated products (purple dot).

(A)

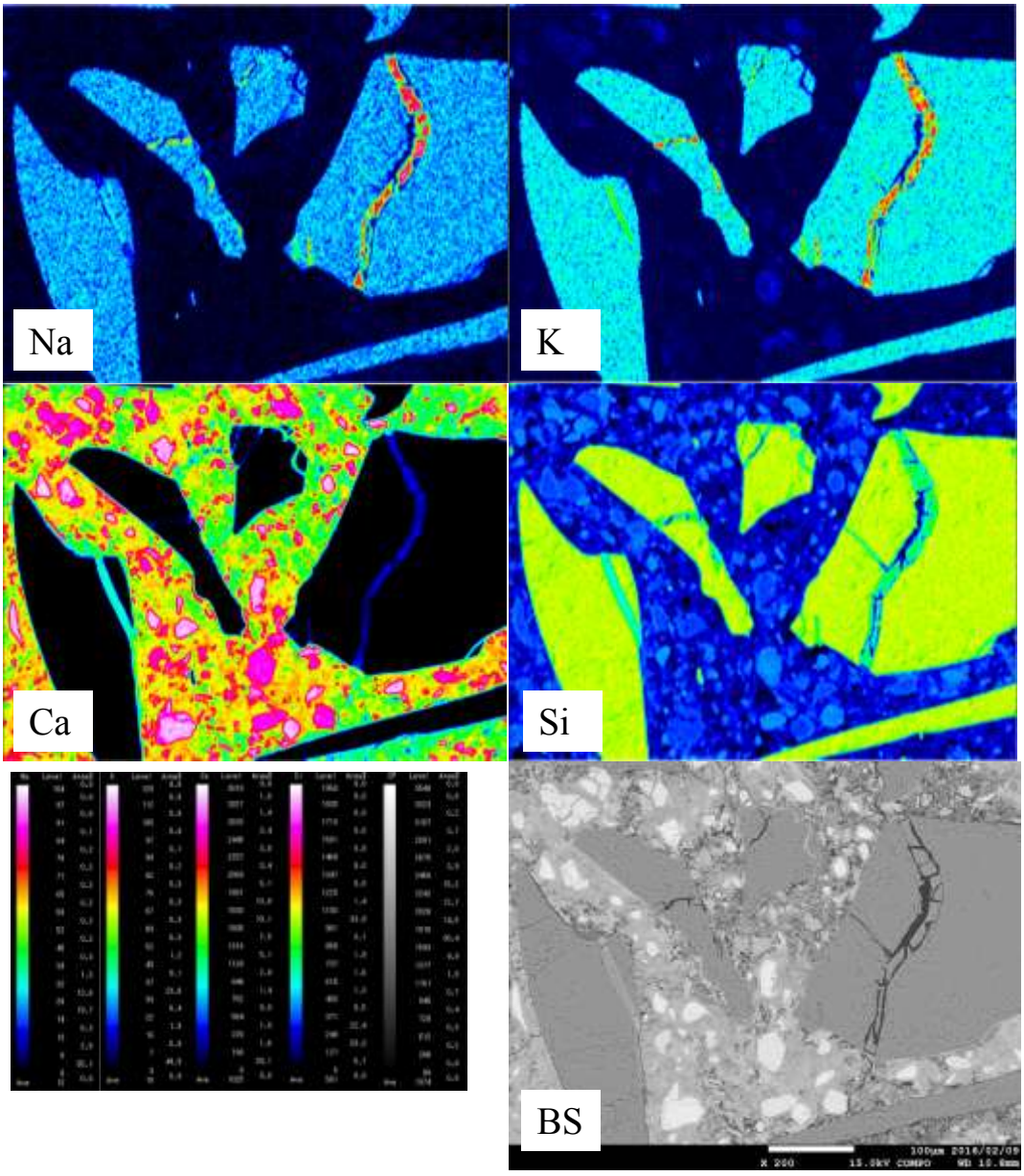

(B)

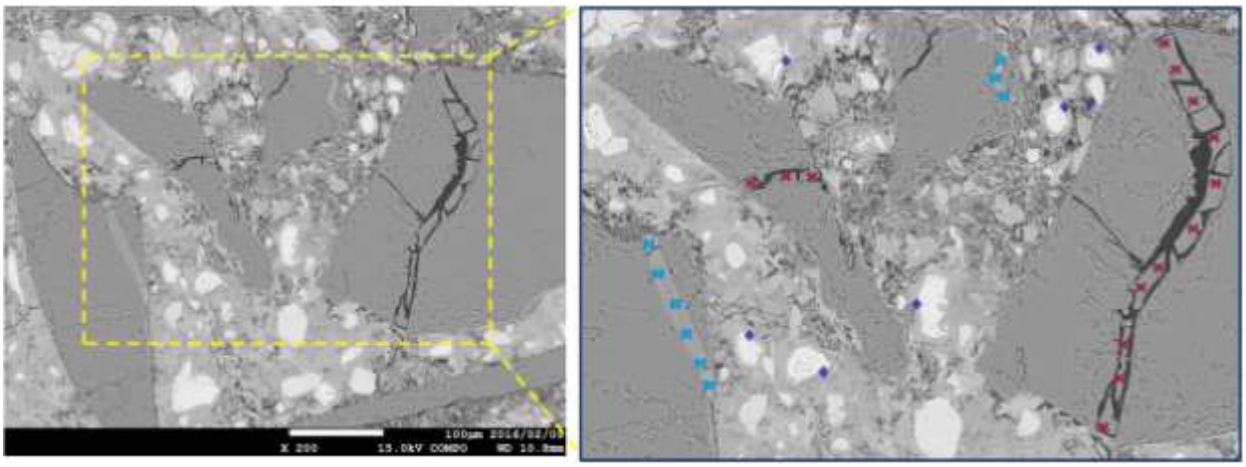

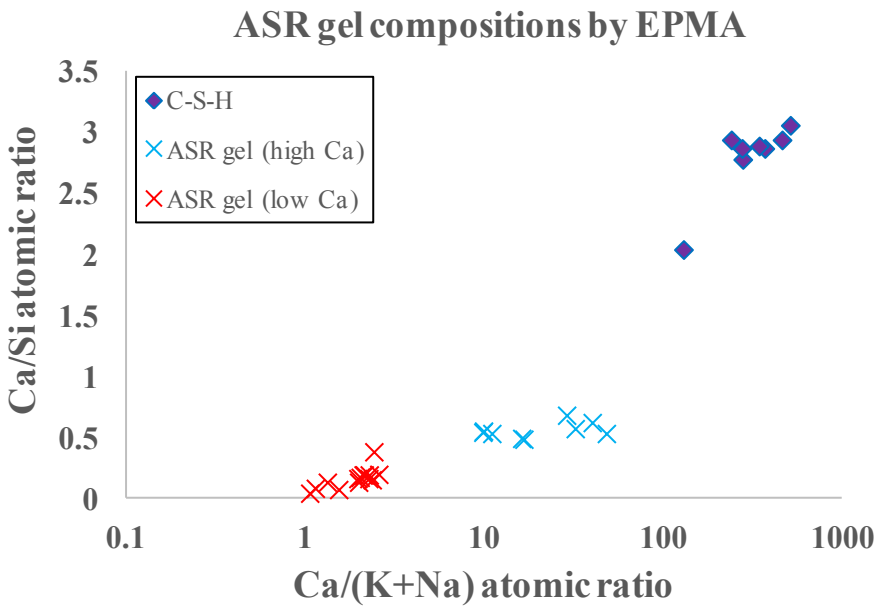

Fig. 6.10 BSE images of PG100 with alkali content of 1.2%: (A) EPMA with mapping method of; (B) Magnification of BSE images showing ASR deposited in the cracked aggregates (red cross), ASR deposited in the rim between aggregate and paste (blue cross) and the hydrated products (purple dot).

REFERENCES

[1] E. Iwatsuki, K. Morino. Characteristics of alkali silica reaction of siliceous sedimentary rocks. J. Mater. Sci, 57(10) (2008), 967-972.

[2] Method of test for alkali-silica reactivity of aggregates by mortar bar method (JIS A1146). Japan Concrete Institute (JCI) 2007.

[3] Test method for potential alkali reactivity of cement-aggregate combinations (mortar-bar method). ASTM international. Retrieved from http://www.astm.org/Standards/C277.htm.

[4] L.F.M. Sanchez et al. (2014), Comparative study of a chemo–mechanical modeling for alkali silica reaction (ASR) with experimental evidences, Construction and Building Materials,72, 301–315.

[5] L.S. Dent Glasser, N. Kataoka, The chemistry of alkali-aggregate reactions, proceedings of 5th ICAAR, Cape Town, South Africa (1981), p. S252/23.

[6] T.N. Jones, A new interpretation of alkali–silica reaction and expansion mechanisms in concrete, Chem. Ind., 18 (1988), pp. 40–44

[7] S. Multon, M. Cyr, A. Sellier, P. Diederich, L. Petit, Effect of aggregate size and alkali content on ASR expansion, Cement and Concrete Research, 40(2010), 508–516

[8] S. Multon, A. Sellier, M. Cyr, Chemo–mechanical modeling for prediction of alkali silica reaction (ASR) expansion, Cement and Concrete Research, 39 (2009),490–500

[9] X .X. Gao, S. Multon, M. Cyr, A. Sellier, Alkali–silica reaction (ASR) expansion: Pessimum effect versus scale effect, Cement and Concrete Research, 44(2013), 25–33.

[10] J. W. Phair, S. N. Tkachev, M. H., Manghnani and R. A. Livingston Elastic and structural properties of alkaline-calcium silica hydrogels, Journal of Materials Research, 20(2) (2005), 344-349

[11] M. Kawamura, K. Iwahori. ASR gel composition and expansive pressure in mortars under restraint. Cem Concr Comp, 26(1) (2004), 47-56.

[12] M.B. Haha, E. Gallucci, A. Guidoum, K.L. Scivener, Relation of expansion due to alkali silica reaction to the degree of reaction measured by SEM image analysis, Cement and Concrete Research, 37 (2007), 1206-1214.

[13] J.K. Kim, S.H. Han, K.M. Lee, Estimation of compressive strength by a new apparent activation energy function, Cem. Concr. Res. 31 (2001) 217–225.

[14] P. Lawrence, M. Cyr, E. Ringot, Mineral admixtures in mortars. Effect of inert materials on short-term hydration, Cem. Concr. Res. 33 (2003) 1939–1947.

[15] F. Ridi, E. Fratini, F. Manelli, P. Baglioni, Hydration process of cement in the presence of a cellulosic additive. A calorimetric investigation, J. Phys. Chem., B 109 (2005) 14727–14734.

[16] K.O. Kjellsen, R.J. Detwiler, Reaction-kinetics of Portland-cement mortars hydrated at different temperatures, Cem. Concr. Res. 22 (1) (1992) 112–120.

[17] T. Kishi, K. Maekawa, Multi-component model for hydration heating of Portland cement, Conc. Lib. JSCE 28 (1996) 97–115.

[18] L.E. Copeland, D.L. Kantro, Hydration of Portland cement, Proc 5th International Congress on the Chemistry of Cement, Tokyo, 1968, pp. 387–420.

[19] L. D'Aloia, G. Chanvillard, Determining the "apparent" activation energy of concrete Ea-numerical simulations of the heat of hydration of cement, Cem. Concr. Res. 32 (2002) 1277–1289.

[20] S. Swaddiwudhipong, D. Chen, M.H. Zhang, Simulation of the exothermic process of Portland cement, Adv. Cem. Res. 14 (2) (2002) 61–69.

[21] D. Bulteel, E. Garcia-Diaz, C. Vernet, H. Zanni Alkali-silica Reaction A Method to Quantify the Reaction Degree. Cem Concr Res, 32 (2002), 1199-1206.

[22] T. Katayama. Late-expansive ASR in a 30-year old PC structure in eastern Japan. Proceedings of 14th ICAAR 030411-KATA-05. Austin;Texas: USA:2012.

CHAPTER 7 CONCLUSIONS AND FUTURE WORKS

7.1 CONCLUSIONS

The concrete deterioration due to ASR has been remained a subject of interest to many researchers in the areas of durability of concrete structures. The expansion process to cause damage in structure occurs due to the formation of gel by the ASR reaction. The simulating ASR formation in concrete with accelerating conditions (highly alkaline and temperatures) was a model experiments to start of this research. This research has become more interest in the sequence of ASR formation related to the content of Ca ions. The chemical compositions and structures of hydrated products with or without Ca ions have been investigated and predicted in this work. Then, the simulated results were compared against experimental data in this model system. The final goal of this dissertation was to associate the rate of dissolution of Si form aggregate in model system and its contribution to ASR-induced expansion of mortar.

The main conclusions with regards to main objectives of this dissertation can be summarized as follows:

- The model system was establish here to simulating the ASR formation that promotes the ASR reactivity of reactive chert aggregates and reactive pyrex glass. Soluble silica in the system was dissolved from reactive compounds by the OH^- activity (NH solution). It was found that the high contents of soluble silica determined by ICP-AES were observed in liquid samples without CH. With increasing temperature, the greater content of soluble silica in liquid samples mostly detected.

- In XRD results, the peak patterns at 7.0°2θ and 29.0 °2θ which changes with reaction time, indicating ASR product incorporation with Ca. The observation of C-S-H in the insoluble products is consistent with a little dissolved silica of liquid samples when CH was present. This implies that Ca ions react with dissolved silica of the liquid samples, precipitated ASR product in solids.

- In spectra of ^{29}Si-NMR results, the change from intensities of Q^1, Q^2 and Q^3 indicates the important role of Ca on the structure of ASR product. The sequence of ASR from model experiment suggests that Na/K-S-H, may be supposed to be the first product in the sequence of the ASR. It is commonly accepted that prior to the completed C-S-H formation, C-N/K-S-H (the Q^1 site dominantly) could be formed by the incorporation of Ca^{2+} ions into N/K-S-H. Later, excess Ca^{2+} ions are closely involved in the precipitation of ASR gel, likely to form a more polymerized structure of C-S-H (dominated by the Q^2 site). With lower amounts of Ca ions, the Q^3 site becomes detectable and finally, the presence of C-N/K-S-H and N/K-S-H may be attributed to the complete consumption of CH.

- It is deduced that the rapid rate of silica dissolution has an influence on the structure of ASR gel formation, in particular the ASR gel likely to C-S-H. For Yoro-chert with moderated ASR reactivity, the C-S-H with low Ca/Si ratios (0.83) appeared and then it tends to be C-N-S-H gel when Ca is almost consumed (**Fig. 1 (A)**). High Ca/Si ratios of C-S-H, like Jennite type C-S-H was detected in solid sample of pyrex glass (**Fig. 1 (B)**). This result is similar to the formation of C-S-H products in case of rapid C_3S reaction, as shown in **Fig. 2**.

- The sequence in the simulated process of ASR by PHREEQC can be divided into 4 steps:
  (i) formation of a stable C–S–H_0.83 for chert aggregate and C-S-H-1.66 for pyrex glass sample by reaction between dissolved Si ions from chert and Ca ions;(ii) after complete consumption of CH, formation of C–Na–S–H by reaction between existing C–S–H, Na ions, and dissolved Si ions;(iii) during the conversion of C–S–H to C–N–S–H, the Si concentration in the solution keeps increasing;(iv) following (iii) there is formation of N–S–H by reaction between dissolved Si ions

from reactive compound and alkali ions. The simulation model tends to give predictions of C-S-H, C–N–S–H, and Na-S-H that are in agreement with the experimental data from the corresponding tests, except for the initial formation of C-N-S-H because the formation occurs in a shorten period (as mentioned previously in the XRD and ^{29}Si-NMR results).

- Expansion measurements made at constant temperature of 40°C, the mortars with alkali content of 1.2% attribute to the ASR activity of PG. To approach the ASR formation, the microstructure of mortars including SS100 and PG100 was investigated by EPMA, indicating that ASR with Ca/Si ratios less than 1.0 mostly deposited in the cracked aggregate, while ASR in the cement paste near reactive site has been found to be high Ca/Si ratios (0.5.-1.5). This is because the low rate of Ca diffusion through the reactive site.

- With dissolution rate of soluble silica, it is associated with the expansion rate of mortar containing siliceous materials, indicating a reaction degree of reactive compounds reach to 0.2 to 0.5%. Although both pyrex glass and chert aggregate are reactive materials, mortar with Pyrex glass expanded rapidly when compared to mortar mixed with chert aggregate. This attributed to differences in the kind of ASR. As expected from gel composition, jennite type C-S-H (Ca/Si ratios=1.66) existed in pyrex glass sample but not found in chert sample. With the high consumption of Ca at early stage for C-S-H_1.66, this tends to yield the ASR gel, like kanemite (Na-S-H) or Ca-kanemite (C-N-S-H). The formation of C-N-S-H and N-S-H is responsible for essential to swelling, inducing the greater expansive pressure in mortar of PG. Therefore, it can be concluded that the rate of expansion due to ASR depends on both the contents of ASR as well as on the capacity available for swelling of the gel. Therefore, ASR gel formation is related to expansion of mortar.

7.2 FUTURE WORKS

Based on the experiment results gained from this dissertation, the following aspects on experiment and simulation are recommended for further research work in order to have a better understanding on ASR Formation of Reactive Siliceous Materials in Conducting Model Experiments at Highly Alkaline and Temperature Conditions

- The model system established in this dissertation contributes to the ASR formation of only four siliceous compounds. It would be a great interest to study other reactive materials and non-deleterious materials in order to gain accurate relationship between the activation energy and expansion of mortar at constant temperature. Moreover, the dissolution rate of soluble silica at different alkali contents should also be investigated in order to explain the pessimum effect of alkali contents on ASR formation and expansion.

- This research focused on the model system to simulate the ASR formation of siliceous compounds (Yo, Se, SS and PG). In particular, the dissolution rate of soluble silica of PG is very rapid and then some reaction product cannot detect in the insoluble products. Thus, to retard the ASR reaction of PG, this model system has to be modified with considering the impact of PG/SS ratio. The effect of PG/SS mixing ratios on dissolution of silica and the chemical sequence of ASR production in model system are recommended for future work. To do this, the contents of soluble silica from mixture will be used to simulate the ASR formation by PHREEQC program. Parallel to the expansion measurement, the mixtures including PG and SS with different ratios should be explored. This could eventually lead to draw the diagram of change of ASR gel formation comparing with the expansion of mortars.

- It should be noted that the reaction rim of ASR was not observed by EPMA analysis from the expanded mortar of PG100. The expansion measurement was investigated until 56 days. This

reaction time was probably not enough for the reaction rim of ASR formed around reactive site. Therefore, the expansion measurements should be extended with considering the reaction time, the temperature conditions, and the mixture ratios between SS and PG. Additionally, the expansion measurements at different temperatures should be investigated in order to determine the pessimum effect of temperatures on expansion of mortars.

- As mentioned above the rate of expansion due to ASR depends on both the contents of ASR as well as on the capacity available for swelling of the gel. Gel swelling depends on the moisture in pore solution that is linked to the viscosity of gel. With the expansion data, this attributes to investigate the viscosity effect of ASR gel by considering the fitting data curve of expansion. The mathematics model is needed to illustrate the relationship of expansion and gel viscosity in future.

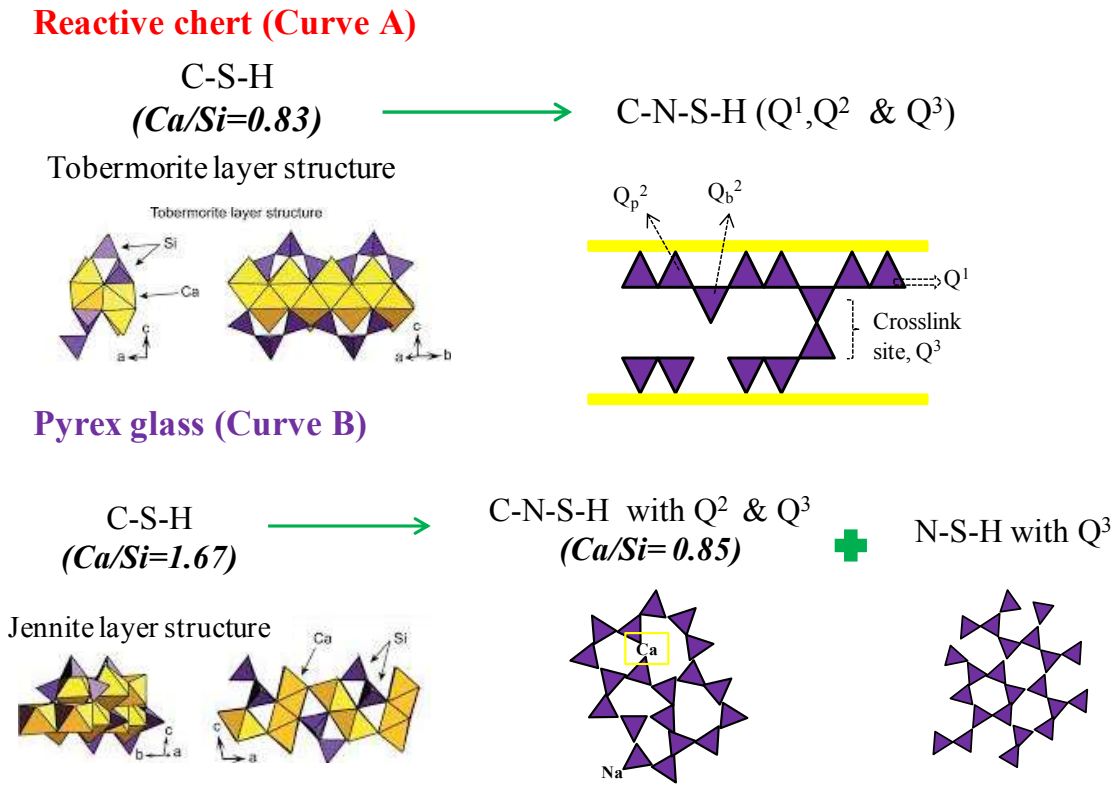

Fig. 1 Product formation: (A) for Yoro-chert mixed with CH; (B) for Pyrex-glass mixed with CH

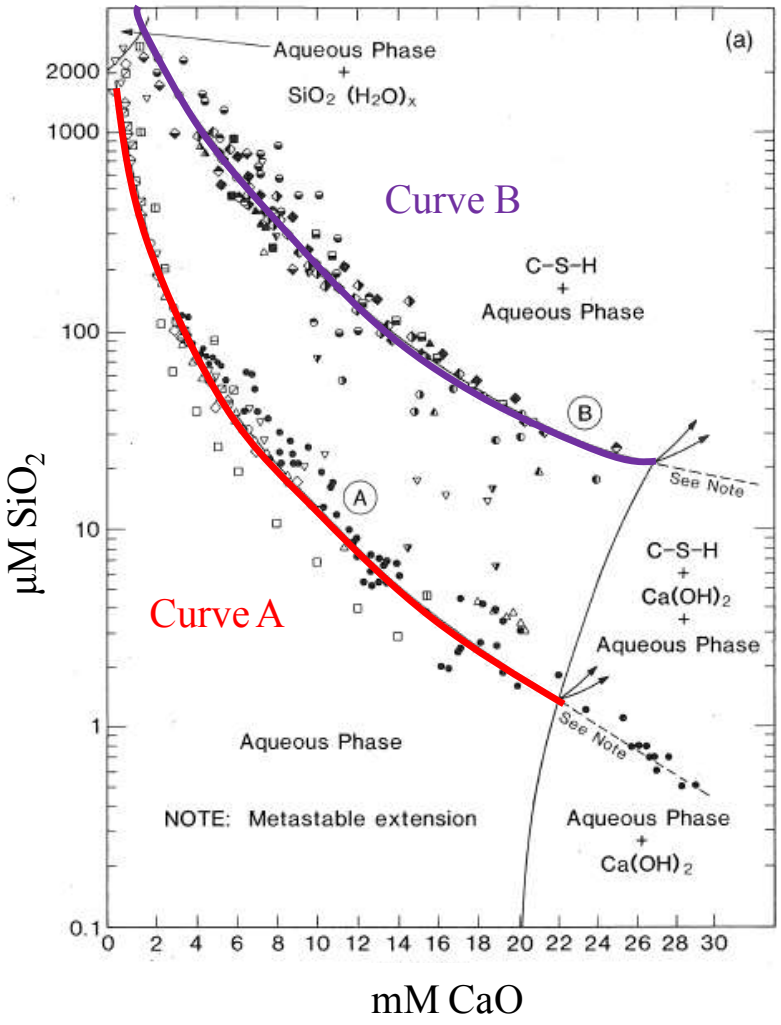

Fig. 2 The product formation due to hydration reaction of C_3S